A Wide-area Analysis of Shifts in Electric Power System Generation Profiles and High-impact Event Scenarios

A Dissertation Presented for the

Doctor of Philosophy

Degree

The University of Tennessee, Knoxville

Micah Joel Till

May 2017

Copyright © 2017 by Micah J. Till
All rights reserved.

ACKNOWLEDGEMENTS

There are many friends and colleagues for whose help and support I am deeply grateful. Unfortunately, a comprehensive list is beyond the scope of the space available here. That said, there are those without whom this work would not be possible.

The first is Dr. Yilu Liu, my advisor and mentor, who trained me how to think about research and explore interesting problems. Her guidance throughout my Ph.D. studies has been invaluable. I am also thankful for the members of my committee, Dr. Kevin Tomsovic, Dr. Kai Sun, and Dr. Lee Riedinger, who shared their time and experience and constantly challenged me.

The next is Dr. Matthew Gardner at Dominion Virginia Power along with Dr. Emanuel Bernabeu, Dr. Kevin D. Jones, Kyle Thomas, and everyone else in Richmond who has invested in my growth. The expertise and the opportunity they extended me were vital in this process. Chapter 4, specifically, would not exist without Dominion's sponsorship.

I would hasten to acknowledge other utility support as well. Engineers at the Tennessee Valley Authority provided data and feedback for Chapter 2. Mahendra Patel (PJM Interconnection, LLC) reviewed the work in Chapter 3. Chapter 5 and Chapter 6 cover research I conducted in partnership with Oak Ridge National Laboratory. Jose Gracia's leadership and Eric Alan's (New Electricity Transmission Software Solutions) expertise were vital for the latter.

I would also recognize my fellow researchers in the FNET/GridEye lab, past and present, for their patient help and comradery. Special thanks to Penn Markham, Hesen Liu, Ye "Zoe" Zhang, Gefei "Derek" Kou, and Yong "Frank" Liu.

I thank God for the identity and purpose He has given me in Christ Jesus and for the body of brothers and sisters He has surrounded me with on every step of this journey—most notably the men and women at both Fellowship Church Knoxville and Redemption Hill Church in Richmond. I am particularly indebted to Austin Womac, a UTK EECS alumnus and spiritual brother, for his friendship and encouragement over the past three years.

Of course, no acknowledgement could be complete without recognizing my family, especially my parents, Lynn and David Till, who taught me how to learn, are usually right, and are never slow to say "I love you." I love you too.

ABSTRACT

Often cited as the largest machine in the world, the electric power grid is a complex system, integral to modern life. Continuous technology advancements over the past hundred years have delivered improvements to both the system itself, e.g., wide-area management systems (WAMS), as well as modeling capabilities in order to better understand how that system functions. Phenomena that could once be simulated only in small, localized settings can now be studied from a wide-area perspective.

Chapter 1 briefly introduces the three major U.S. electric interconnections along with wide-area power system analysis tools and the benchmarked models used in this work. It also puts forward two topics that wide-area modeling must address: the effect of generation portfolio changes on dynamic system response and the assessment and hardening of the grid against high-impact, interconnection-wide events.

The first topic is investigated in Chapter 2 and Chapter 3. Specifically, Chapter 2 examines dynamic response repercussions of the recent shift from coal-fired generation plants to natural gas turbines. Chapter 3 extends this discussion to the increase in low-inertia renewable sources.

Modeling and analysis of wide-area events in line with the second topic, including extreme weather phenomena, solar storms, and physical attacks, as well as methodologies to harden the grid, are investigated in the remainder of this work. Chapter 4 begins with an example of modeling geomagnetically induced current (GIC) effects while Chapter 5 discusses high-altitude electromagnetic pulse (HEMP) components and impacts. Chapter 6, guided by the 2015 Fixing America's Surface Transportation (FAST) Act, extends the scope of these scenarios and presents a methodology to find the most critical elements for any given system and determine the minimum required spare large power transformer (LPT) reserve that should be available.

Conclusions and potential future research directions are presented in Chapter 7.

TABLE OF CONTENTS

Chapter 1: Introduction 1
1.1 An Introduction to the U.S. Interconnections 1
1.1.1 Interconnection Governance 2
1.1.2 Industry Planning Models 3
1.1.3 Simulation Tools 3
Chapter 2: Dynamic Effects of the Eastern Interconnection's Transition from Coal to Natural Gas 4
2.1 Impact of EPA Regulations on Frequency Response 5
2.2 Dynamic Model Creation 7
2.3 Dynamic Simulation Results 9
2.4 Conclusions 15
Chapter 3: The Ramifications of Loss of Inertia and Generator Controls 16
3.1 EI Model and Study Scenarios 17
3.1.1 Modifications to Generator Controls and Inertia Constants 17
3.2 Simulation Results 18
3.2.1 Event 1: Loss of 2,550 MW Generator 18
3.2.2 Event 2: Loss of 1,517 MW Generator 20
3.2.3 Event 3: Loss of 1,056 MW Load Site 24
3.2.4 Event 4: Comparison of Responses to Different Imbalance Magnitudes 24
3.3 Conclusions and Recommendations 27
Chapter 4: Wide-area Analysis of Geomagnetically Induced Current Harmonics 28
4.1 Background 28
4.2 Purpose and Procedure 28
4.2.1 Demonstration of Harmonic Current Injection Interactions 29
4.2.2 Modeling Methodology 31
4.2.3 Harmonic Current Injections 32
4.2.4 GMD Scenario 32
4.3 Simulation Results 33
4.3.1 Model Validation 36

4.3.2 Sensitivity Analysis 37
4.4 Conclusions 37
Chapter 5: Evaluating the Impact of a High Altitude Electromagnetic Pulse 39
5.1 Background 39
5.1.1 HEMP Components 40
5.1.2 HEMP Models 41
5.2 HEMP E1 Impact Study 42
5.2.1 Input Event Assumptions 42
5.2.2 Modeling Methodology 43
5.2.3 Simulation Results 44
5.2.4 NPCC Participation 45
5.3 Conclusions and Future Work 52
Chapter 6: Strategic Transformer Reserve Interconnection-wide Grid Security Assessment 53
6.1 Problem Formulation 53
6.2 Methodology 54
6.2.1 Incremental Thermal Transfer Capacity 55
6.2.2 Reactive Power Generation Headroom 59
6.2.3 Application of Ranking Methodology 61
6.2.4 Combinatorial Scenarios 63
6.2.5 Spare Transformer Identification 75
6.3 Substation Pair Analysis 76
6.3.1 European Analysis Results 76
6.3.2 Comparison with Other Systems 81
6.4 Further Combinatorial Studies 82
6.5 Findings and Conclusions 90
Chapter 7: Conclusions and Recommendations 92
7.1 Future Work 93
References 94
Appendices 101

Appendix A: Fuel Transition Simulation Results 102
Appendix B: Loss of Inertia Simulation Results 116
Appendix C: Python Helper Functions Created for PSS®E 126
Appendix D: Substation Bus List Script 133
Appendix E: Transformer Replacement Locator Script 137
Vita 141

LIST OF TABLES

Table 2.1. Summary of yearly base case changes versus original MMWG model 7
Table 2.2. Summary of case changes inside each year 8
Table 2.3. Range of inertia and damping constant values by fuel type 8
Table 5.1. Megawatt summaries for the original, dropped, and recovered load by region 44
Table 5.2. Maximum and minimum measurements by scenario 45
Table 6.1. Illustrative results from an example combinatorial outage scenario 64
Table 6.2. Illustrative results from an example combinatorial outage scenario with transformer replacement 74
Table 6.3. Summary of EU paired substation scenario convergence 78
Table 6.4. Summary of WECC and EI paired substation scenario convergence 81
Table 6.5. Proximity-based impact study results 90

LIST OF FIGURES

Figure 1.1. A map of the North American Interconnections and EROs 2
Figure 2.1. A map of all buses in the MMWG 2010 series case for summer 2015 peak load [9].. 6
Figure 2.2. Base case frequency response for 2003 MW east coast generation loss 10
Figure 2.3. Year 2015 frequency response for 2003 MW east coast generation loss 10
Figure 2.4. Anomalous behavior due to bad initial power flow solutions 11
Figure 2.5. Base case frequency response for 5~ southeast bolted bus fault 11
Figure 2.6. Year 2015 frequency response for 5~ southeast bolted bus fault 12
Figure 2.7. Base case frequency response for southwest 230 kV line trip 12
Figure 2.8. Year 2015 frequency response for southwest 230 kV line trip 13
Figure 2.9. Base case frequency response for 800 MW southeast load shed 14
Figure 2.10. Year 2015 frequency response for 800 MW southeast load shed 14
Figure 3.1. Event 1, Case 1: Frequency response 19
Figure 3.2. Event 1, Case 1: Voltage response 19
Figure 3.3. Event 1, Case 2: Frequency response 21
Figure 3.4. Event 1, Case 2: Voltage response 21
Figure 3.5. Event 2, Case 1: Frequency response 22
Figure 3.6. Event 2, Case 1: Voltage response 22
Figure 3.7. Event 2, Case 1: Frequency response 23
Figure 3.8. Event 2, Case 2: Voltage response 23
Figure 3.9. Event 3, Case 2: Frequency response 25
Figure 3.10. Event 3, Case 2: Voltage response 25
Figure 3.11. Event 4, Base Case: Proportional frequency response 26
Figure 3.12. Event 4, Case 1: Proportional frequency response 26
Figure 4.1. ETAP diagram of IEEE 14 bus system 30
Figure 4.2. Bus voltage THD in the IEEE 14 bus system under case 1 and case 2 31
Figure 4.3. Harmonic current injection spectrum for particular transformer design [50] 33
Figure 4.4. Voltage THD box plot across major bus voltage levels [50] 34
Figure 4.5. GIC injections for 1-in-100 year GMD event [50] 35
Figure 4.6. Bus voltage THD for 1-in-100 year GMD event [50] 35

Figure 4.7. Voltage THD caused by monitored in-rush events 37
Figure 5.1. Illustrative qualitative example of transient HEMP components on a log-log graph 40
Figure 5.2. Map of HEMP detonation and impact locations 42
Figure 5.3. Frequency deviation for 5% load loss with 75% recovery at t = 4 seconds 46
Figure 5.4. Voltage profile for 5% load loss with 75% recovery at t = 4 seconds 46
Figure 5.5. Frequency deviation for 5% load loss with 75% recovery at t = 10 seconds 47
Figure 5.6. Voltage profile for 5% load loss with 75% recovery at t = 10 seconds 47
Figure 5.7. Frequency deviation for 10% load loss with 75% recovery at t = 4 seconds 48
Figure 5.8. Voltage profile for 10% load loss with 75% recovery at t = 4 seconds 48
Figure 5.9. Frequency deviation for 10% load loss with 75% recovery at t = 10 seconds 49
Figure 5.10. Voltage profile for 10% load loss with 75% recovery at t = 10 seconds 49
Figure 5.11. Frequency deviation for 15% load loss with 75% recovery at t = 4 seconds 50
Figure 5.12. Voltage profile for 15% load loss with 75% recovery at t = 4 seconds 50
Figure 5.13. Frequency deviation for 15% load loss with 75% recovery at t = 10 seconds 51
Figure 5.14. Voltage profile for 10% load loss with 75% recovery at t = 10 seconds 51
Figure 6.1. Linear projection technique 56
Figure 6.2. Illustrative ordered criticality index plot using thermal ranking 62
Figure 6.3. Illustrative ordered criticality index plot using VAR support ranking 62
Figure 6.4. Example system one line diagram 67
Figure 6.5. LPTs at top removed from service 68
Figure 6.6. Local voltage collapse leads to a divergent solution state 69
Figure 6.7. Alternative solution process: Begin by removing entire load center from service 70
Figure 6.8. Then bring sections back into service in stages 71
Figure 6.9. This allows the numeric solver to calculate more feasible VAR flow patterns 72
Figure 6.10. The final result is a valid system with only the LPTs under test removed from service 73
Figure 6.11. Ordered thermal criticality index ranking for high voltage EU substations 77
Figure 6.12. Ordered VAR support criticality index ranking high voltage EU substations 77
Figure 6.13. Thermal analysis box plots for paired high voltage EU substations ordered by single substation rank 79

Figure 6.14. VAR support analysis box plots for paired high voltage EU substations ordered by single substation rank 80
Figure 6.15. Map of Case A impact zone 83
Figure 6.16. Map of Case B impact zone 83
Figure 6.17. Map of Case C impact zone 84
Figure 6.18. Map of Case D impact zone 84
Figure 6.19. Map of Case E impact zone 85
Figure 6.20. Map of Case F impact zone 85
Figure 6.21. Map of Case G impact zone 86
Figure 6.22. Map of Case H impact zone 86
Figure 6.23. Map of Case I impact zone 87
Figure 6.24. Map of Case J impact zone 87
Figure 6.25. Map of Case K impact zone 88
Figure 6.26. Map of Case L impact zone 88
Figure 6.27. Map of Case M impact zone 89
Figure 6.28. Map of Case N impact zone 89
Figure A.1. Base case frequency response for 2003 MW east coast generation loss 102
Figure A.2. Year 2012 frequency response for 2003 MW east coast generation loss 102
Figure A.3. Year 2013 frequency response for 2003 MW east coast generation loss 103
Figure A.4. Year 2014 frequency response for 2003 MW east coast generation loss 103
Figure A.5. Year 2015 frequency response for 2003 MW east coast generation loss 104
Figure A.6. Year 2016 frequency response for 2003 MW east coast generation loss 104
Figure A.7. Year 2017 frequency response for 2003 MW east coast generation loss 105
Figure A.8. Base case frequency response for 5~ southeast bolted bus fault 105
Figure A.9. Year 2012 frequency response for 5~ southeast bolted bus fault 106
Figure A.10. Year 2013 frequency response for 5~ southeast bolted bus fault 106
Figure A.11. Year 2014 frequency response for 5~ southeast bolted bus fault 107
Figure A.12. Year 2015 frequency response for 5~ southeast bolted bus fault 107
Figure A.13. Year 2016 frequency response for 5~ southeast bolted bus fault 108
Figure A.14. Year 2017 frequency response for 5~ southeast bolted bus fault 108

Figure A.15. Base case frequency response for southwest 230 kV line trip 109
Figure A.16. Year 2012 frequency response for southwest 230 kV line trip 109
Figure A.17. Year 2013 frequency response for southwest 230 kV line trip 110
Figure A.18. Year 2014 frequency response for southwest 230 kV line trip 110
Figure A.19. Year 2015 frequency response for southwest 230 kV line trip 111
Figure A.20. Year 2016 frequency response for southwest 230 kV line trip 111
Figure A.21. Year 2017 frequency response for southwest 230 kV line trip 112
Figure A.22. Base case frequency response for 800 MW southeast load shed 112
Figure A.23. Year 2012 frequency response for 800 MW southeast load shed 113
Figure A.24. Year 2012 frequency response for 800 MW southeast load shed 113
Figure A.25. Year 2014 frequency response for 800 MW southeast load shed 114
Figure A.26. Year 2015 frequency response for 800 MW southeast load shed 114
Figure A.27. Year 2016 frequency response for 800 MW southeast load shed 115
Figure A.28. Year 2017 frequency response for 800 MW southeast load shed 115
Figure B.1. Event 1, Case 1: Frequency response 116
Figure B.2. Event 1, Case 1: Voltage response..... 116
Figure B.3. Event 1, Case 2: Frequency response 117
Figure B.4. Event 1, Case 2: Voltage response..... 117
Figure B.5. Event 2, Case 1: Frequency response 118
Figure B.6. Event 2, Case 1: Voltage response..... 118
Figure B.7. Event 2, Case 1: Frequency response 119
Figure B.8. Event 2, Case 2: Voltage response..... 119
Figure B.9. Event 3, Case 1: Frequency response 120
Figure B.10. Event 3, Case 1: Voltage response..... 120
Figure B.11. Event 3, Case 2: Frequency response 121
Figure B.12. Event 3, Case 2: Voltage response..... 121
Figure B.13. Event 4, One Unit, Case 1: Frequency response..... 122
Figure B.14. Event 4, One Unit, Case 1: Voltage response..... 122
Figure B.15. Event 4, Two Units, Case 1: Frequency response 123
Figure B.16. Event 4, Two Units, Case 1: Voltage response..... 123

Figure B.17. Event 4, One Unit, Case 2: Frequency response 124
Figure B.18. Event 4, One Unit, Case 2: Voltage response 124
Figure B.19. Event 4, Two Units, Case 2: Frequency response 125
Figure B.20. Event 4, Two Units, Case 2: Voltage response 125

CHAPTER 1: INTRODUCTION

The electric power grid is a complex system, integral to modern life. Sustained development since the first alternating current (AC) transmission system over 100 years ago [1] has earned the grid the title of the largest machine in the world [2]. Continuous technological advancements allow improvements to both the system itself, e.g., wide-area management systems (WAMS), as well as modeling capabilities. The former increases the efficiency and control capabilities of the grid from electricity generation to end-use consumption. The latter provides deeper understanding of how the system works at a fundamental level.

Phenomena that once could be simulated only in a small, localized setting can now be studied from a wide-area perspective—often even in real time. Two related topics immediately rise to the forefront when considering such a perspective: future buildout scenarios and extreme event analysis.

Inquiry into the first seeks to answer the question of how changes in infrastructure will effect electric grid performance. With the recent shift in generation portfolios toward fuel sources that produce lower CO_2 emissions than traditional coal-fired plants, this is a timely issue.

The second topic relies on similar wide-area models to focus on the response of the present grid to high impact events. Geomagnetically induced current (GIC), high-altitude electromagnetic pulse (HEMP) detonations, and interconnection-wide security and resiliency assessments all require analysis techniques capable of evaluating impacts across the entire system.

1.1 An Introduction to the U.S. Interconnections

The United States is divided into three dynamically isolated, three-phase, 60 Hz alternating current electric grids: the Eastern Interconnection (EI), the Western Electricity Coordinating Council (WECC), and the Electric Reliability Council of Texas (ERCOT). The EI extends from the Atlantic Ocean to the Rocky Mountains—minus most of Texas which, as the name implies, is run by ERCOT—and from Florida to parts of Canada. WECC covers the rest of the continental U.S. and a large western section in Canada. Alaska and Hawaii are not members of an interconnection, but are both subdivided by geography into multiple island-like grids [3].

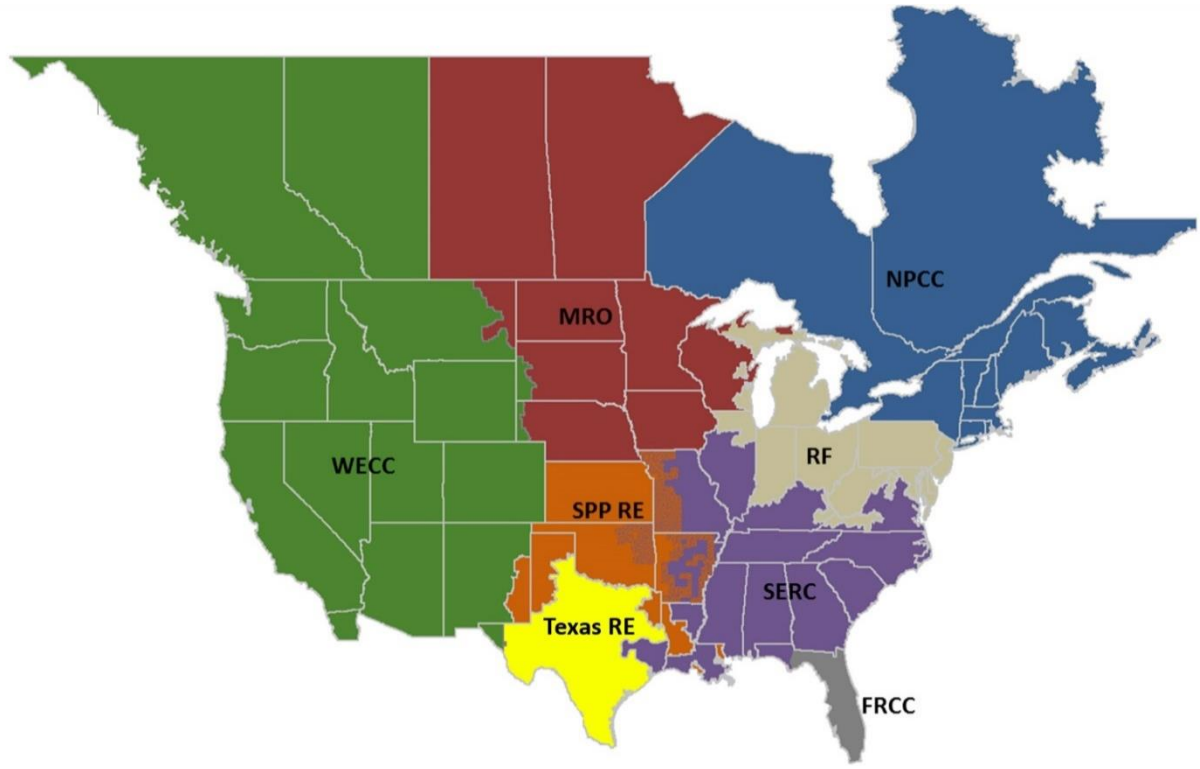

Figure 1.1. A map of the North American Interconnections and EROs

1.1.1 Interconnection Governance

WECC and ERCOT both have a central governing council for reliability concerns, WECC and Texas Reliability Entity, Inc. (TRE), respectively. The EI is composed of six independent regional entities (EROs). The location of each is shown in Figure 1.1 [3]. All six of these reliability bodies must meet standards set by the North American Electricity Reliability Corporation (NERC) under the oversight and authority of the Federal Energy Regulatory Commission (FERC). One requirement is the creation of interconnection planning models with both load flow (steady state) and dynamic information for all elements that are a part of the bulk electric system (BES) [4]. Typically the summer peak load model is considered the most important with the winter peak load model coming in as a close second. Spring shoulder load models are also used, but not produced for every study year.

1.1.2 Industry Planning Models

As the sole EROs in their interconnections, the models released by WECC and ERCOT are considered definitive and referred to simply as the WECC and ERCOT models, respectively. In the EI, the Multiregional Modeling Working Group (MMWG), under the oversight of the Eastern Interconnection Reliability Assessment Group (ERAG), is responsible for developing models for the interconnection [5]. Due to the size of the EI, the full 60,000 three-phase bus MMWG model is often equivalized to reduce model complexity. Depending on the purpose of the study and the geographical area of interest, significant compression is possible.

This work utilizes models from all three interconnections kindly provided through the Tennessee Valley Authority (TVA), Dominion Virginia Power (DVP), Energy Visuals, Inc., and FERC. In all cases, industry models are made available through non-disclosure agreements (NDAs) that require that no detailed parameters from the models be released. Under the agreements, results and analysis may still be discussed, provided no critical energy infrastructure information (CEII) is disclosed.

1.1.3 Simulation Tools

The main analysis tool used in this work for both power flow and dynamic simulation is PSS®E (Power System Simulation for Engineers). This software suite is based in Fortran (FORTRAN at the time) with an extensive Python application programing interface (API). All MMWG and ERCOT models are specifically designed with PSS®E in mind and it is generally considered the gold standard for power system simulation by engineers in those regions. WECC prioritizes PSLF (Power System Load Flow) as the main power flow engine for interconnection studies, but ensures all cases also run correctly in PSS®E.

Harmonic load flow is conducted in ETAP (Electrical Transient and Analysis Program).

Hardware-in-the-loop electromagnetic transient program (EMTP) simulations are designed in RSCAD (Real-time Simulation Computer Aided Design) and run on RTDS (Real-time Digital Simulator).

CHAPTER 2: DYNAMIC EFFECTS OF THE EASTERN INTERCONNECTION'S TRANSITION FROM COAL TO NATURAL GAS

The generation profile of America's power grids is changing. Over the last decade, many synchronous coal-fired plants have been retired and replaced by other fuel forms [6]. While steady state power flow analysis may yield similar results after this shift—postulating general topology and generation levels remain similar, without respect to fuel type—dynamic simulation will not [7], [8]. Differing control structures and inertia constants strongly affect system response and oscillation damping. The effects of these changes are generally considered muted by large, strongly connected systems such as the Eastern Interconnection (EI), but the scale of the current generation shift is unprecedented [9]. In Tennessee, electricity generated from natural gas increased over four-fold in 2012 alone and is replacing coal as the dominant fuel resource [10]. This trend holds true across most of the country and the United States Energy Information Administration (EIA) predicts that every state will pivot away from coal-fueled electricity generation, whether to natural gas-fueled generation or not, in the near future [6].

Motivating Factors behind this Shift

This shift has several underlying causes, but the dual prime drivers are Environmental Protection Agency (EPA) regulations and the rise of hydraulic fracturing (fracking).

The EPA finalized the Cross-state Air Pollution Rule (CSAPR) in July 2011 and the Mercury and Air Toxic Standards (MATS) in December of the same year. CSAPR requires power plants that contribute to air quality pollution in other states to reduce ozone and fine particle emissions [11]. MATS requires power plants to limit emissions of mercury, arsenic, and metals [12]. After the Supreme Court upheld CSAPR [13], utilities filed reports of their plans to shift generator fuel types away from coal [9]. The EPA subsequently proposed standards for CO_2 emissions from electrical power generation with the Clean Power Plan in June 2014 and released the final version in August 2015. The Clean Power Plan is intended to reduce CO_2 emissions from electrical power generation sources by 32% by 2030, relative to 2005 levels [14]. While the Clean Power Plan faces legal challenges, some stakeholders are already moving toward implementation [15]-[23].

Burning methane (natural gas) produces about half the CO_2 emissions as burning coal, giving natural gas a distinct advantage in conversations about greenhouse gas emissions [24]. This advantage now extends to economic concerns due to the ubiquitous expansion of hydraulic fracturing. The sudden glut of natural gas released into the market led to a significant decrease in cost [6]. With the possibility of new regulations and the changes in fuel markets, utilities are pivoting away from coal-fired turbines in favor of other fuel sources [25].

Dynamic Response Degradation

The dynamic response of the electric grid will change as the underlying generation infrastructure does. Coal-fired plants, which historically act as the majority baseline of the generation profile, respond to changes in power demand slowly, but also have the ability to match reactive power needs quickly. Gas turbines are historically used as smaller spinning reserve for the system since they have the ability to quickly change both real and reactive output power [1]. Gas-powered turbines have much lower inertia constants though, and the proliferation of baseline natural gas units and low, or zero, inertia renewable generation sources, i.e., wind turbines and photovoltaics, are often represented as a cause of degradation in the frequency response of the EI [26]. The conversation over the existence and causes of potential dynamic response degradation must not simply be discussed as theoretical arguments between utilities and vendors—the planned system must be modeled and analyzed to understand the impacts of shifting generation profiles on system performance and reliability.

2.1 Impact of EPA Regulations on Frequency Response

The six regional reliability entities across the EI provide data to the Eastern Interconnection Reliability Assessment Group (ERAG) so that planning studies (typically using a five to twenty year horizon) can be performed to ensure the reliability of the electric transmission system across the interconnection. The Multiregional Model Working Group (MMWG) is responsible for synthesizing these data into models that can be used as baseline planning cases. Each year the MMWG releases a set of seasonal power flow cases and associated dynamic model data [27]. In a previous study by Penn Markham [9], an MMWG 2010 series case representing the peak summer 2015 load is used to model the steady state buildout of several predicted scenarios caused by EPA emissions regulation. The original model contains

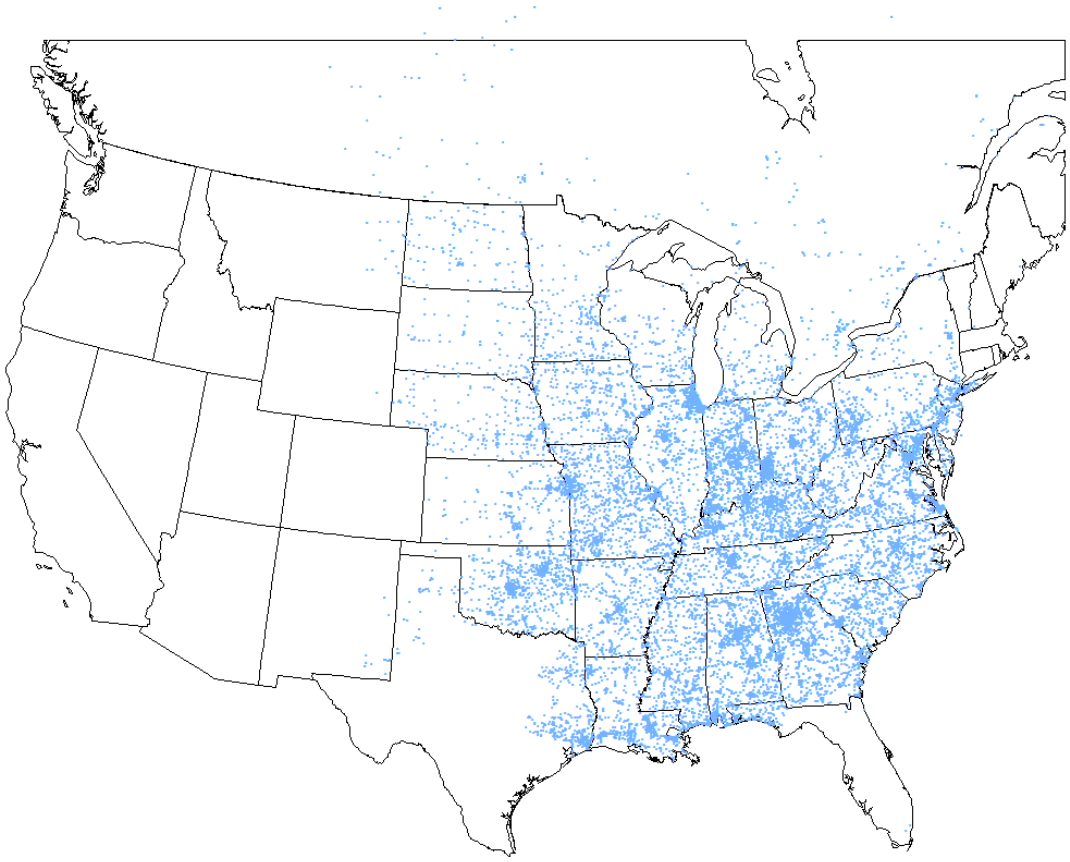

Figure 2.1. A map of all buses in the MMWG 2010 series case for summer 2015 peak load [9]

29,051 three-phase buses with 3,398 generating plants and 19,729 loads. 4,030 machines have associated dynamic data. Due to a set of generators with artificial upper limits of 9,999 MW, the total capacity of the system is immaterial, but the total system load and generation are 580,140 MW and 589,124 MW, respectively. A map of all modeled buses is provided in Figure 2.1 [9].

The initial study used information available from the Institute for Energy Research (IER), 2010 U.S. EIA Form 860 data filings, and the Nuclear Regulatory Commission (NRC) to locate and size generation sites that were expected to be retired or built [18]-[23]. A set of cases were created for different generation profiles and years. Each is able to converge to a solution using the fixed-slope decoupled Newton-Raphson method for power flow, but several of the solutions required swing bus operation beyond its given limits—the sign of a highly stressed system and in reality an infeasible set point.

First, base cases for the summers of 2012 through 2017 were created. These do not have any extra generation compared to the original 2015 MMWG case, but used the in-service date of each plant to determine if it should run or not and scaled the load to match expected forecasts [20]. Then, a set of cases were created where all coal plants expected to be shuttered by EPA regulations were removed from service based on the dates found in the IER, EIA, and NRC filings. Finally, a third set of cases was constructed where new natural gas turbines were added to replace coal generation. These are extensions of the second, retired coal case buildouts, except in the case of 2016, where the case does not converged cleanly. Instead, the coal retirement and gas expansion stages were combined using the 2016 base case as a starting point so that the numerical solver could find a stable steady state system solution. Note that new gas units are run close to their real power limits. These cases are identified by the last two digits of the base year (12-17) and the letter "a," "b," or "c" for base case, coal plant retirement, or additional natural gas units, respectively. Table 2.1 and Table 2.2 summarize each of these cases.

2.2 Dynamic Model Creation

In this work, the dynamic data for each case are created from the summer 2015 base case dynamic data supplied with the original MMWG model. The data for each machine are chosen based on representative sampling of existing dynamic models of similarly sized machines with matching fuel types. The inertia constant of a machine, H, is defined as the kinetic energy stored in the rotating mass at nominal speed divided by the generator rating. The damping coefficient, D, is a measure of how strongly a machine acts to minimize any difference in the angular velocities of the physical rotor and the air gap field [45]. Table 2.3 shows the range of inertia and damping values found across both the retired coal units and the additional natural gas generators.

Table 2.1. Summary of yearly base case changes versus original MMWG model

Case	Year	Capacity Change (MW)	Total Load (MW)
12a	2012	+13,328	554,798
13a	2013	+14,809	563,120
14a	2014	+10,571	571,567
15a	2015	-	580,140
16a	2016	+632	588,842
17a	2017	+722	597,675

Table 2.2. Summary of case changes inside each year

Case	Year	Retired Coal (MW)	Additional Gas (MW)
12a	2012	-	-
12b	2012	2,489	-
12c	2012	2,489	5,732
13a	2013	-	-
13b	2013	2,489	-
13c	2013	2,489	6,354
14a	2014	-	-
14b	2014	6,685	-
14c	2014	6,685	7,174
15a	2015	-	-
15b	2015	19,043	-
15c	2015	19,043	10,102
16a	2016	-	-
16b	2016	20,611	-
16c	2016	20,611	10,449
17a	2017	-	-
17b	2017	20,611	-
17c	2017	20,611	10,505

Adapting the original MMWG summer 2015 dynamic data to align with the base cases for years 2012-2017 is a trivial task. Modifying the dynamic data for cases where coal plants are retired to meet expected MATS/CSAPR compliance actions is also fairly straightforward. For these eleven cases, reaching a reasonable power flow solution to act as the initialization state for dynamic simulation is the most challenging problem. The 2016 coal retirement case, case 16b, cannot reach a stable power flow solution without pushing the swing bus to over 8,000 MW of generation—well outside the machine's upper limit. Since convergence in the power flow solution is not robust, pushing the limits of that solution even further in dynamic simulations produces problematic results that are discussed later

Table 2.3. Range of inertia and damping constant values by fuel type

Parameter	Retired Coal	Additional Gas
Inertia (H)	0.045–9.5	0.05–1.39
Damping (D)	1.39–10.64	1.39–12.66

With the next set of cases, accounting for new natural gas generation in place of retired coal plants requires significantly more care and several iterations of fine-tuning. It should be noted that the additional gas case for 2017, case 17c, like case 16b, initializes from a questionable power flow solution where the system is stable, but draws real power beyond the stated limit of the swing bus unit.

2.3 Dynamic Simulation Results

The frequency response of the system in each case is tested using several events. First, a large, dual reactor nuclear plant is dropped along the east coast. This location is both tightly tied to the interconnection and nearby several of the additional natural gas units in the third set of cases. Two representative sets of case results are discussed here. The results of this event across the full case suite are shown in Appendix A.

With the loss of 2,003 MW of generation, the frequency response across the base cases for 2012 to 2017 is fairly similar, as seen in Figure 2.2. As Figure 2.3 demonstrates, only small differences in damping are created by the retirement of larger coal plants across the system. As seen in Appendix A, this trend continues across all cases with the exceptions of case 16b and case 17c. These are the two cases with infeasible swing bus operation in the power flow and clear stressed system markers. The anomalous dynamic behavior in both cases (visible in Figure 2.4) is a result of their invalid initial conditions.

The second event was a three-phase bolted fault on a 500 kV bus in the southeast, cleared after 5 cycles (0.8333 seconds at 60 Hz). As shown in Figure 2.5 and Figure 2.6, the removal of coal-fired units does not significantly alter frequency response, but the addition of natural gas turbines does noticeably improve recovery. It should be noted that in the scope of the entire interconnection, much of the additional natural gas-based generation is located relatively close to the fault location. The 50% improvement in settling frequency makes a strong argument for the merits of gas turbines' fast ramping rates. This result occurs across all six years studied.

A third event is created to examine the result of redirecting line flows and rebalancing output generation. The loss of a 230 kV line in the southwestern part of the EI is simulated. In all cases, the plotted results overlap almost perfectly—even for the clear frequency spike that marks automatic dispatching as seen in Figure 2.7 and Figure 2.8. Since case 15a is the original

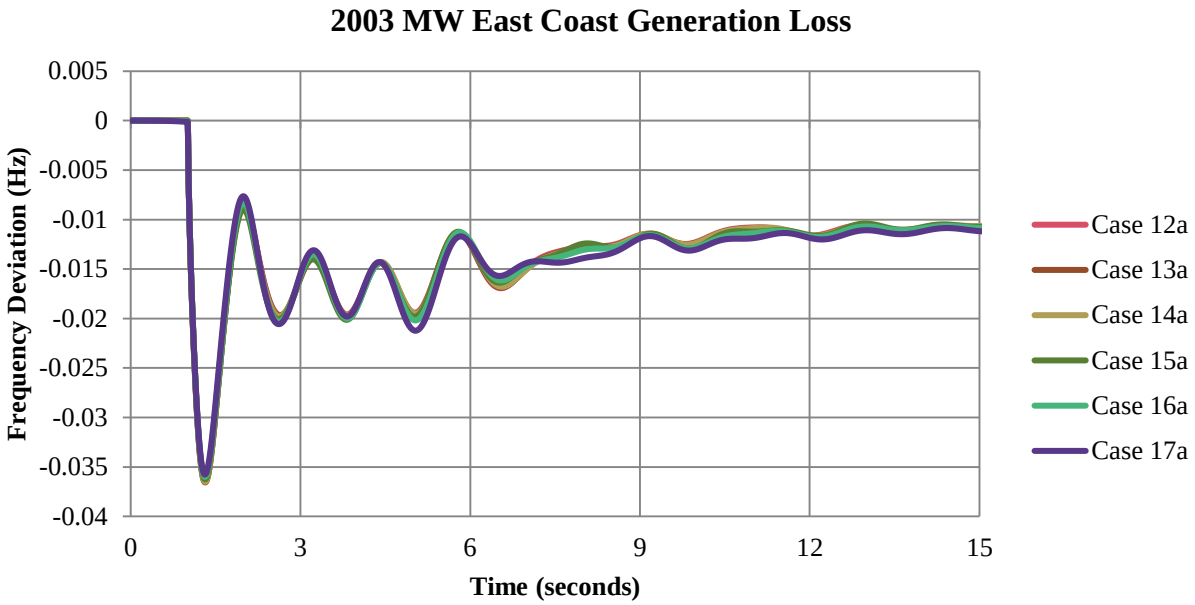

Figure 2.2. Base case frequency response for 2003 MW east coast generation loss

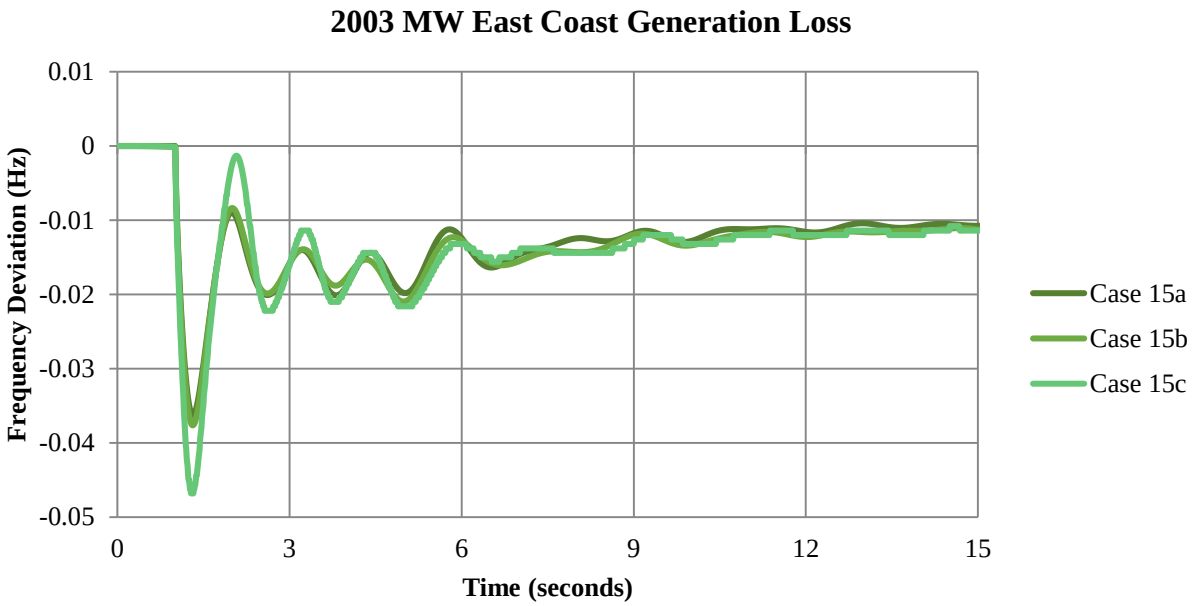

Figure 2.3. Year 2015 frequency response for 2003 MW east coast generation loss

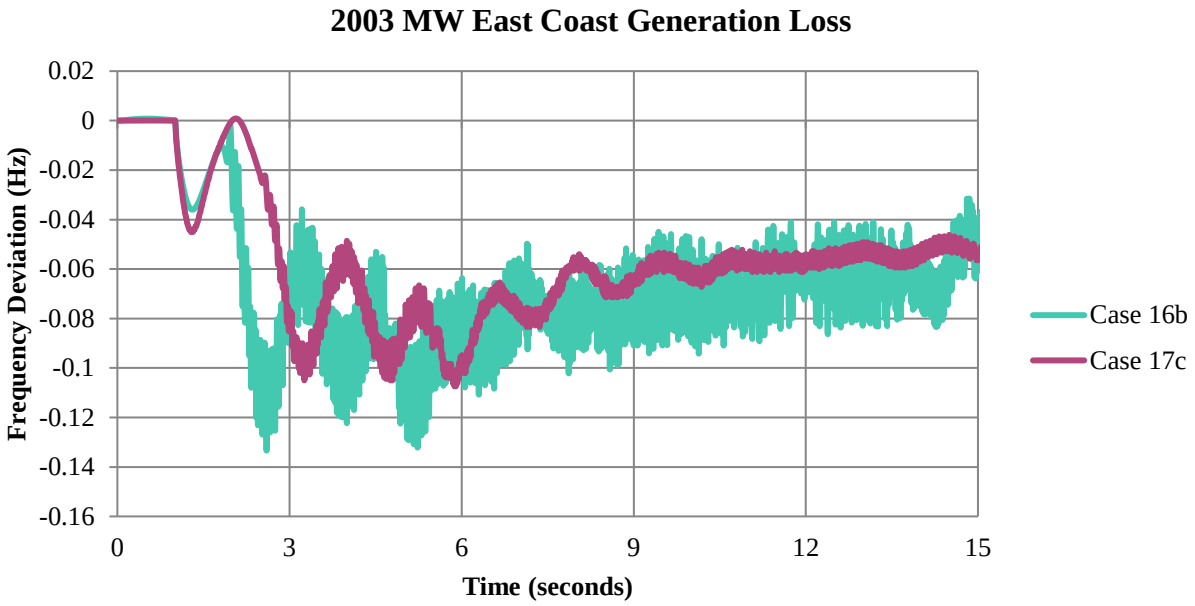

Figure 2.4. Anomalous behavior due to bad initial power flow solutions

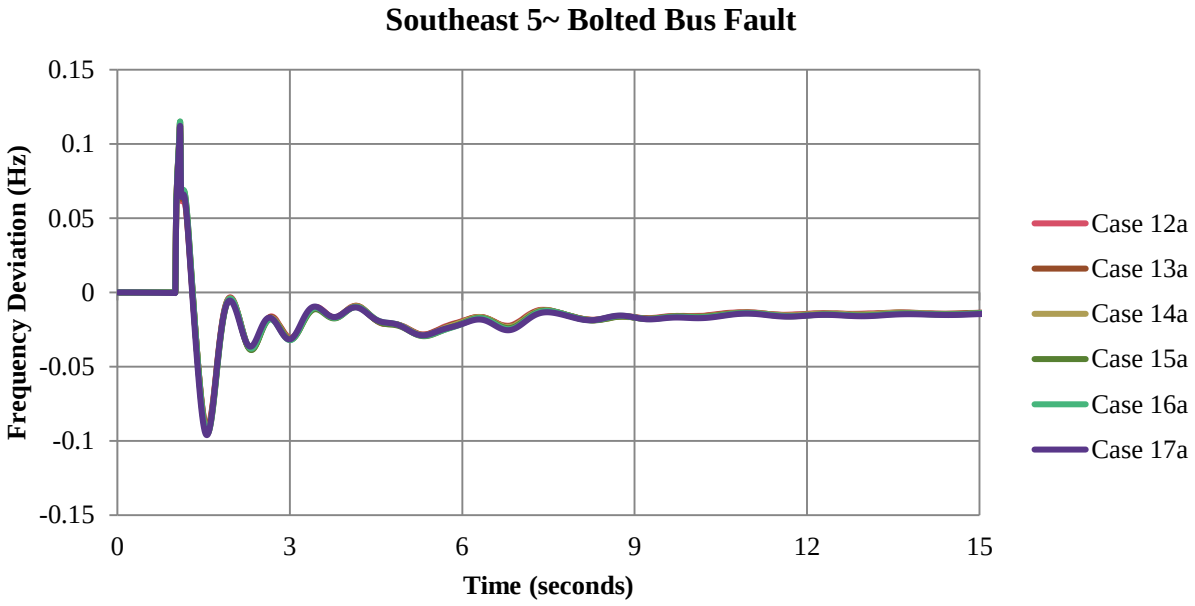

Figure 2.5. Base case frequency response for 5~ southeast bolted bus fault

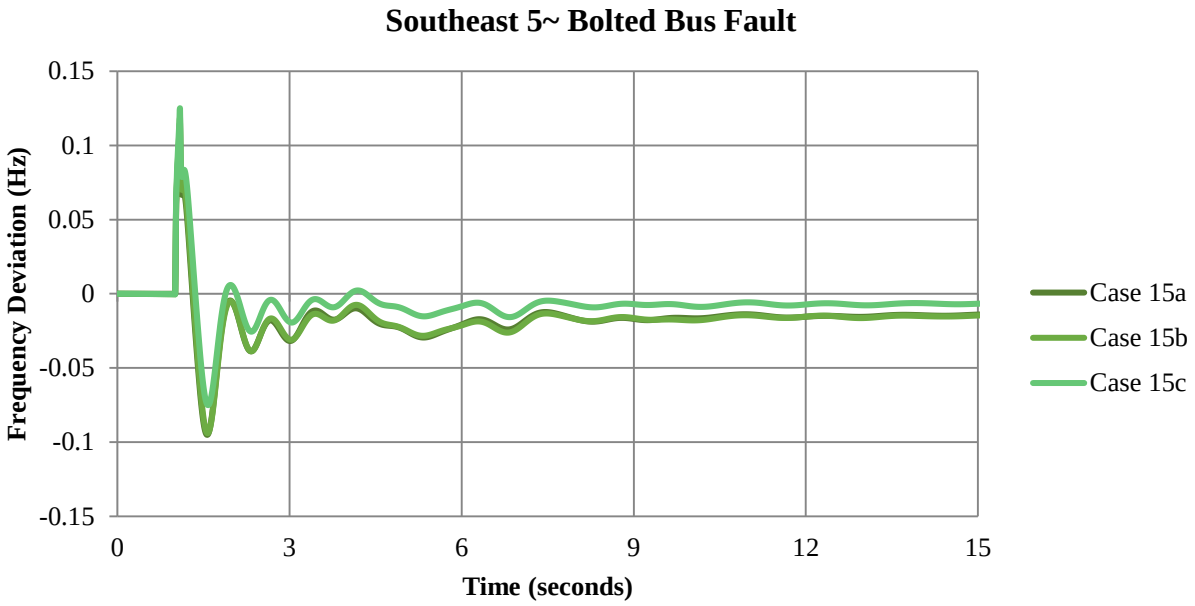

Figure 2.6. Year 2015 frequency response for 5~ southeast bolted bus fault

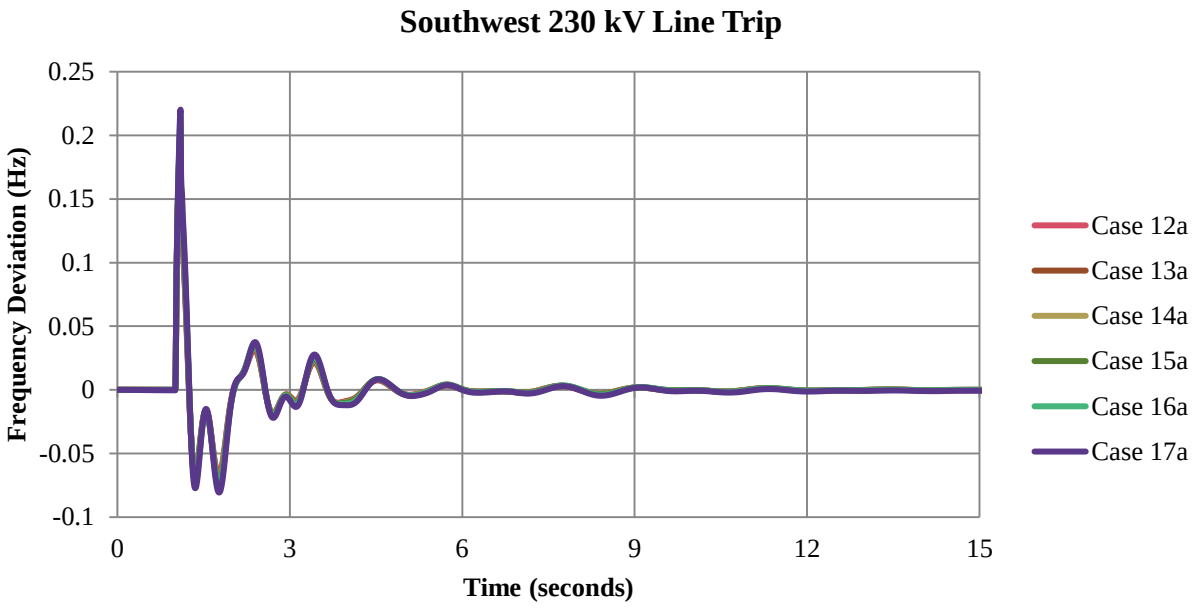

Figure 2.7. Base case frequency response for southwest 230 kV line trip

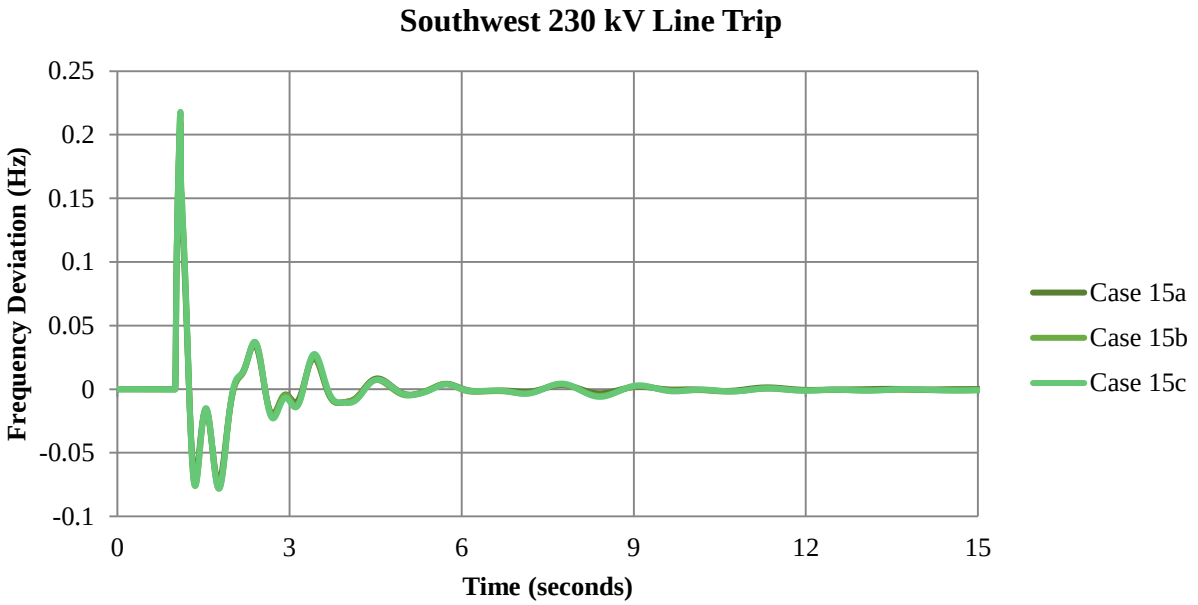

Figure 2.8. Year 2015 frequency response for southwest 230 kV line trip

MMWG model, this serves to prove the flexibility of the system and reasonableness of the dynamic control data added for this work.

Finally, a fourth event representing the loss of 800 MW of load in the southeast is studied. As expected in a loss-of-load situation, the final system frequency rises from the original value. As seen in Figure 2.9 and Figure 2.10, the number and timing of oscillations does not significantly differ, but the magnitude of each local maximum and minimum improves with each step further from the original case (case 15a), partially because more weight is given to generation from high inertia nuclear plants as coal-fired plants are removed.

As a rule, the different build-out cases in 2015 do not have the dramatically altered dynamic profiles for a large (2 GW generation loss) event that were originally predicted by opponents of EPA emissions regulation (whether MATS, CSAPR, or the Clean Air Act). In reality, simulation results across most cases appear very close to each year's base case dynamic frequency response. This intuitively makes sense for two reasons: First, both coal-fired and natural gas turbines are synchronous machines with similar control devices. The main two difference are output generation size—coal-fired plants are traditionally larger—and that gas turbines often do not have power system stabilizers (PSS) to damp forced oscillations; typically

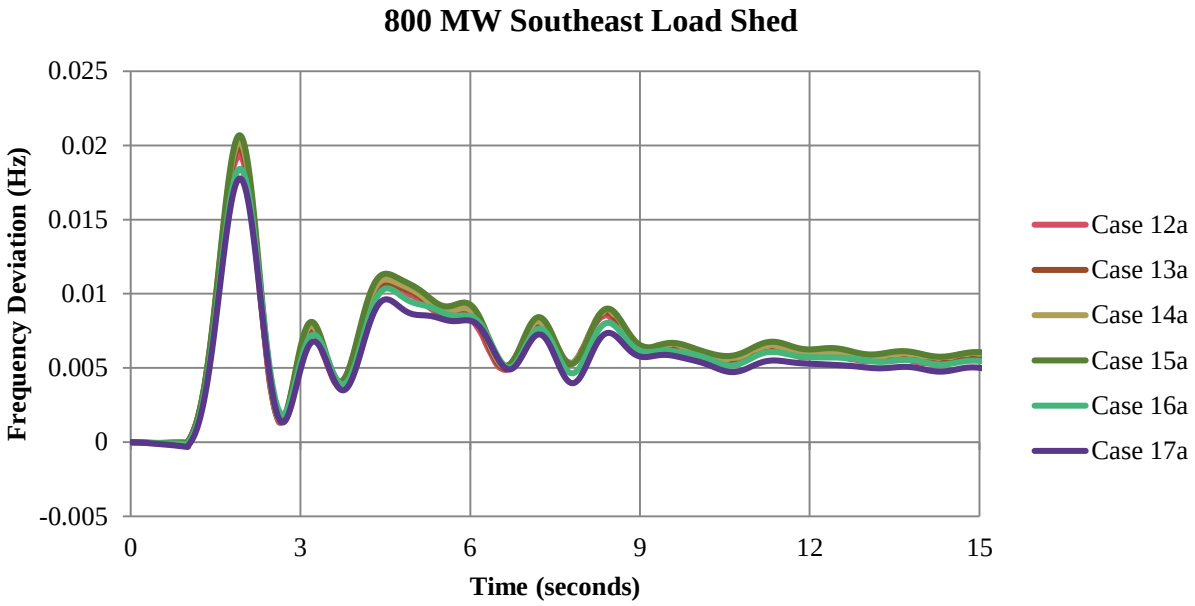

Figure 2.9. Base case frequency response for 800 MW southeast load shed

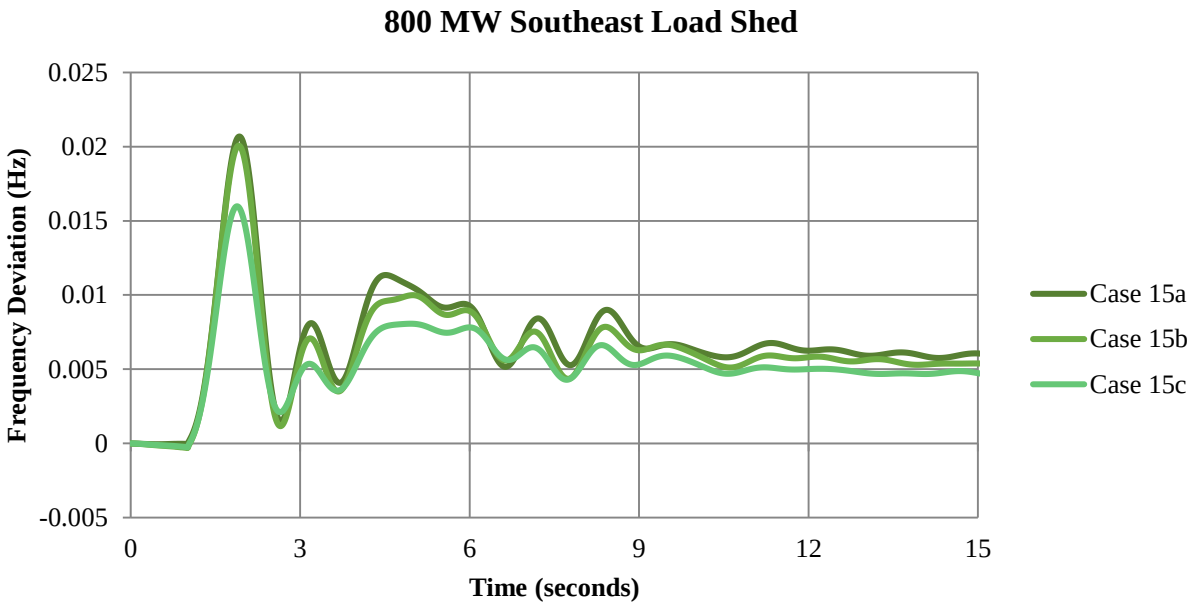

Figure 2.10. Year 2015 frequency response for 800 MW southeast load shed

their nimbler ramp rates allow them to forgo PSS control loops. Second, while a loss of 20.6 GW of coal-fired generation is no small event, these retirements only account for 3.5% of real power generation in the original MMWG model and there is enough capacity to continue meeting load even before the addition of natural gas units (which in cases 12c, 13c, and 14c more than make up for retired coal).

The impact to system stability mainly comes from the loss of system inertia—and while a decrease of 3.5% may have local impacts, it barely affects the system when taken as a whole. Looking further into EIA predictions [6], [18], renewables (e.g., wind turbines and photovoltaics), which are notorious for their low inertia constants, are expected to eventually replace both coal-fired and gas-fired plants. Thus, stiffer widespread loss of system inertia must also be addressed.

2.4 Conclusions

EPA regulations and economic factors are together driving the shift from coal-fired generators to natural gas turbines. This change in fuel type does represent a measurable loss of inertia in the Eastern Interconnection. Local dynamic response to generation losses is worse for locations nearby retired/new generation sites, but the overall impact will hardly destabilize the electric grid and the dynamic response to load losses actually improves with the addition of natural gas turbines. The total system inertia of the EI is great enough to absorb the overall effect of the small inertia loss of changing from one synchronous generation source to another. This result naturally leads to the question of how switching from traditional synchronous generation sources to nonsynchronous renewable generation (e.g., wind turbine and solar photovoltaic) sources will affect the dynamic response of the system. This topic is investigated in Chapter 3.

CHAPTER 3: THE RAMIFICATIONS OF LOSS OF INERTIA AND GENERATOR CONTROLS

Renewable generation is not merely a prediction or future goal. In 2012 alone, 13,131 MW of wind generation capacity was constructed in the United States, bringing the total installed capacity to over 60 GW [28]. In 2013, wind-powered generation supplied 4.5% of the nation's electricity [29]. While the business as usual case no longer aligns with the 2008 U.S. Department of Energy (DOE) goal of 20% by 2030, the total continues to grow and the agency still reports several potential scenarios where that goal is either met or surpassed [29], [30].

This sizable increase in the number of wind turbines on the grid must be met with careful study. At the unit level, voltage control, reactive power output, power quality requirements, and fault ride-through have already been considered in detail and commercial solutions are available to address known issues [31]-[35].

Potential problems for the grid as a whole must also be addressed. Traditional synchronous generators provide frequency control that defines the dynamic response of the EI through governor units, generator inertia, and exciter controls. Variable-speed wind turbines do not provide synchronizing torque and cannot damp oscillations as effectively as traditional generation because of the resulting lower inertia they have available to exert [36]-[38]. Most wind turbines are also not equipped with governor or exciter units [39]. As a result, a higher percentage of wind generation in the EI portfolio will lead to a decrease of system inertia and alter the interconnection's frequency response [36]-[42]. The effects of displacing generation from traditional coal-fired units with variable-speed wind turbines in the EI are not straightforward and are thus best determined by system simulation. Generic wind turbine models introduce numerical instability when simulated in large quantities though. This problem can be avoided by starting with traditional generation models, removing governor units, decreasing generator inertia, and disabling exciter controls to create pseudo-models that mimic some characteristics of large sets of equivalized wind turbines.

This study, originally published and discussed in [43], uses a 16,000 bus dynamic EI model created from an MMWG model as the base case scenario to investigate how large groups of wind turbines would collectively act to affect the EI dynamic frequency response.

3.1 EI Model and Study Scenarios

The 16,000 bus dynamic EI model was originally created from the full MMWG model designed to run in PSS®E. In total, the model contains 16,013 three-phase buses and 3,248 generators with a total generation capacity of just under 600 GW across the entire system. The original model does not include wind turbines.

3.1.1 Modifications to Generator Controls and Inertia Constants

Several generic wind turbine models exist for dynamic PSS®E simulation. For smaller models, these are perfectly acceptable, but substituting these generic models for traditional synchronous machines can create numerical instability during runs [43]. This effect compounds as the number of turbines grows. Due to this, the EI system is too large to employ generic models for high levels of wind penetration.

Alternatively, it is possible to simulate the effect of wind farms using traditional synchronous generator models. By lowering the inertia constants of existing machines, the frequency response can be simulated. While newer wind turbines may provide voltage support capabilities [44], disabling the associated exciter units is also required to mimic the voltage support capabilities of the generic wind turbine models.

A Python script was written to modify the base case and create two cases with this pseudo-wind generation model method applied throughout the system. Case 1 removes governor units from a percentage of generators in the system and decreases individual generators' inertia constants. Case 2 covers the loss of governor units and lower unit inertia like Case 1 while additionally disabling a percentage of exciter control participation in the model as well.

Four different percentages are used to scale down generator inertia constants and disable governor and exciter control units to simulate different levels of wind penetration in the system. This yields five scenarios within each of the two cases: the base case or 0% change (original model values; identical between case 1 and case 2), 20% scaling, 40% scaling, 60% scaling, and 80% scaling. These percentages are simultaneously used to scale generator inertia and disable control units throughout the model.

Disturbances are introduced to the system by tripping generation or load offline. The frequency response and voltage profile for each event are then captured. Descriptions of specific events and the associated simulation results are presented in the next section.

3.2 Simulation Results

The events presented in this section compare the simulated EI frequency response and voltage profile between case 1 and case 2 (with 0% change representing the base case) during four loss-of-generation events and a loss-of-load event. The last two loss-of-generation events occur at the same plant, but represent different power imbalances, removing topological considerations from the comparison.

3.2.1 Event 1: Loss of 2,550 MW Generator

During the first event a 2,550 MW loss-of-generation scenario is simulated. The plant is tripped off line one second into the simulation and the frequency and voltage responses are recorded for each case.

Figure 3.1 shows the case 1 frequency response profile. When 20% of inertia and governor control is lost, the change in frequency increases by about 50% from the base case. With 60% and 80% scaling, the response is further off, but the marginal difference between the two high percentage scenarios is small. Decreasing inertia constants of individual units does not significantly affect the settling frequency, but does cause the drop to occur faster with each successive value.

When exciters are also disabled in case 2, shown in Figure 3.2, the same effect can be seen on the rate of change as in case 1. The nadir also becomes noticeably more pronounced with each decrease in system inertia. The settling frequency, however, is significantly altered. Without voltage exciters, the system compensates for a lack of VARs by ramping generation output. This also increases real power output and causes the frequency to rise dramatically. With only a portion of the base case governor control, the system takes a long time to settle.

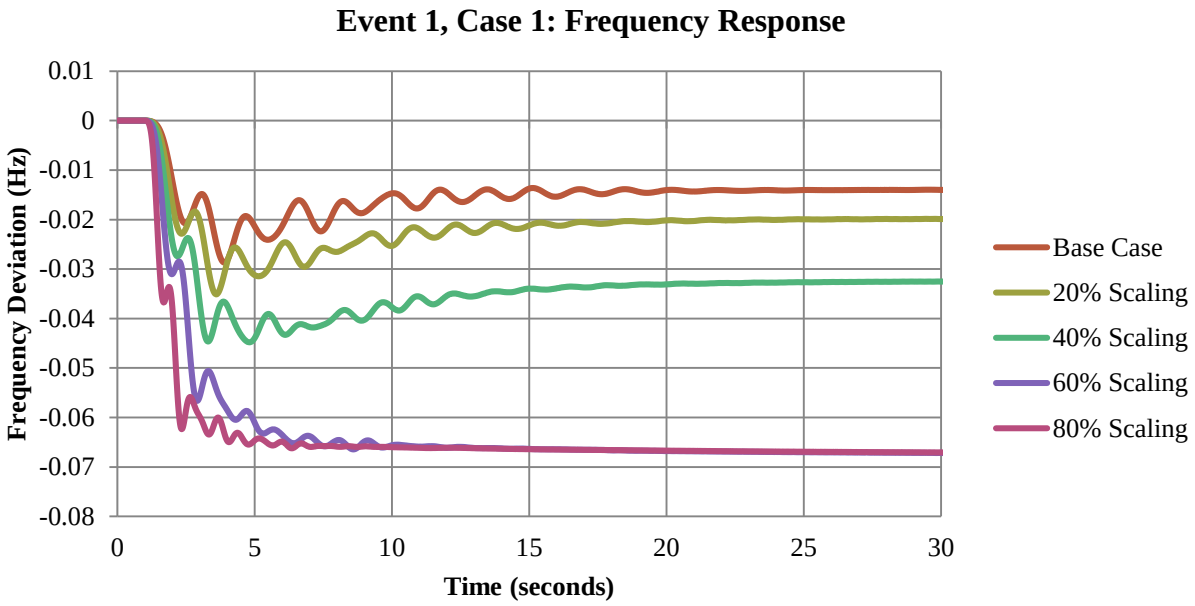

Figure 3.1. Event 1, Case 1: Frequency response

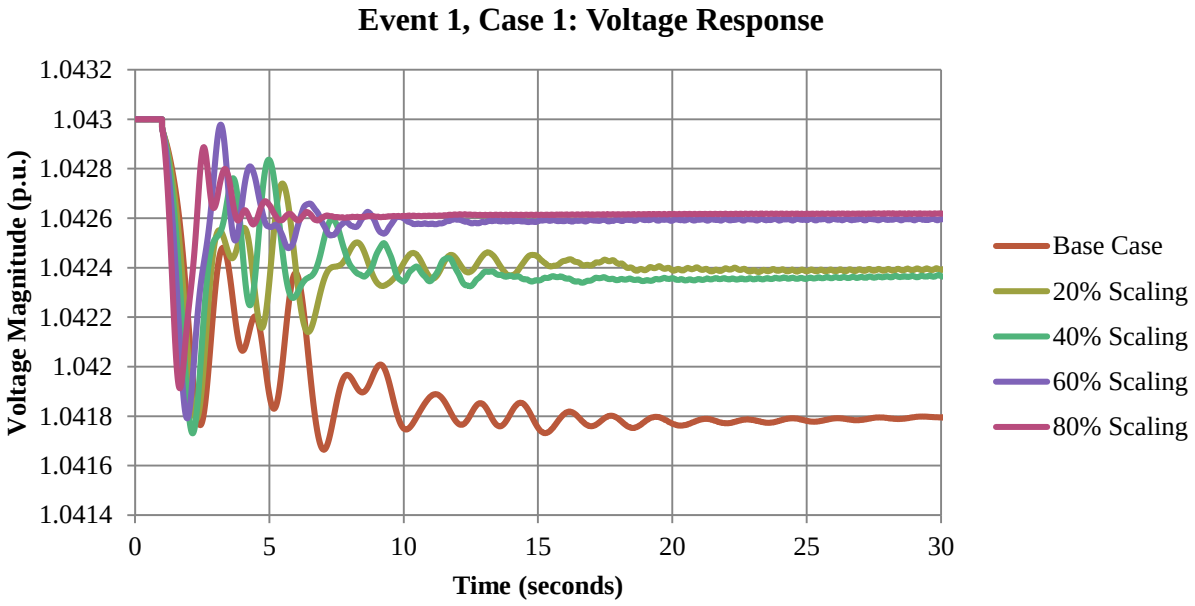

Figure 3.2. Event 1, Case 1: Voltage response

Figure 3.3 presents the voltage profile of case 1 under the same contingency. The first oscillation still drops noticeably lower as inertia is lost, but with less inertia to push against, control systems are more effective than in the base case. The settling voltage is improved by 50% to 75% under all case 1 scaling compared to the base case value.

This is not true for case 2. As seen in Figure 3.4, the loss of exciter systems causes the voltage to drop dramatically. As should be expected, losing governor units and exciter systems is clearly detrimental to the system's ability to keep voltage levels constant during events.

3.2.2 Event 2: Loss of 1,517 MW Generator

A second event is simulated for the loss of a 1,517 MW source. The same procedure is used as in the first event; the generator is dropped one second into the run and the frequency and voltage response are captured. Figure 3.5 through Figure 3.8 show the case 1 and case 2 frequency and voltage responses.

As with the first event, the settling frequency with 20% scaling is about 50% further from the nominal value than in the base case and further loss of governor control causes this gap to grow. The loss of governor units clearly has a measurable impact on the system that must be considered when planning for increased renewable penetration.

The voltage profile in case 1 is again improved from the base case since the lower system inertia allows exciter systems to act more effectively. There is a noticeable ripple in the final voltage levels. This probably results from a small level of numerical instability in the solver, but may indicate that the system is physically less stable at this point.

Removing the exciters in case 2 has a similar effect on the frequency and voltage response as in the previous event. Comparing the two shows that the 1,517 MW profile is actually worse since the 40% scaling response now groups with the 60% and 80% curves. The same instability seen in case 1 is present in all four scaled case 2 results, although to a lesser degree.

Under a full comparison, the results of the 1,517 MW loss-of-generation event are consistent with those of the 2,550 MW event.

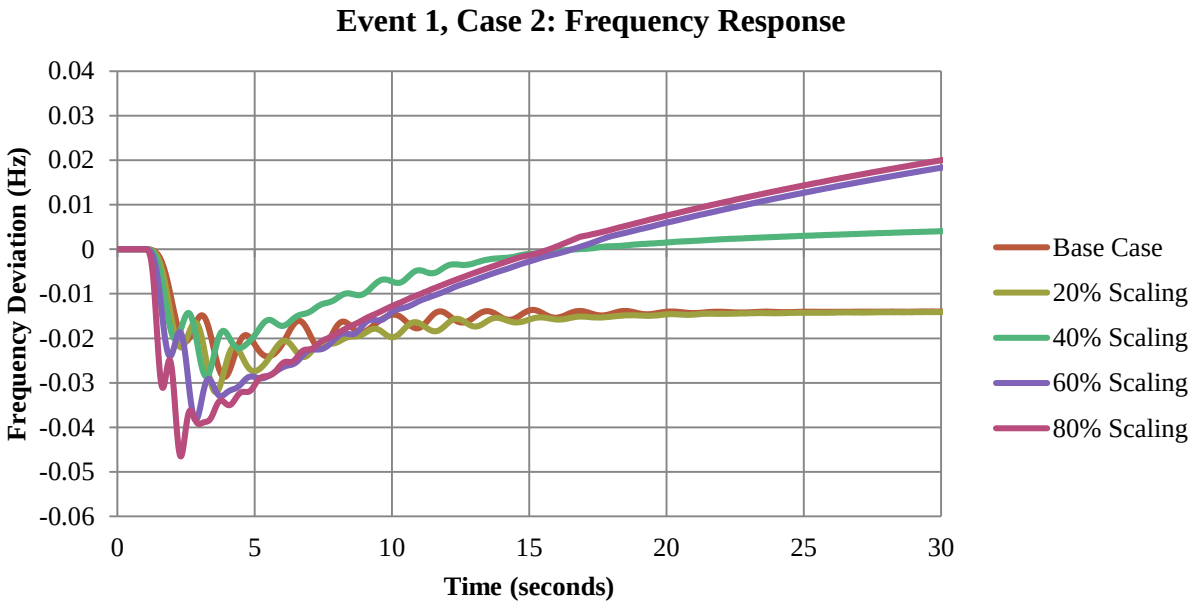

Figure 3.3. Event 1, Case 2: Frequency response

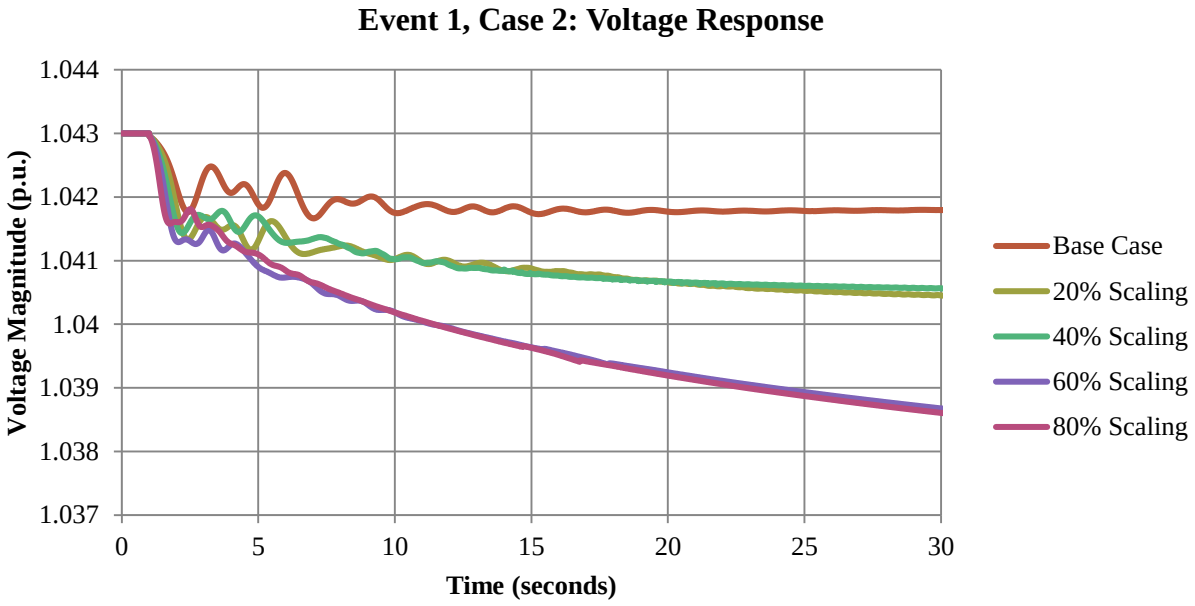

Figure 3.4. Event 1, Case 2: Voltage response

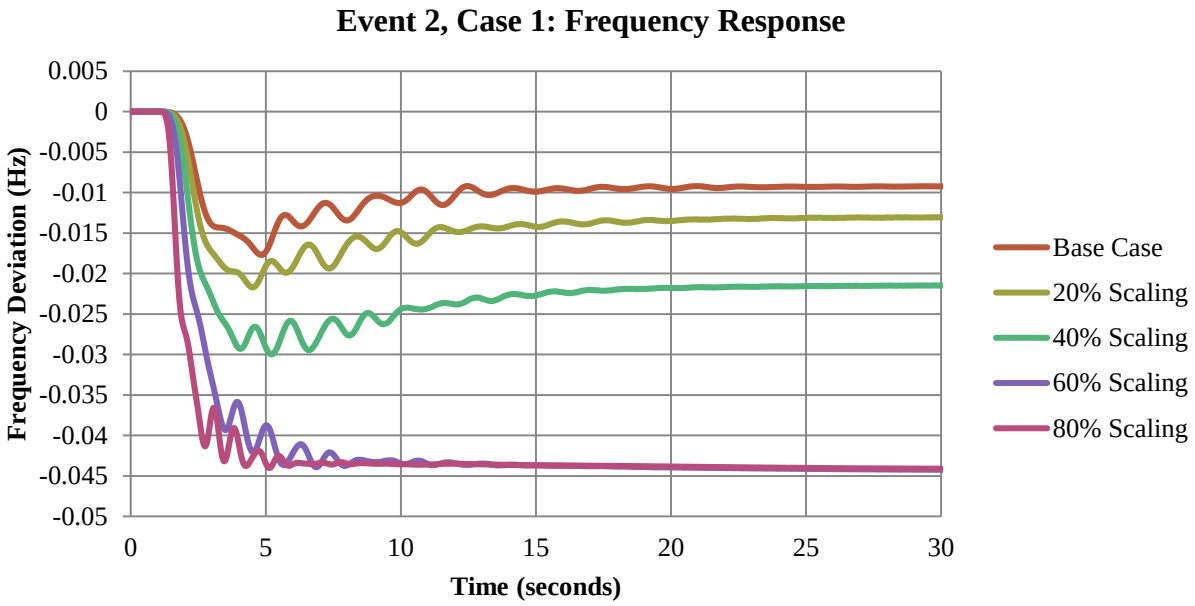

Figure 3.5. Event 2, Case 1: Frequency response

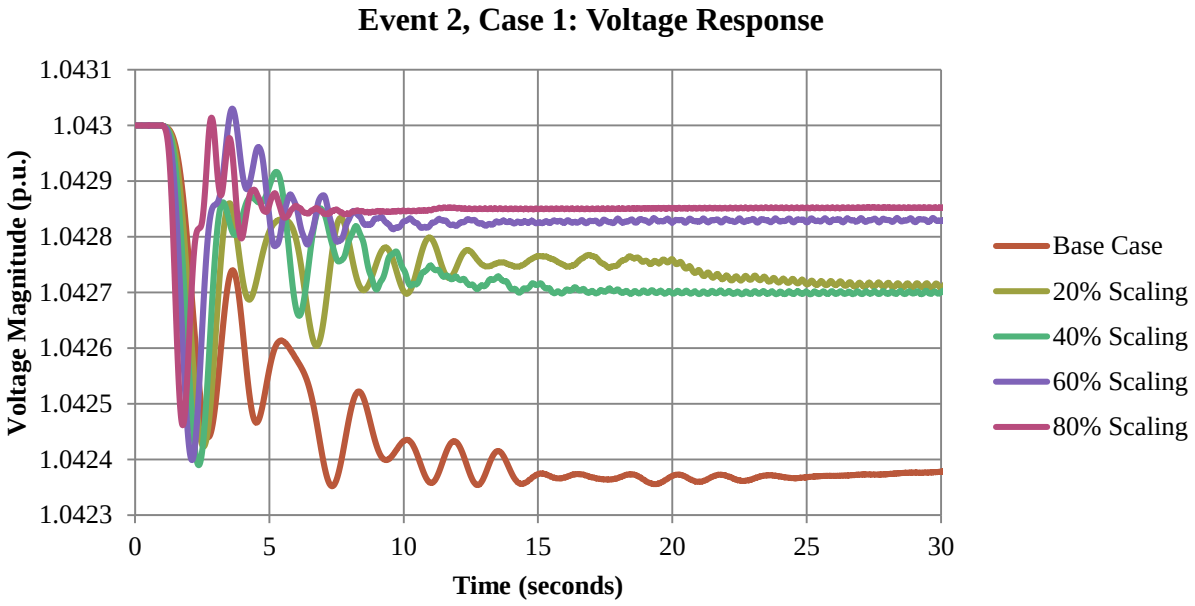

Figure 3.6. Event 2, Case 1: Voltage response

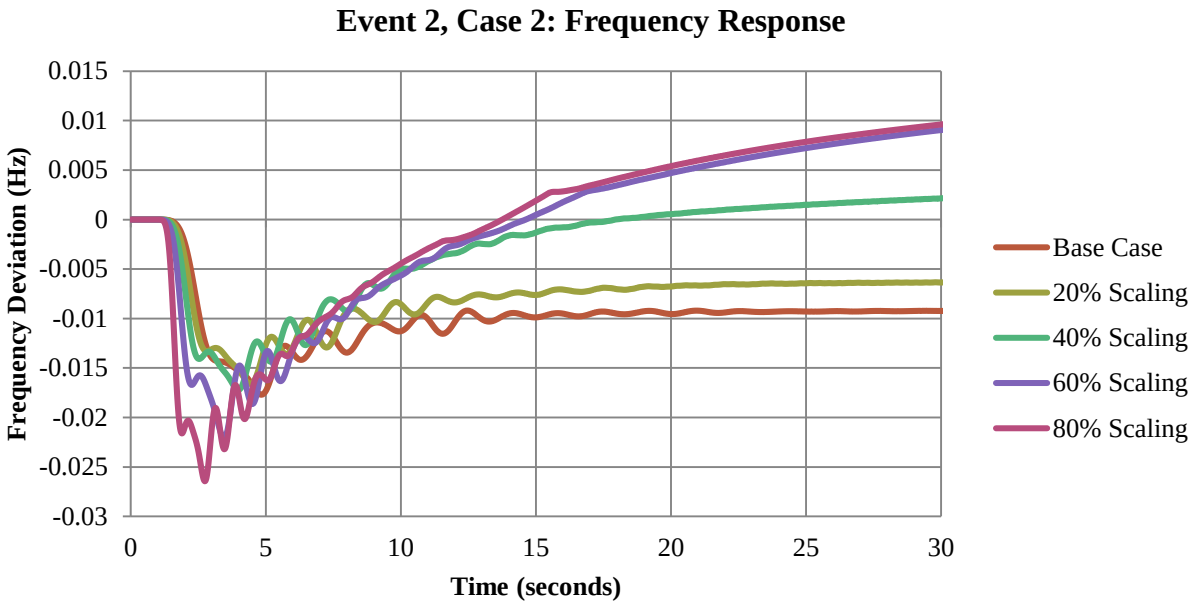

Figure 3.7. Event 2, Case 1: Frequency response

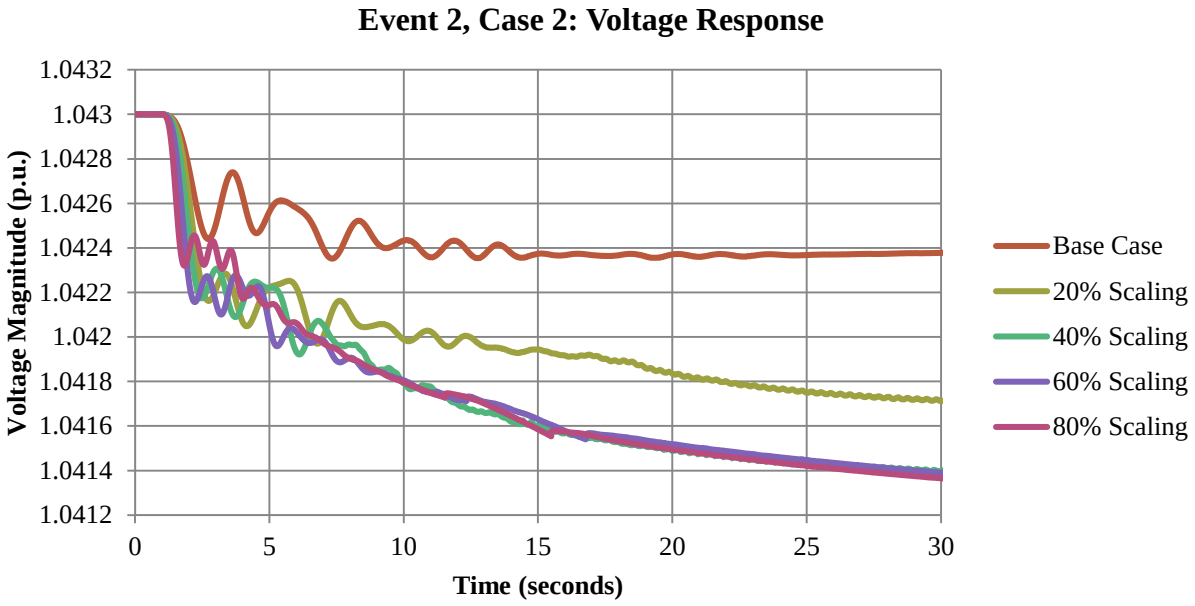

Figure 3.8. Event 2, Case 2: Voltage response

3.2.3 Event 3: Loss of 1,056 MW Load Site

A loss-of-load event designed so that a 1,056 MW load site was tripped offline one second into the run is proffered for comparison with event 2. The four case 2 scaling scenarios are contrasted with the base case frequency response and voltage profiles.

As seen in Figure 3.9, the system frequency stabilizes as fast as or faster than in the base case for all scaling scenarios. Losing 20% of the automated control systems throughout the EI leads to a significantly muted recovery after the event though. At 40%, the system barely moves back toward the nominal frequency and at 60%, the frequency plot simply diverges completely from the previous trends. As with event 2, each greater inertia scaling percentage causes the nadir to increase.

The oscillations in Figure 3.10 cover a wider range than in the previous event and the final steady state voltages are more varied. In the 20% and 40% scaling scenarios, enough exciter control exists in the system to take advantage of the lower system inertia and actually improve the voltage response. Both curves show the same ripple as event 2. As in the frequency plot, the 60% and 80% scaling scenarios settle at much higher values. These curves take longer to settle, but remain smooth. As this event again demonstrates, high penetrations of wind energy will require replacement control systems to take the place of traditional exciter controls.

3.2.4 Event 4: Comparison of Responses to Different Imbalance Magnitudes

The change in frequency experienced during an event is generally proportional to the imbalance of power in the system. This is observable in real measurements from the EI [45]. The scaling in case 1 should not negate this property. Two generators at the same station worth 2,000 MW each are employed to create frequency drops in both the base case and case 2 for events with identical topology but different magnitudes.

Figure 3.11 shows the frequency response of the base case for the loss of a single 2000 MW unit versus dropping both units for a total 4000 MW loss. The nadir is 15.5 mHz or 68.6% lower in the double contingency, while the settling frequency is 7.76 mHz or 70.6% lower.

These values are nearly identical to those in case 1, shown in Figure 3.12, where the nadir

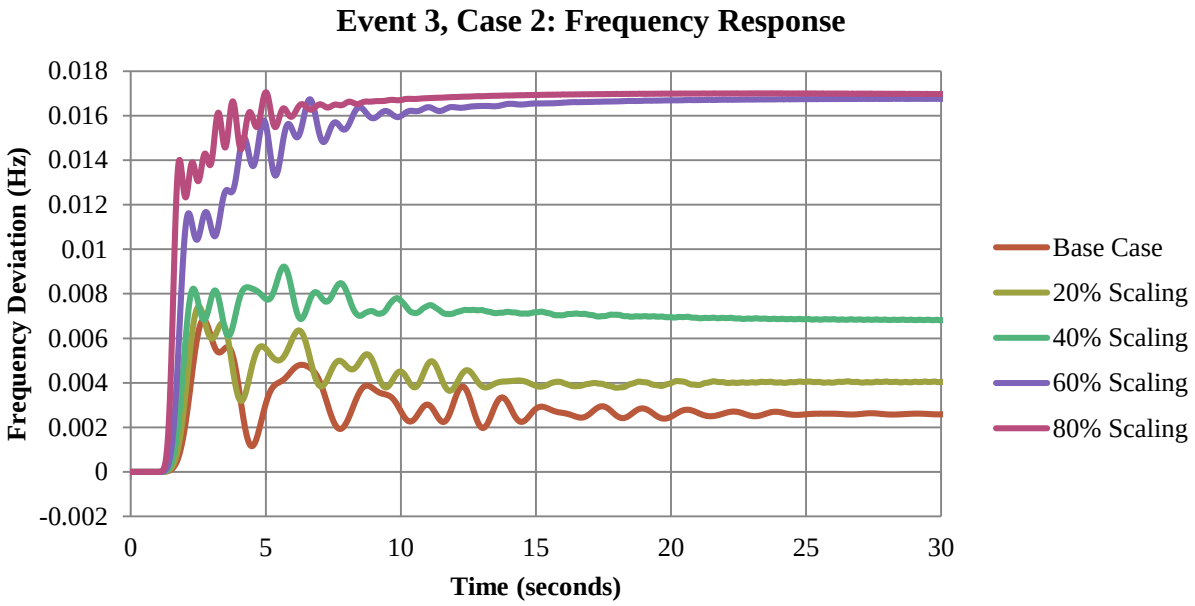

Figure 3.9. Event 3, Case 2: Frequency response

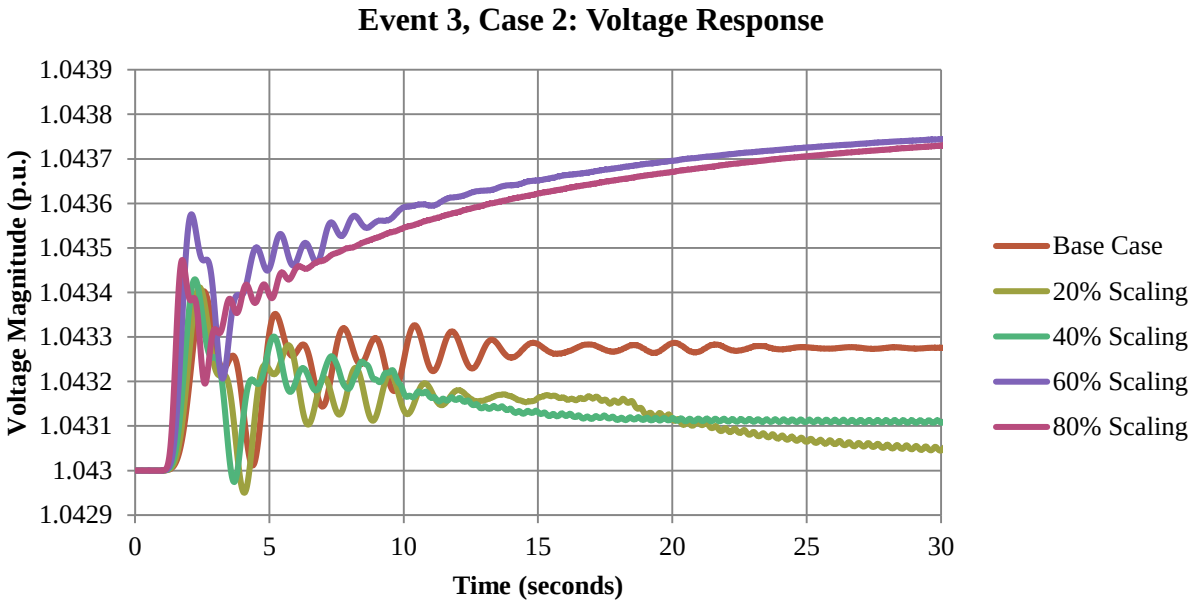

Figure 3.10. Event 3, Case 2: Voltage response

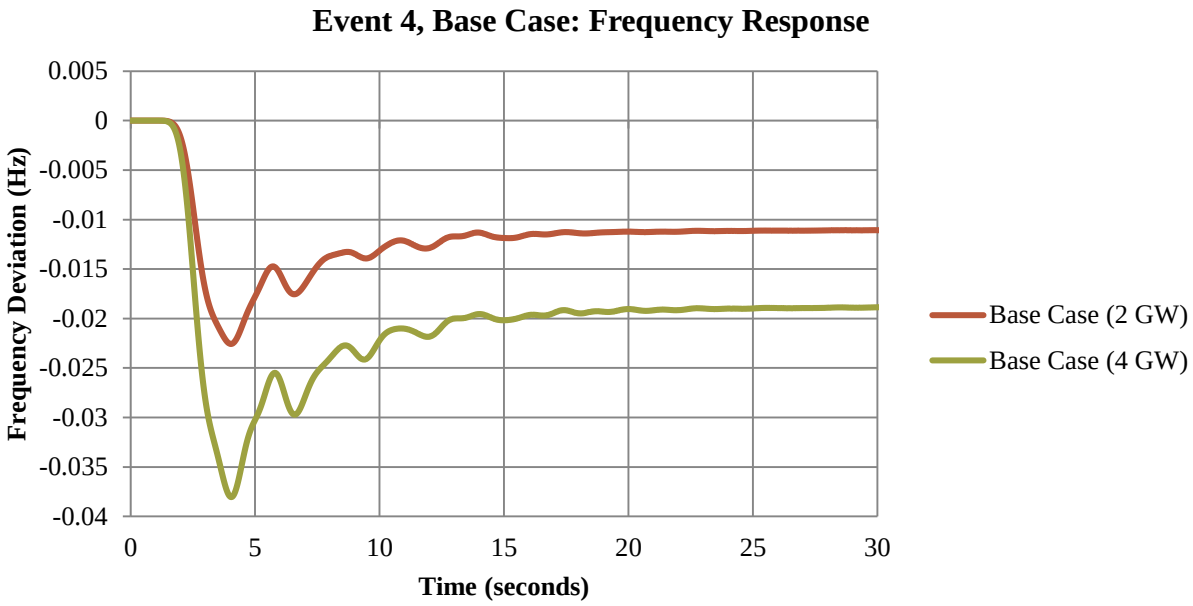

Figure 3.11. Event 4, Base Case: Proportional frequency response

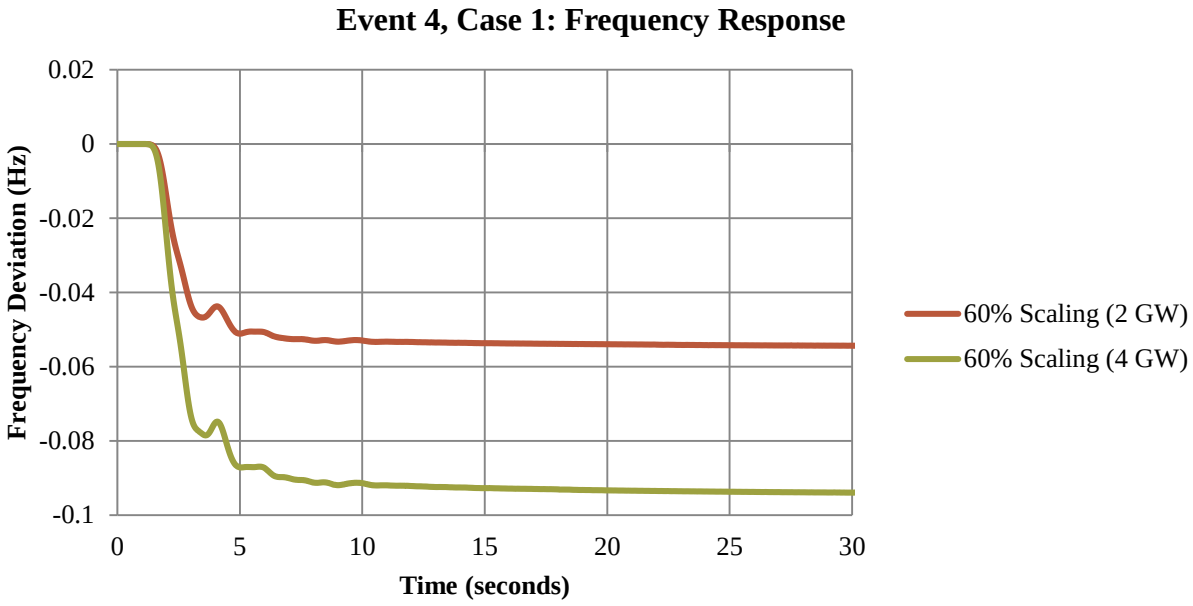

Figure 3.12. Event 4, Case 1: Proportional frequency response

and settling frequency (due to lack of recovery) is 39.71 mHz or 72.8% lower than the initial value.

These results, along with the analysis of the two generation trips, show that the imbalance of power and change in frequency remain proportional to each other, even as the relationship between those values changes with the inertia of the system. From this, the results of this study (plotted in full in Appendix B) may be scaled to find the frequency response of the EI for power imbalances of any size.

3.3 Conclusions and Recommendations

Increasing wind penetration in the EI lowers the average inertia of generator units and the percentage of generators with governor and exciter controls. This changes the characteristic dynamic frequency and voltage response of the system. The scenarios presented show that contingencies will create greater frequency oscillations and require further mitigating control to return post-event steady state conditions at nominal values quickly. With the current policy and technology implementation there is a strong limit to the support that wind turbines can provide. Governor and excitation systems, or their functional equivalents, must become commonly available and be enabled in commercial installations so that wind plants will be able to aid in frequency and voltage recovery.

CHAPTER 4: WIDE-AREA ANALYSIS OF GEOMAGNETICALLY INDUCED CURRENT HARMONICS

4.1 Background

While power system dynamics are usually studied in the context of a wide-area or interconnection view, investigations of many other phenomena are often limited to smaller models with reduced boundary conditions. One example of this is harmonic load flow for geomagnetically induced current (GIC) [46]-[49]. GIC is caused by geomagnetic disturbances (GMD), usually solar activity or other radiation from space. Electromagnetic (EM) waves associated with this "space weather" cause induced current in equipment with a physical ground connection. These elements act as sources or sinks and, compared to the 60 Hz nominal frequency of the grid, appear as quasi-direct current (DC) or zero-sequence sources.

Power transformers under significant DC effects can enter half-cycle saturation. In this state, transformers require significantly more reactive power to maintain their internal magnetic fields and will inject even and odd harmonics (waveforms oscillating at multiples of the 60 Hz system frequency) into the grid. Half-cycle saturation carries a high potential for equipment damage due to the formation of thermal hot spots.

By nature, GMD events effect a wide area—potentially covering all three U.S. interconnections simultaneously. Even though there is extensive research on GIC in isolated pieces of equipment, considering the interplay of GIC across an appropriately sized area is a novel approach. This chapter discusses work conducted on behalf of Dominion Virginia Power (DVP) to model harmonic load flow across their entire extra-high voltage (EHV) transmission system to capture full wide-area GIC impacts and determine what, if any, protection and control systems could be compromised.

4.2 Purpose and Procedure

Much of the existing literature on this topic was published in response to the Hydro Quebec blackout of 1989, which was caused by a GMD event with an aurora that could be seen as far south as Texas [49]. Each of these studies is concerned with the performance of a single transformer—none considers the effects of network-wide harmonics. They also focus heavily on

northern latitudes. As the association with aurora phenomena implies, GMD impact is stronger close to the magnetic poles and typically does not reach very far south into the continental United States. There are events, e.g., Virginia capacitor bank protection misoperations in 1989, 1993, and 2003 [50], which prove exceptions. Additionally, lower order harmonic injections, especially at the second harmonic (120 Hz), are known to travel significant electrical distances.

4.2.1 Demonstration of Harmonic Current Injection Interactions

The IEEE 14 bus system [51] is enlisted to demonstrate the construction and deconstruction of harmonic flows from multiple sources and the necessity of a wide-area approach. Figure 4.1 presents a diagram of the model in ETAP, an electrical power system analysis and operation software capable of both load flow solutions and harmonic analysis. ETAP default values are substituted for any parameters missing from the original IEEE data, e.g., generator zero-sequence impedance. Two transformers, the unit connecting bus 4 with bus 7 and the unit connecting bus 4 with bus 9, will act as harmonic current sources. Two cases are examined. In the first, the two sources are completely identical. In the second, the magnitude of the two sources remains identical, but the phase angle of the input harmonic currents through the transformer between bus 4 and bus 7 is shifted 180°. In both cases the harmonic sources on the magnetizing branch of the transformers inject current from the second to the ninth harmonic at 10.00%, 5.00%, 2.50%, 1.25%, 0.63%, 0.31%, 0.15%, and 0.08% of the fundamental value, respectively. The injection of wide-spectrum harmonics is more material to the problem at hand than the exact values used.

The base power flow solution angles at all three buses are similar (−10.3°, −13.4°, and −15.0°, respectively) so in the first case the harmonic currents join and create a high level of voltage THD throughout the system. In the second, the harmonic currents have disparate phase angles and thus deconstruct each other, leading to significantly lower voltage THD at every bus. Figure 4.2 provides a comparison of bus voltage THD from both cases.

This example clearly demonstrates the importance of capturing the interaction of harmonic sources over a wide area from a valid base case power flow solution. A realistic assessment of GMD impact will require the full model of an actual system with appropriate phase angle information.

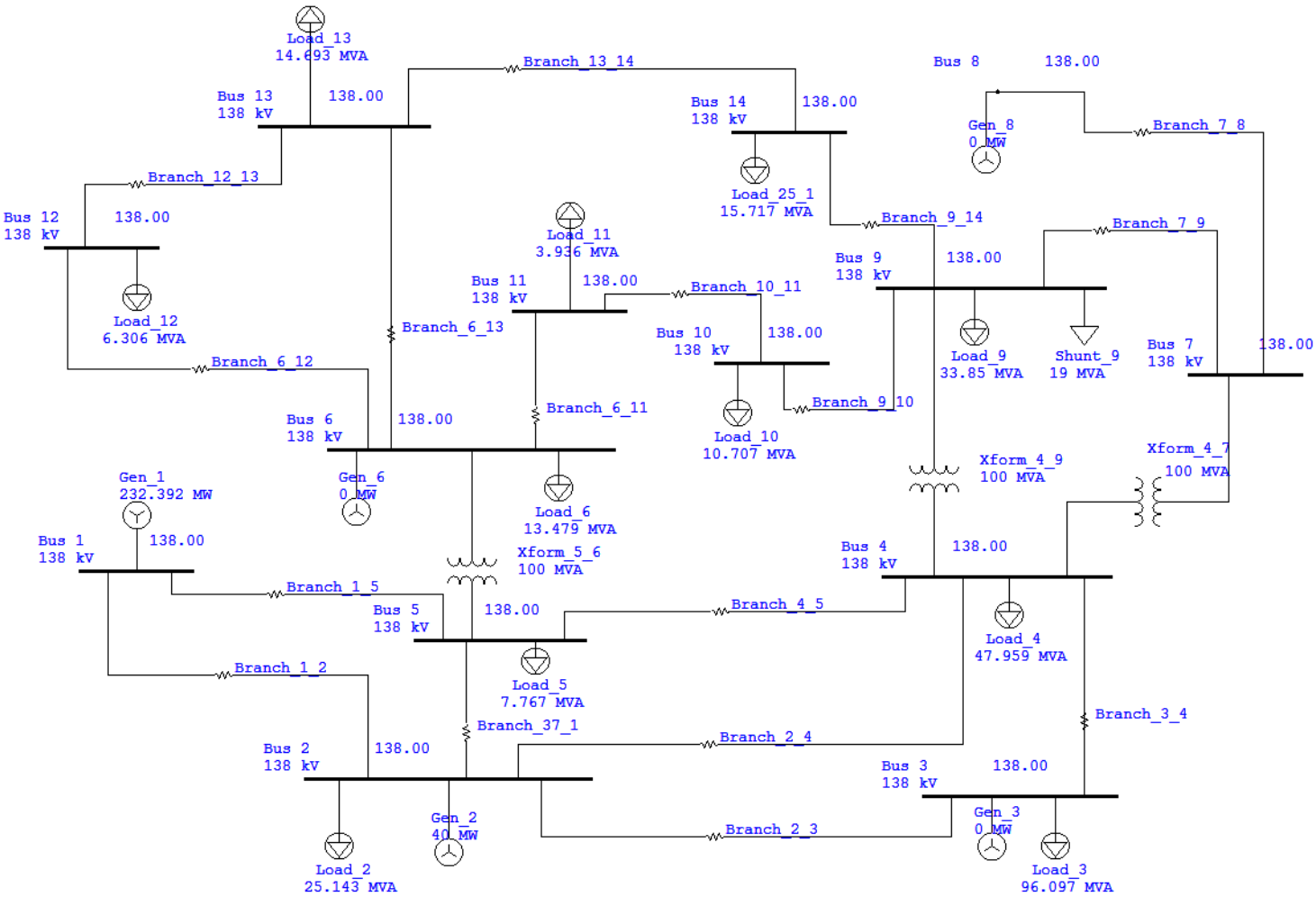

Figure 4.1. ETAP diagram of IEEE 14 bus system

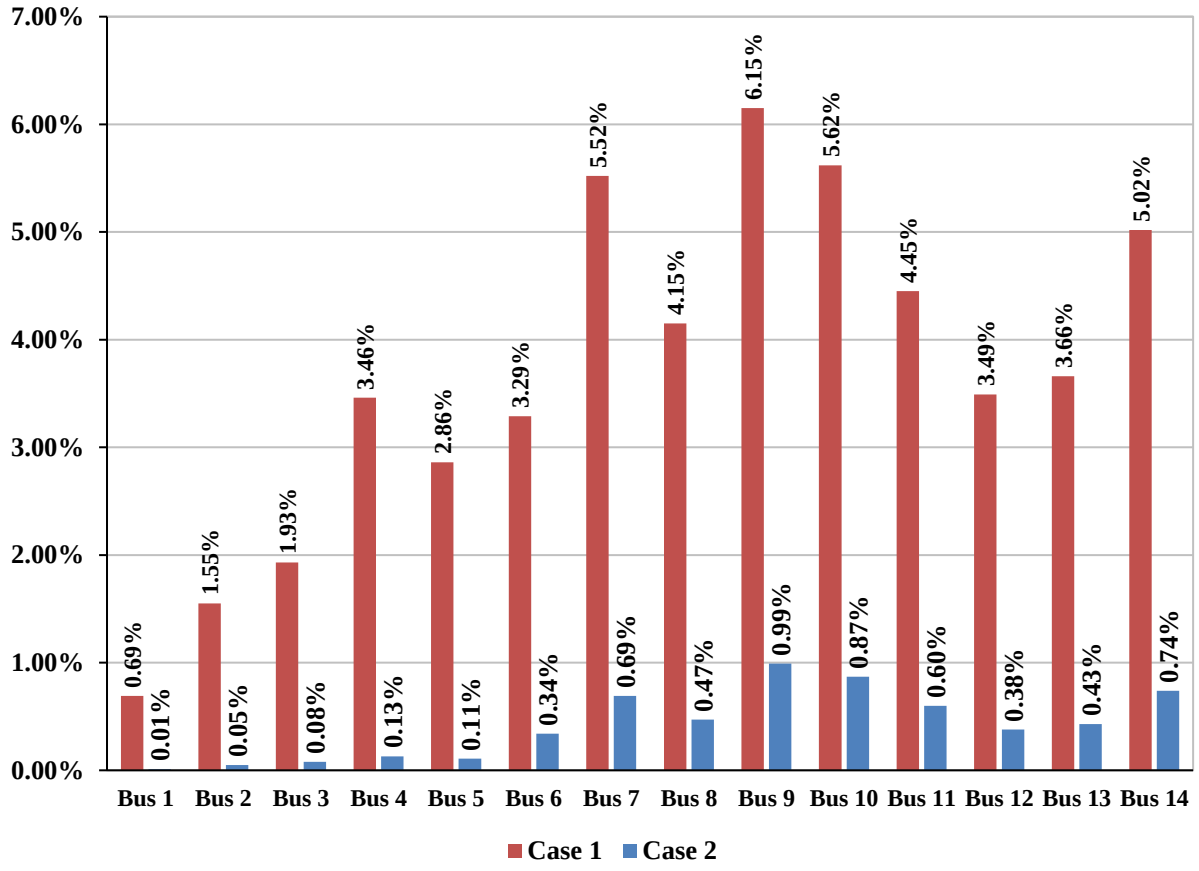

Figure 4.2. Bus voltage THD in the IEEE 14 bus system under case 1 and case 2

4.2.2 Modeling Methodology

In this project, Dominion's system is investigated though the use of a detailed 4,000 bus transmission model of the DVP grid that encompasses 24.6 GW of generation. The model is constructed specifically for this study in ETAP based on information taken from DVP's MMWG-based bus-branch planning model and the more detailed protection model that includes full station topology, transformer winding configurations, and sequence network information. Combining information from these sources into a single cohesive whole proved to be the most demanding task of this project. This is not surprising as the sources of input data were each originally compiled for unique purposes with different levels of required detail and topology.

Generators are modeled using their negative sequence impedances. Negative sequence impedance equivalents are created at least one bus away from the boundary of Dominion's system. Loads are modeled as impedances (see Model A in [52]) as opposed to more detailed induction motor models (e.g., Model C in [52]) to match ETAP functionality. Transmission lines, transformers, and reactors are modeled with frequency dependent impedances. Generator and load impedances are not frequency dependent in ETAP. Harmonic damping in the model is conservative as a result and somewhat understated compared to the actual system.

4.2.3 Harmonic Current Injections

In this model it is assumed that all three phases are balanced based on Dominion's mean unbalance (defined as $\frac{V_2}{V_1}$) of 0.3% and the project's focus on the bulk electric system as a whole. In a balanced system, harmonic orders are related to specific sequence components such that the 1st harmonic is positive sequence, the 2nd is negative sequence, and the 3rd is zero sequence. This pattern repeats ad infinitum. Symmetrical sequence network data must still be included in the model to capture the effects of all harmonics from GIC.

Individual GIC harmonic injections can be set for each transformer using the magnetizing branch; this is a reasonable practice given Dominion's transformer fleet. Doing so yields over 200 injection points on Dominion's EHV grid. Other sources of harmonics (e.g., loads) are considered negligible in comparison. Total harmonic distortion (THD) of all bus voltages and line currents in the system are then obtained after the harmonic load flow is solved. With multiple harmonic sources, analysis requires complex load flow instead of simple superposition so injection angles are as important as current magnitudes. Analysis is performed in the frequency domain (as opposed to using EMTP in the time domain) due to the scale of the model.

4.2.4 GMD Scenario

A 1-in-100 year GMD scenario is considered, leading to a geoelectric field magnitude of 2 V/km. Both west-east and north-south incidence orientations are investigated. GMD input for this study is as described in [53] and [54]. Dr. Bernabeu's calculations as originally presented in [55] are used for each transformer's GIC magnitude input. The harmonic spectrum of the first

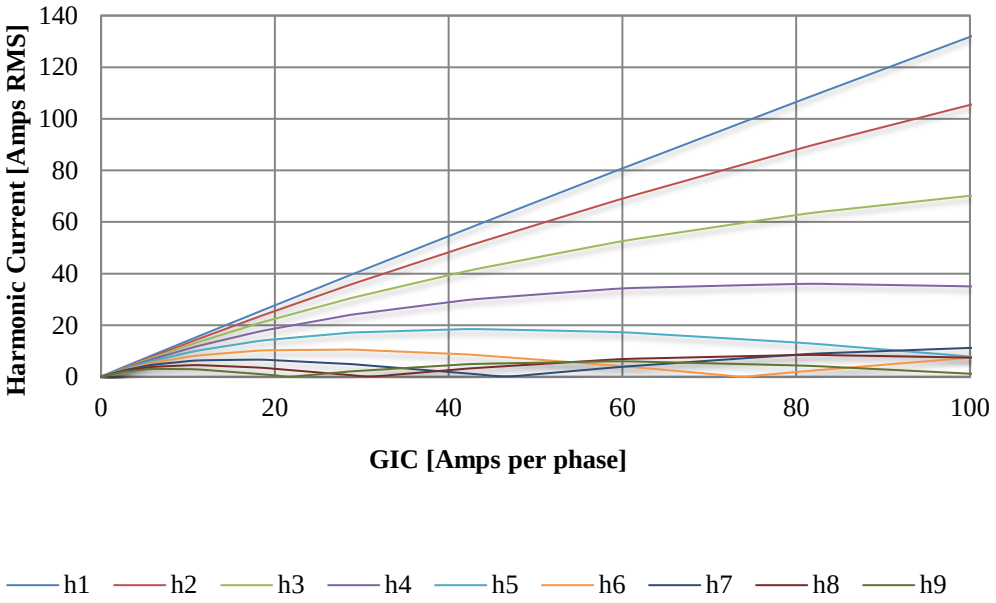

Figure 4.3. Harmonic current injection spectrum for particular transformer design [50]

nine harmonics for a specific transformer in Dominion's system is given in Figure 4.3 [50]. Phase angles for each injection align with the base load flow solution.

4.3 Simulation Results

Harmonic load flow analysis for a 1-in-100 year GMD scenario with a west-east field orientation yields voltage THD across buses of different voltage levels as shown in Figure 4.4 [50]. (Due to an NDA with DVP, more detailed output tables are not provided to preserve a level of location anonymity.) The central line marks the median. The lower box edge falls at the 25th percentile, the upper edge at the 75th percentile. Whiskers extend to 2.7 standard deviations and extreme values are marked in red.

As documented in [55], the largest GIC amplitudes are typically observed in substations located at the edges of the transmission system and substations with multiple transmission lines with abrupt changes in line orientation. Both statements hold true in this simulation. Figure 4.5 shows the amplitude of GIC experienced during the 1-in-100 year GMD event simulated with

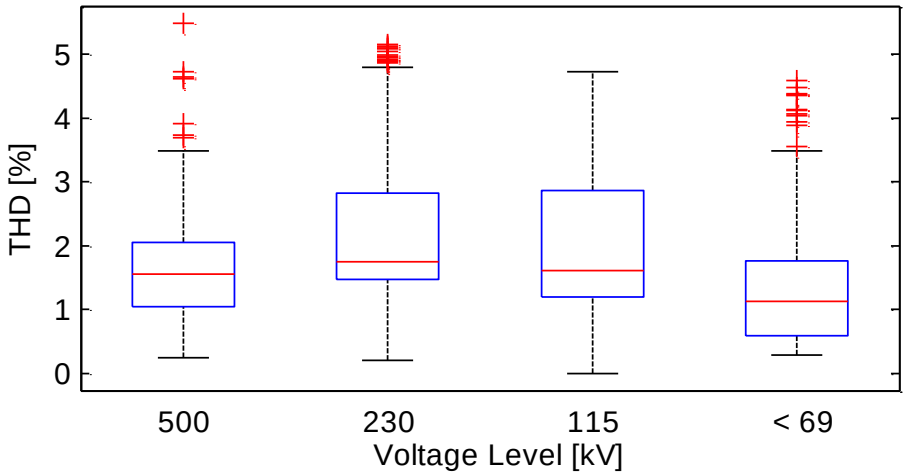

Figure 4.4. Voltage THD box plot across major bus voltage levels [50]

blue representing harmonic current sources and red representing sinks [50]. Bus voltage THD does not conform to this pattern though. Under half-cycle saturation, the magnetizing current injects currents with large magnitudes at a wide range of harmonic frequencies. Lower order frequencies have the ability to propagate over significant electrical distances before being damped. Higher order frequencies are damped sooner as frequency-dependent impedance values increase with the harmonic order. Figure 4.6 shows the resulting voltage THD resulting from this simulation [50]. Clearly, bus voltage THD does not exhibit the same clustering as GIC injections, but spreads throughout the system. Since THD is a result of complex harmonic load flow with the over 200 injection sites working to boost or counteract one another, it cannot be assumed, as is done previous literature, that a few elements with equivalized boundary points will accurately represent a full system simulation. The assumption that buses with the largest GIC injections will experience the greatest voltage THD is clearly incorrect.

The effects of the east-west orientation are generally worse in magnitude than the north-south orientation scenario. Even so, the latter yielded similar results for locations of both GIC injections and THD across DVP's system.

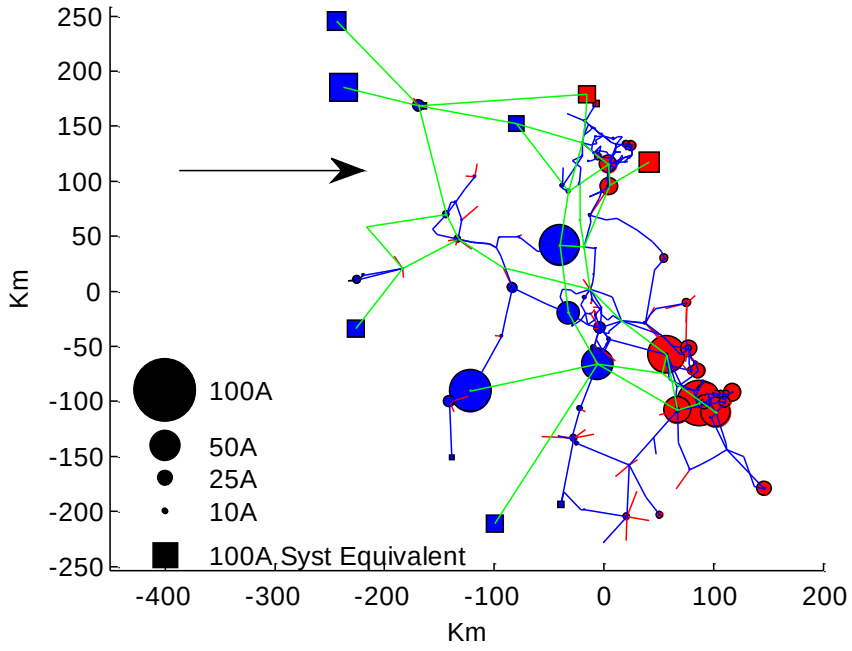

Figure 4.5. GIC injections for 1-in-100 year GMD event [50]

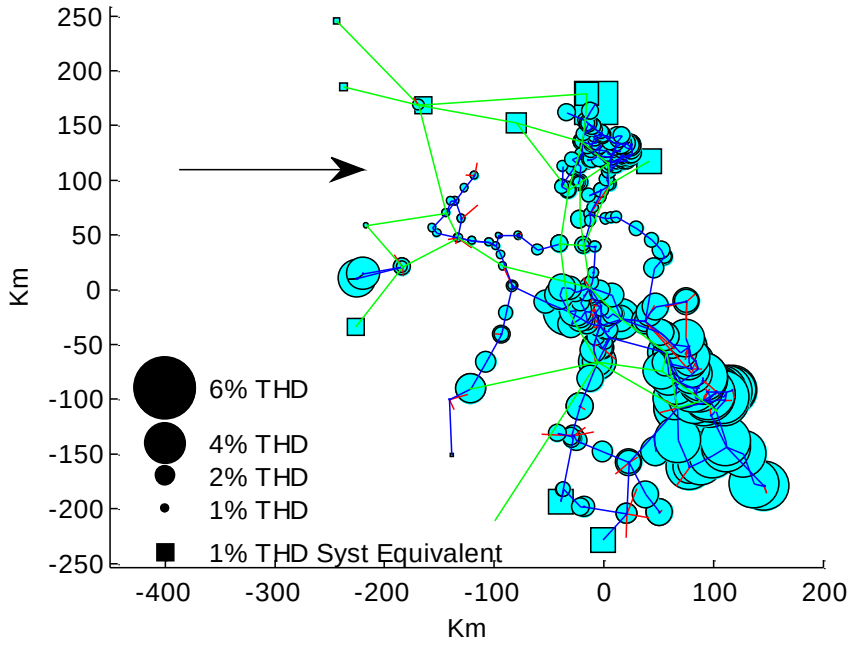

Figure 4.6. Bus voltage THD for 1-in-100 year GMD event [50]

4.3.1 Model Validation

The ideal validation for this study is an actual GMD event. Dominion has installed a system of monitoring devices known as GICnet across their grid in partnership with PJM Interconnection, LLC (PJM) and the National Aeronautics and Space Administration (NASA). GICnet measures power transformer neutral DC current, harmonic currents associated with transformer magnetizing currents, harmonic voltages and currents at capacitor banks, and transmission line DC currents. Unfortunately, (or fortunately, depending on the point of view,) while procedures are in place to validate harmonic load flow as data are acquired, DVP has not experienced a significant GMD event since GICnet was established.

Without an accurate set of real world measurements or previous accepted research on wide-area GIC flow, transformer in-rush currents are chosen as a stand-in for validation purposes. Figure 4.7 shows THD measurements during in-rush events at several 500 kV and 230 kV buses. These values are comparable to the simulation results presented in Figure 4.4.

These two events are not strictly congruent. First, GMD will affect a wide area and create multiple harmonic sources; in-rush current causes only a single harmonic source. Second, depending on the closing angle and remnant core flux, transformer energization can fully offset core flux. The GIC current required to reproduce this effect is far beyond any expected value. E.g., the largest distortion in Figure 4.7, 11.3% THD, comes from a magnetizing current of approximately 1,200 A_{DC}. The largest effective GIC predicted for a 1-in-100 year storm is 90 A per phase [55]. Still, given the similarity between the two phenomena [49], the comparison is useful to establish that the simulation results fall inside a reasonable range.

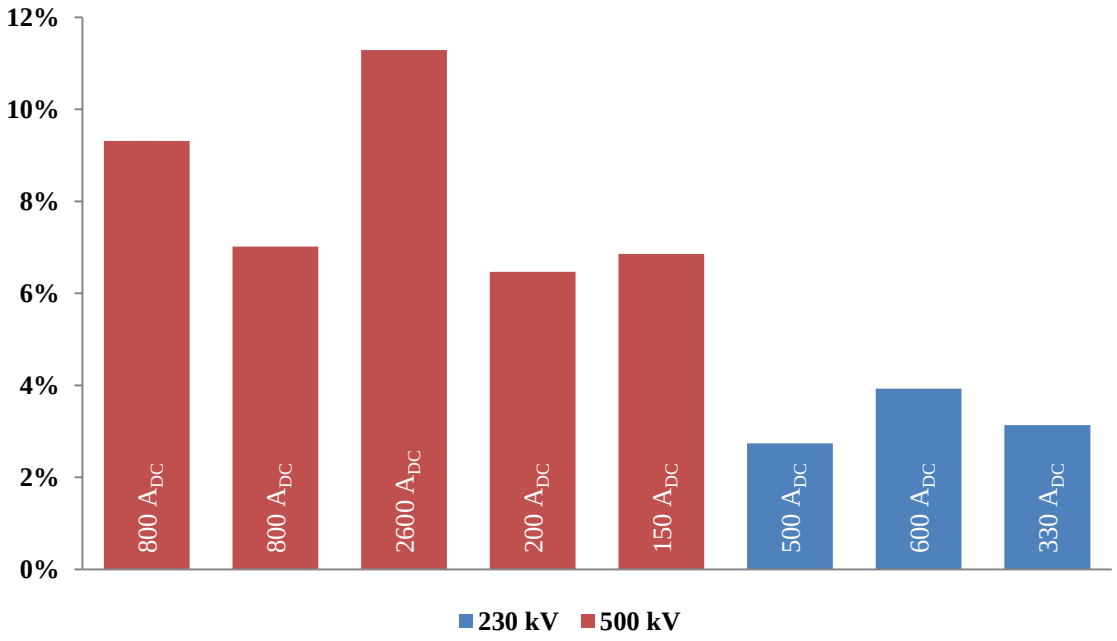

Figure 4.7. Voltage THD caused by monitored in-rush events

4.3.2 Sensitivity Analysis

Sensitivity analysis is performed by switching capacitor banks out of service in several sequential sets. No resonant frequencies are excited by these topology changes, leading to the conclusion that these harmonic load flow results are valid for a range of operating points. Comparing the baseline THD to that found during this sensitivity analysis, the maximum increase is 0.13% while the maximum decrease is -1.7%.

4.4 Conclusions

NERC requires all system planning coordinators to assess potential GMD impact in their system and determine additional thermal loading that transformers may be required to sustain [56]. Harmonic load flow and THD has only a minor impact on this thermal loading though, as GMD-related heating is strongly tied to physical parameters of each transformer's design and stray flux conditions. The results of the model created in this work are more useful in determining generator thermal loading and potential misoperation of protection and control

equipment across the system, both of which are highly sensitive to THD. Since several historic GMD events led to such misoperations, this function is equally important.

From this study, Dominion found that

- due to their current standard design of fuseless wye-grounded capacitor banks with voltage differential per phase primary protection and the high thermal capacity of all-film capacitors, the likelihood of capacitor bank failure under a 1-in-100 GMD scenario is extremely low;
- while possible, it is unlikely that STATCOM/SVC controllers would experience operation errors due to the maximum expected THD (6%); and that
- DVP-owned generators should not experience nuisance tripping due to negative sequence current and generally be free from thermal overheating unless significant negative sequence current exists before the GMD event.

DVP engineers did note that a discussion on the difference between negative sequence current due to faults vs. that due to loads may be in order with generator relay settings used across the utility industry reviewed as appropriate to avoid nuisance tripping. This analysis and Dominion's full discussion of the findings were originally documented in [56].

The clear overarching finding is that GMD must be studies at the wide-area level. Reduced boundary conditions designed to target only a few elements such as a single generator connected to a step-up transformer cannot capture the complex interplay of harmonic current injections or the resulting voltage THD across the grid. Limiting studies to these conditions produces shortsighted results and, at best, will lead to suboptimal policy decisions.

CHAPTER 5: EVALUATING THE IMPACT OF A HIGH ALTITUDE ELECTROMAGNETIC PULSE

In 2015, Oak Ridge National Laboratory (ORNL) along with CSRA Inc. and the University of Tennessee, Knoxville (UTK) began a survey on the available methodologies to assess high altitude electromagnetic pulse (HEMP) impacts to power grids. The final goal of this project was to summarize accepted methodologies, critique critical findings as necessary, and suggest possible research directions. Differences in methodologies were found to lead to discrepancies in key results and the ultimate determination on whether a single high altitude EMP could lead to the collapse of the U.S. power grid. This author performed the HEMP E1 power system impact simulations that are discussed in this chapter.

5.1 Background

Starfish Prime, a high-altitude nuclear test conducted by the U.S. government above Johnston Atoll on July 8, 1962, was the initial trigger event leading to research on HEMP impacts in electrical system, both military and civilian. The detonation created a peak electric field of 5.6 kV/m [57] over Honolulu on the island of Oahu, 800 miles from the test site. This peak amplitude is relatively small compared to targeted HEMP scenarios, but it is still enough when paired with the orientation of street light wiring on the island to cause a coherent buildup of surges that resulted in the failure of 30 strings of streetlights. Over time, the Department of Defense (DoD) and Bell Labs developed unclassified models that represent what they consider the most damaging features of HEMP without fully describing the phenomena [58]. These models are referred to as bounding waveforms since they contain only the most basic information about magnitude and timescale. While these models are useful for basic research, hardening the electric grid against attacks requires more detailed information. With the recent push for development on that front by the Federal Energy Regulatory Commission (FERC) [59]-[61], it is necessary to demonstrate the need for—and specific requirements of—more complete models.

5.1.1 HEMP Components

HEMP can be divided into three transient components: early-time E1, intermediate-time E2, and late-time E3 [59], [62]. In addition to acting on different timescales, the magnitude of each component is significantly distinct. Figure 5.1 presents an illustrative plot of a HEMP signal divided into constituent components.

E1 electric field magnitude caused by the initial gamma burst is strong, but usually decays within half a microsecond. As such, E1 is a steep-front, short-duration (SFSD) pulse waveform with a duration measured in nanoseconds. It is possible for a large majority of the 48 contiguous states to experience E1 with an amplitude in the order of tens of kilovolts per meter from a single HEMP burst. Due to the strength of the field, E1 is the component traditionally studied when assessing nuclear EMP effects [59].

After the SFSD pulse passes, the intermediate-time E2 component caused by scattered—or "delayed"—gamma pulses is observed. The peak E2 electric field magnitude is notably

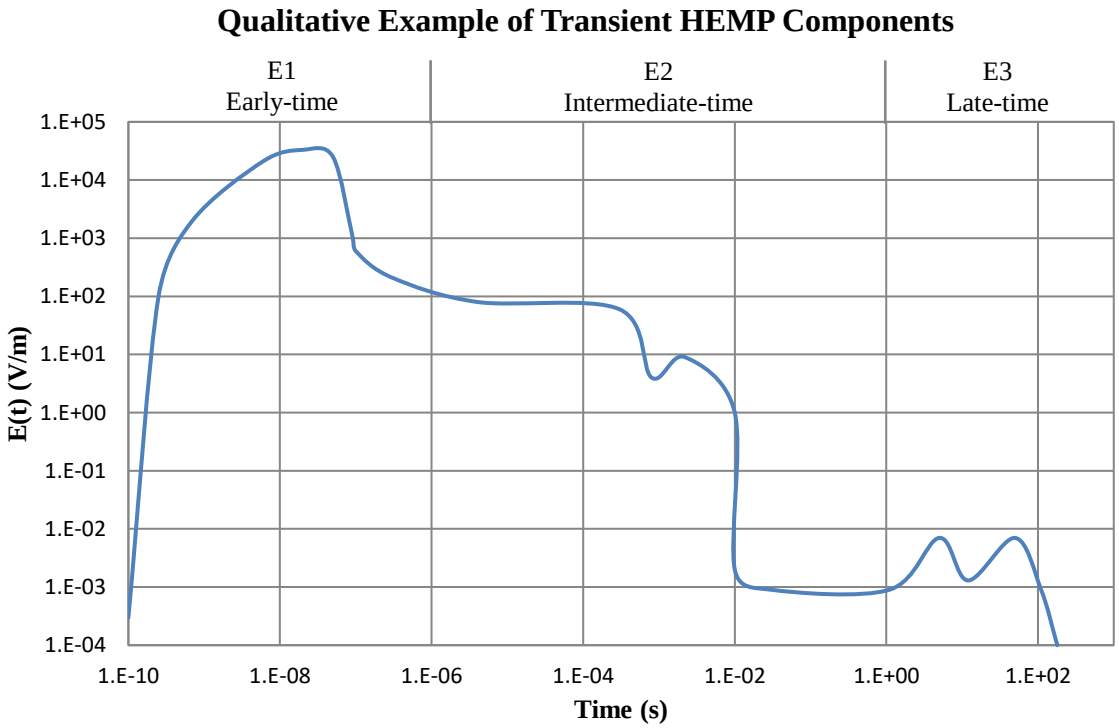

Figure 5.1. Illustrative qualitative example of transient HEMP components on a log-log graph

weaker at several hundred volts per meter and exhibits less time variance. The E2 component typically lasts several hundred microseconds.

The final late-time E3 component, also known as magnetohydrodynamic (MHD) EMP, follows. E3 resembles a short, intense natural geomagnetic disturbance (GMD) since it results from geomagnetic perturbations caused by the initial HEMP event. The peak E3 electric field is usually on the order of tens of volts per kilometer and the component duration is measured in hundreds of seconds.

5.1.2 HEMP Models

Determining the potential effects of HEMP on a power grid requires detailed specifications of the E1, E2, and E3 electric field components. As shown in Chapter 4, system reduction can significantly influence simulation results. In contrast, the original HEMP model developed by Bell Labs contains only generic worst-case E1 components [62]. In order to obscure or remove waveform detail to prevent users from ascertaining confidential data regarding the delivery system, spatial considerations outside the altitude of the detonation are ignored and only ground-zero is considered when calculating the waveform envelope.

The Compton High Altitude Pulse (CHAP), a more advanced HEMP model, was designed at Los Alamos National Laboratory (LANL) and validated at ORNL to incorporate the other two time components as well as crescent- and circle-shaped impact zones [62], [63]. Maps of these zones are typically referred to as “smile diagrams” due to the visual aesthetic of seeing crescent outlines inside larger circles. CHAP offers a more complete picture, but obtaining useful component waveforms requires a thorough understanding of the gamma pulse input parameters and the ability to form reasonable assumptions surrounding them. This is a barrier to many researchers in the field and even more so for electric utilities attempting to understand potential HEMP affects.

In an attempt to address this issue, Metatech further developed CHAP to provide more complete E1 data [59]. This Metatech model is currently the one used by ORNL and FERC for electric grid oriented HEMP studies [59]-[61]. As a tradeoff to keep the model unclassified, almost all input values from the original CHAP code are hidden in the Metatech implementation.

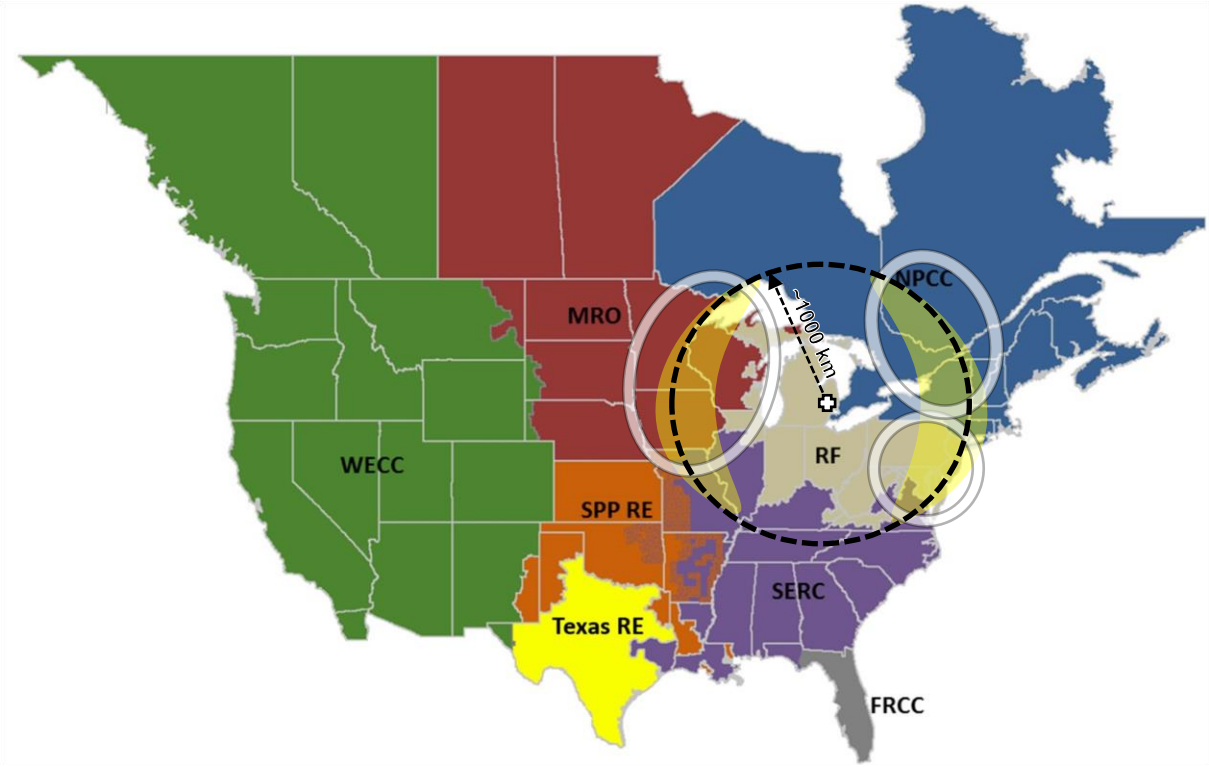

Figure 5.2. Map of HEMP detonation and impact locations

5.2 HEMP E1 Impact Study

This study is designed to simulate loss and recovery of load after a HEMP detonation over the northern states using information available from unclassified models. The assumptions used are consistent with assuming only E1; E3 may cause a wider area loss of load due to total harmonic distortion. Specifically, it is postulated that a HEMP detonation will occur as shown in Figure 5.2 with impacted load areas in the Midwest Reliability Organization (MRO), ReliabilityFirst (RF), and Northeast Power Coordinating Council (NPCC) reliability council regions.

5.2.1 Input Event Assumptions

Impacted areas are selected based on the results of previous ORNL HEMP studies [59], [64]-[66] showing that HEMP will create two crescent-shape areas (highlighted in yellow in Figure 5.2) to the east and west of the detonation on the edge of the area under bombardment.

The detonation site is selected so that the two areas are on a circle approximately covering the major load centers (within the white circles) of the reliability/coordinating regions of interest.

In the 2003 blackout, initial load loss was limited. Grid collapse was caused by over-reaching protection relays and a failure of operators to assess the danger of the situation as quickly as it developed. Unclassified models do not provide the information necessary to determine the amount of load that will be lost as a result of E1, but due to coupling analysis there is a high probability it will be located in the highlighted tangential regions. This region has the highest probability of flashover on distribution networks [65]-[67].

The impact map is based upon knowledge of general "smile diagram" characteristics but is not an actual "smile diagram" simulation. It is representative of a relatively low burst that provides an effected area with about a 1000 km diameter. The worst case for coupling occurs at low angles of incidence and near end-on orientation of the coupled line to the burst point. An extensive discussion of this topic is available in [59], [64]-[67].

This study examines the frequency and voltage impact of losing load equivalent to a given percentage of the total MRO and RF demand and, after a delay, a recovery of 75% of the lost load. The objective is to estimate the minimum load drop that leads to a system collapse. Under the direction of HEMP experts at ORNL, three load loss percentages, 5%, 10%, and 15%, and two recovery periods, four seconds and 10 seconds, are considered. A conservative assumption is made that generators are shielded well enough that there will be no generation loss throughout the system. Simulation results including loss of load within the NPCC region are discussed separately.

5.2.2 Modeling Methodology

The base case is a 16,000 bus PSS®E model of the Eastern Interconnection (EI) derived from the Eastern Interconnection Reliability Assessment Group (ERAG) Multiregional Modeling Working Group (MMWG) model. The model includes complete dynamic data information and realistic dead-band governor response validated using FNET/GridEye measurements [68]. In order to drop and reconnect load in appropriate quantities, additional dummy load buses are created at appropriate locations across the Northeast and the original loads are scaled to preserve the correct aggregate sum at every location. A total of 2,432, 3,363, and 4,002 new nodes are

added to the 5%, 10%, and 15% load loss cases, respectively. A breakdown of the original, dropped, and recovered load by region is shown in Table 5.1.

Note that as each individual load is broken into component pieces in order to facilitate the 75% recovery the system power flow is resolved. This multi-step solution avoids large numerical jumps that can lead to convergence problems when using Newton-Raphson-based algorithms. If the new solution state is only sought after the thousands of dummy buses are added, the amount of load that is shifted is too great for PSS®E to resolve even though they are connected to the original buses by zero-impedance branches.

Six dynamic scenarios are simulated to account for all combinations of the three percentage load loss values and two recovery delays. All six scenarios extend to a total simulation time of 30 seconds. (Load loss occurs at t = 1 second; recover at t = 5 seconds for the 4 second delay and t = 11 seconds for the 10 second delay.) Frequency and voltage are recorded at all base case buses with a voltage rating between 500 kV and 765 kV throughout the EI. System protection is not modeled in the base case so the effects of over- and under-frequency, current, or voltage relays are not contemplated.

5.2.3 Simulation Results

The resulting frequency deviation and voltage profiles for the six HEMP E1 impact scenarios are presented in Figure 5.3 through Figure 5.14. While the first five simulations show no convergence errors, the solution in the final scenario (15% load loss with 75% recovery after

Table 5.1. Megawatt summaries for the original, dropped, and recovered load by region

MW Totals		**5% Case**	**10% Case**	**15% Case**
All EI	Original	578,207	578,207	578,207
	Dropped	12,602	25,188	37,797
	Recovered	9,451	18,891	28,347
MRO	Original	53,585	53,585	53,585
	Dropped	2,679	5,369	8038
	Recovered	2,679	4,027	6,028
RF	Original	19,8176	19,8176	198,176
	Dropped	9,922	19,819	29,758
	Recovered	7,442	14,864	22,319

10 seconds) ceases to converge at t = 7.7198 seconds. This may indicate numerical instability in the PSS®E model, but appears to stem from small signal or voltage instability within the system itself and possibly portends a threat such as cascading faults. Reducing the dynamic simulation time step has no noticeable impact on this result (other than moving the decimal point to match the new step size).

Maximum and minimum frequency values and the largest voltage dip for each scenario are shown in Table 5.2. Note that all three metrics increasingly deviate from their respective nominal values as the scenario definitions become more extreme. The minimum frequency and minimum voltage values would almost certainly trigger local protection relays. Whether this would arrest the spread of cascading blackouts or lead to them through systematic load shedding cannot be ascertained from the data available from the original MMWG model.

5.2.4 NPCC Participation

Several attempts are made to include the NPCC region circled in Figure 5.2 in the simulated scenarios. Every attempt to drop loads or buses in the region immediately results in non-convergent solutions. While underlying issues such as insufficient VAR support cannot be completely ruled out, it is worth noting that when all loads across the NPCC are universally lightened in the initial state power flow analysis but no elements are dropped during dynamic simulation, no convergence errors are reported. The NPCC control areas are represented by sparse matrices in the original model and all indicators point to numerical issues within the solution algorithm caused by further thinning the node connection matrix instead of problems truly present in the physical system.

Table 5.2. Maximum and minimum measurements by scenario

Load Loss Percentage	Recovery Time (seconds)	Maximum Frequency	Minimum Frequency	Minimum Voltage
5%	4 sec	60.2598 Hz	60.0000 Hz	0.9615 pu
5%	10 sec	60.2720 Hz	59.9369 Hz	0.9546 pu
10%	4 sec	60.5156 Hz	59.9009 Hz	0.8880 pu
10%	10 sec	60.5156 Hz	59.7983 Hz	0.8596 pu
15%	4 sec	60.8189 Hz	59.5921 Hz	0.7256 pu
15%	10 sec	--	--	--

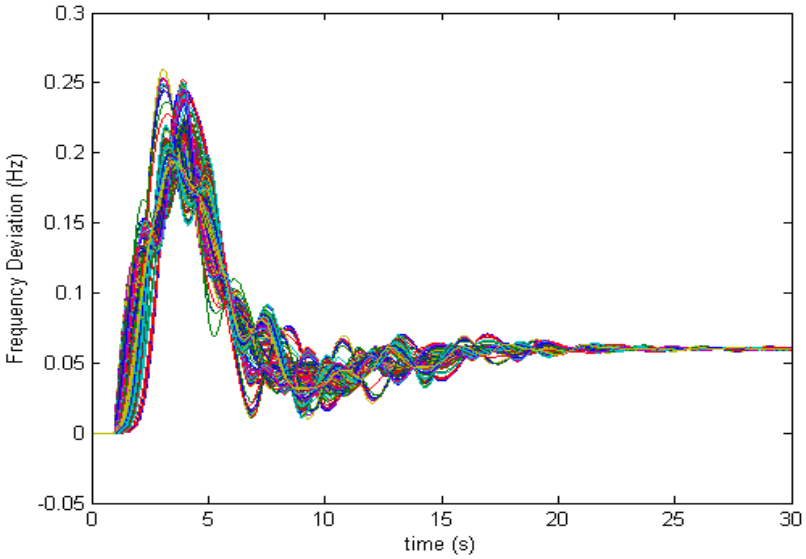

Figure 5.3. Frequency deviation for 5% load loss with 75% recovery at t = 4 seconds

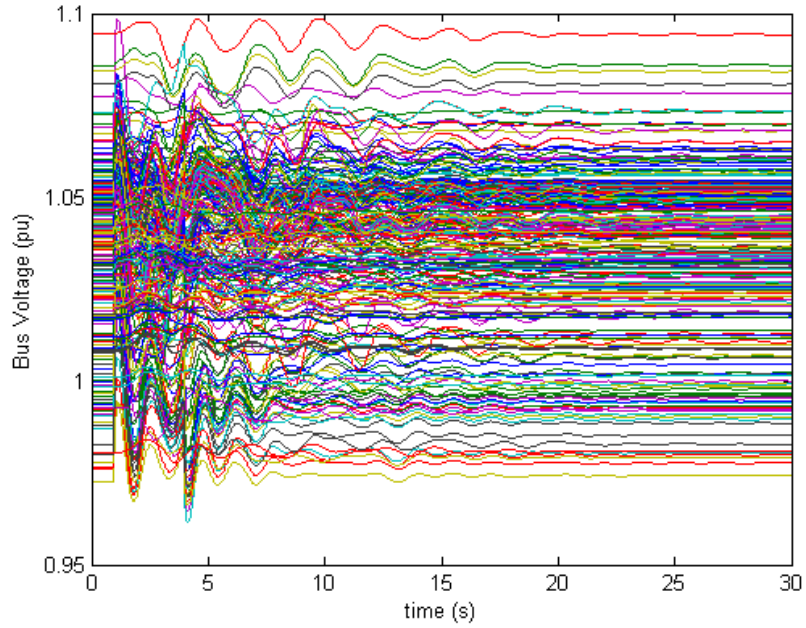

Figure 5.4. Voltage profile for 5% load loss with 75% recovery at t = 4 seconds

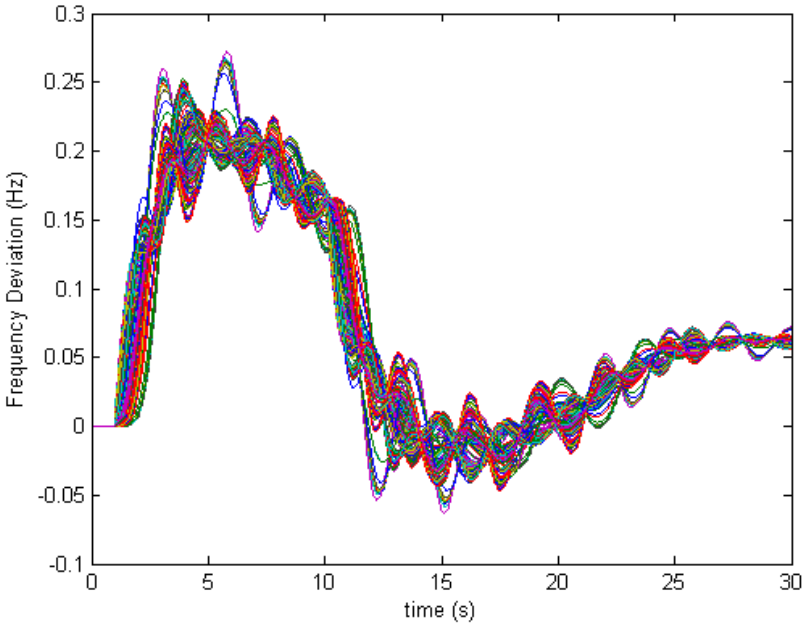

Figure 5.5. Frequency deviation for 5% load loss with 75% recovery at t = 10 seconds

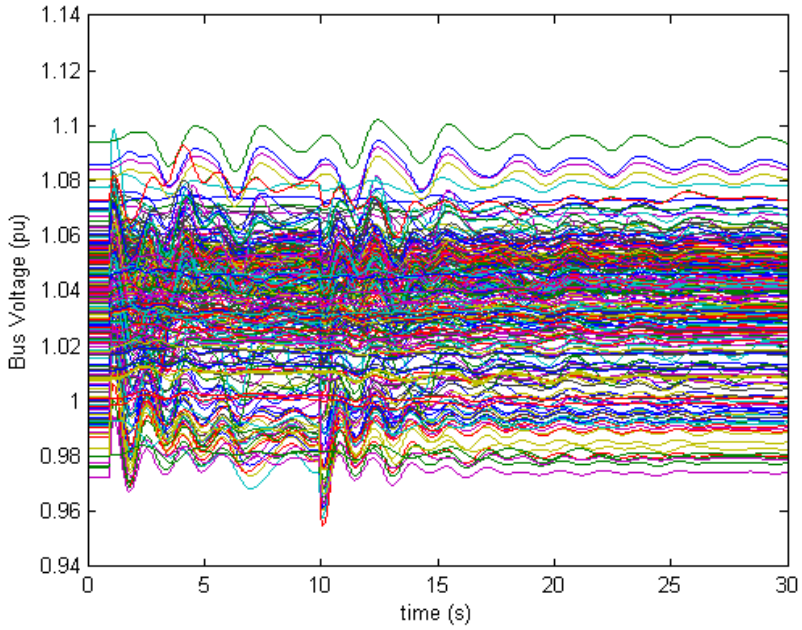

Figure 5.6. Voltage profile for 5% load loss with 75% recovery at t = 10 seconds

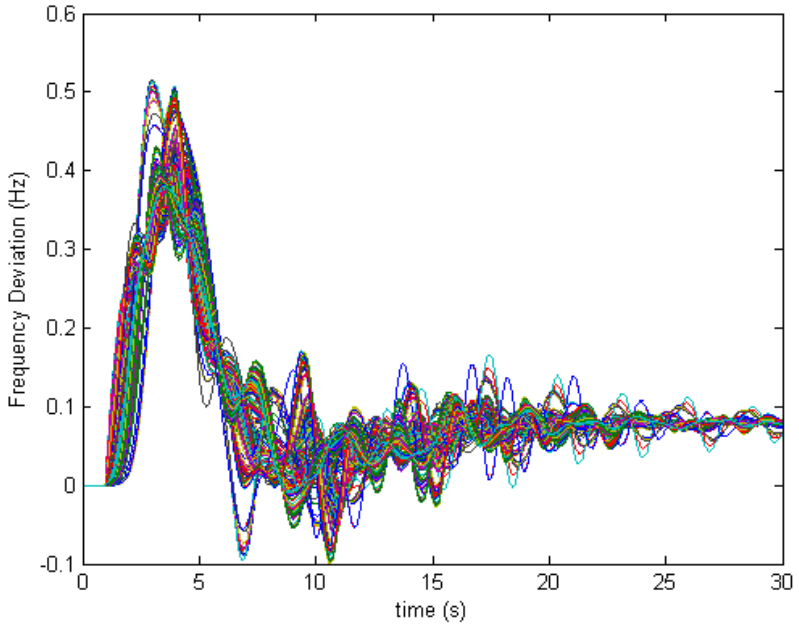

Figure 5.7. Frequency deviation for 10% load loss with 75% recovery at t = 4 seconds

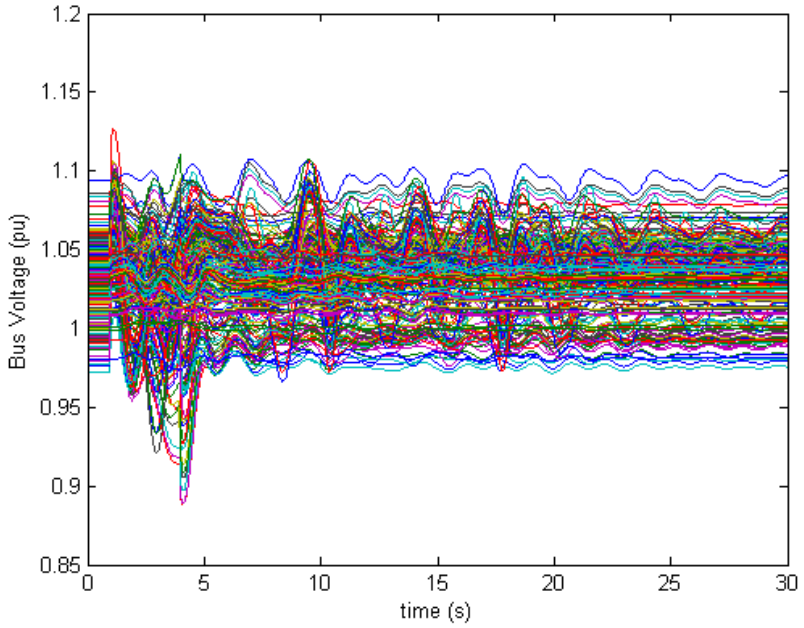

Figure 5.8. Voltage profile for 10% load loss with 75% recovery at t = 4 seconds

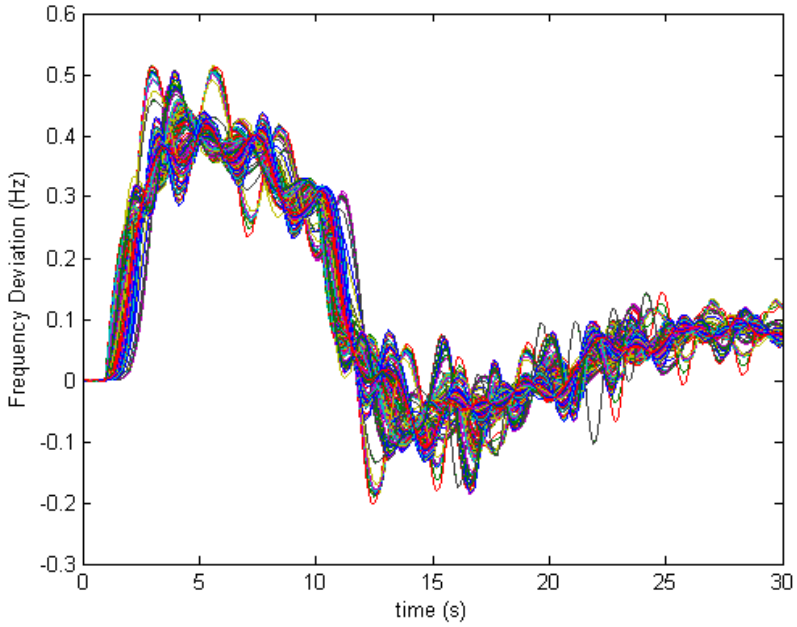

Figure 5.9. Frequency deviation for 10% load loss with 75% recovery at t = 10 seconds

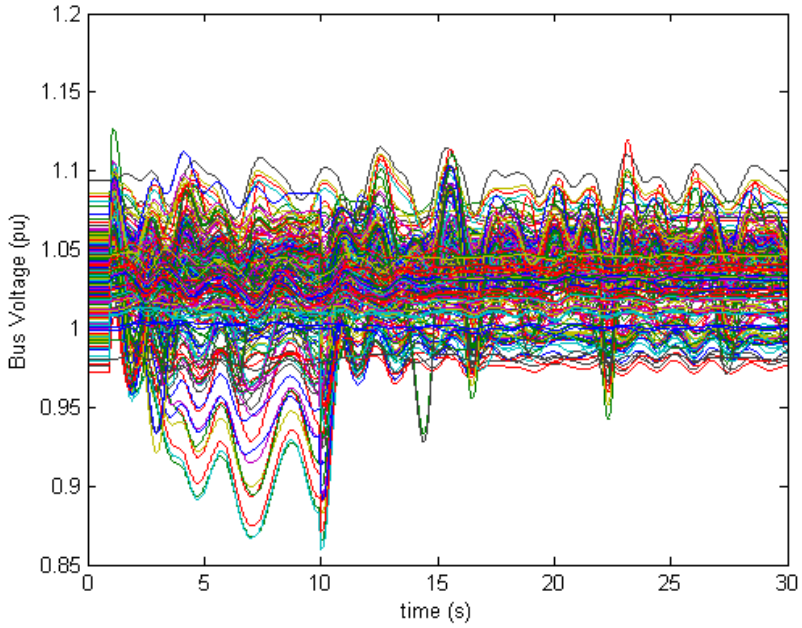

Figure 5.10. Voltage profile for 10% load loss with 75% recovery at t = 10 seconds

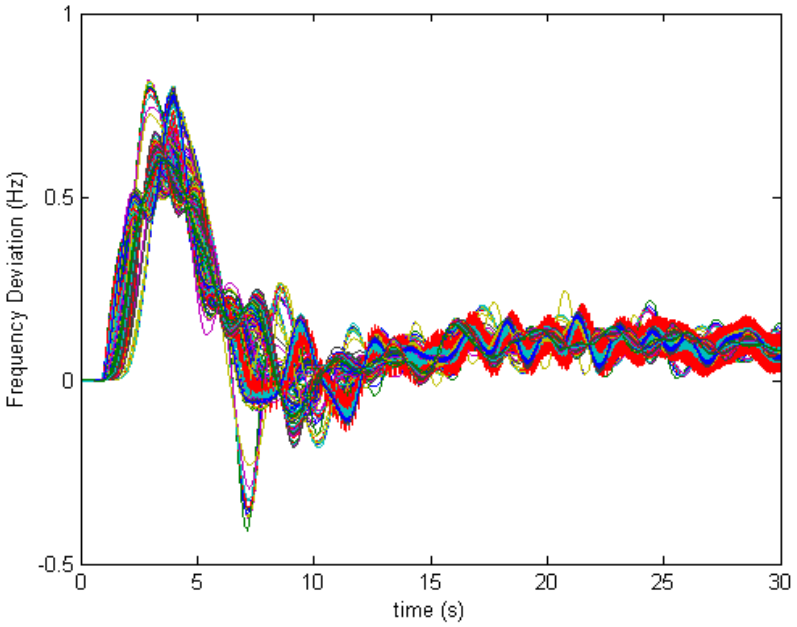

Figure 5.11. Frequency deviation for 15% load loss with 75% recovery at t = 4 seconds

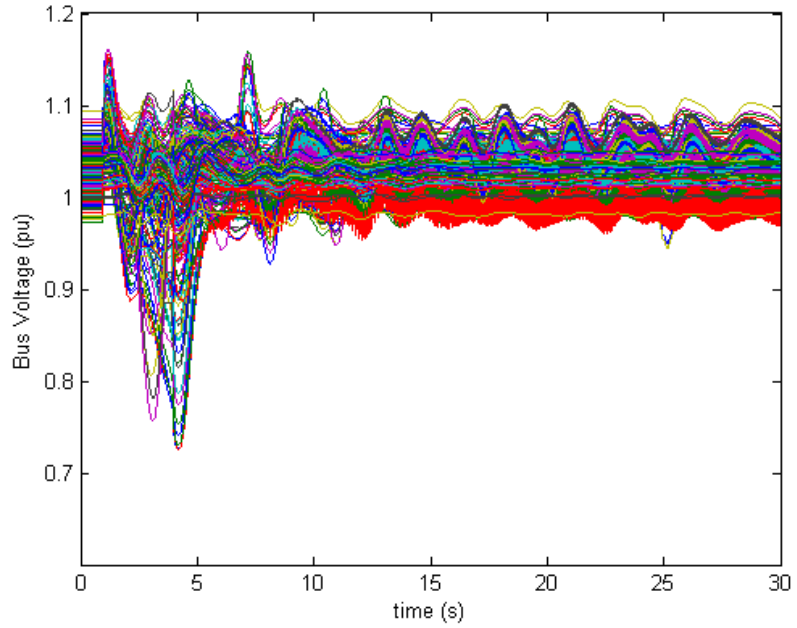

Figure 5.12. Voltage profile for 15% load loss with 75% recovery at t = 4 seconds

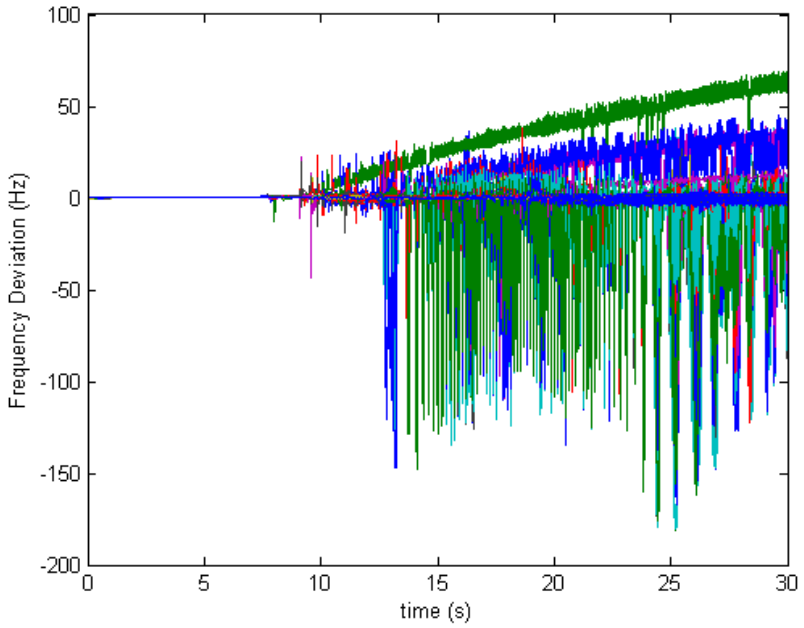

Figure 5.13. Frequency deviation for 15% load loss with 75% recovery at t = 10 seconds
Solution ceases to converge at t = 7.7198 seconds

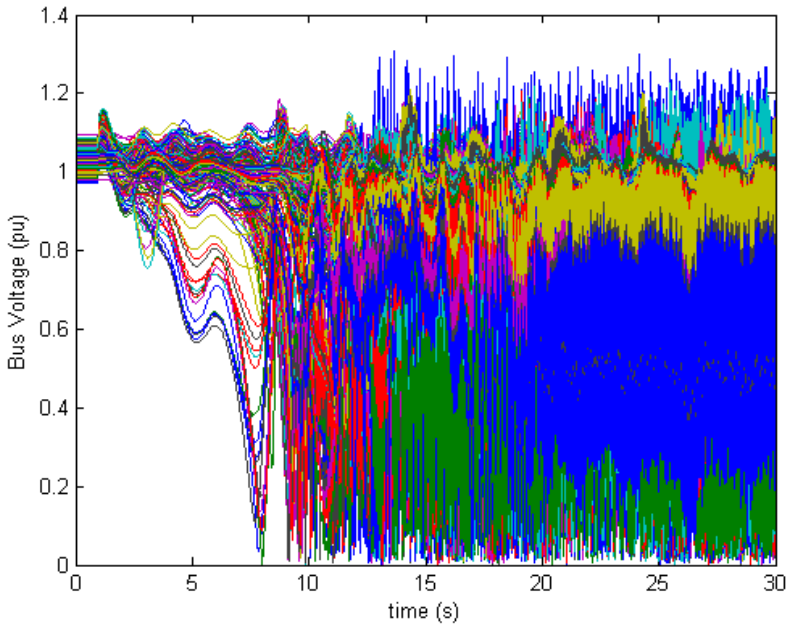

Figure 5.14. Voltage profile for 10% load loss with 75% recovery at t = 10 seconds
Solution ceases to converge at t = 7.7198 seconds

5.3 Conclusions and Future Work

This range of results shows the need for further advances in unclassified HEMP models before the electric grid can be truly hardened against attacks. Flashover in distribution systems caused by HEMP E1 will mainly occur on the eastern and western edges of HEMP impact areas, but the ability of the grid to deal with load loss cannot be assessed without more detailed input information. From the results in Table 5.2, the input data ORNL can currently provide allows for anything from a non-event to a catastrophic wide-area blackout. Due to their sequential nature, the further effects of E2 and E3 HEMP components cannot be contemplated without dependable E1 simulations. Researchers at ORNL continue to work toward producing the required unclassified comprehensive HEMP models while protecting sensitive data. This study serves to fuel that conversation.

CHAPTER 6: STRATEGIC TRANSFORMER RESERVE INTERCONNECTION-WIDE GRID SECURITY ASSESSMENT

In December of 2015, Congress passed the Fixing America's Surface Transportation (FAST) Act. Sec. 61004 of the act contains a mandate for a Strategic Transformer Reserve plan that must address

> the number and type of large power transformers necessary to provide or restore sufficient resiliency to the bulk-power system, critical electric infrastructure, and defense and military installations to mitigate significant impacts to the electric grid resulting from—
>
> (i) physical attack;
> (ii) cyber attack;
> (iii) electromagnetic pulse attack;
> (iv) geomagnetic disturbances;
> (v) severe weather; or
> (vi) seismic events [69]

The Secretary of Energy was to consult FERC and other stakeholders before presenting the Strategic Transformer Reserve plan to Congress. The U.S. Department of Energy contracted Oak Ridge National Lab (ORNL) and the University of Tennessee, Knoxville (UTK) to provide technical analysis of the issues at hand.

6.1 Problem Formulation

If a critical set of large power transformers (LPTs) exists whose unavailability could lead to a cascading power failure, then the Strategic Transformer Reserve plan should anticipate their loss. Most scenarios the plan must address occur within a radial geographic footprint. As the Metcalf substation attack demonstrated though, targeted strikes on individual transformers are not out of the question [70]. Also, as address in Chapter 4, it is possible for GMD or other natural phenomena to affect large areas, or even the entire country, simultaneously. As such, the criticality of power transformers in the bulk electric system (BES) must be assessed using an event agnostic method. To this end, the U.S. electric system is examined for crucial large power

(+100 MVA) transformers at transmission-level substations and the impact each has on the rest of the system when removed from service, both individually and in targeted sets.

This chapter deals specifically with the methodology and results of simulations performed to determine the criticality of large power transformers as originally performed by this author—mainly for the WECC interconnection, but with some EI and European analysis included for the sake of comparison. Two distinct ranking methods are presented. The first details a ranking system based on thermal line loading constraints. The second covers a ranking system based on available reactive power (VAR) support. The practical application of each of these systems is also discussed.

The contracted team's full technical analysis for the Strategic Transformer Reserve includes results for all three major U.S. grids using the same process along with discussion on existing mitigation systems and the recommended number, design, and placement of transformers for the proposed reserve. The final technical report is published in [71].

6.2 Methodology

The ultimate purpose of the BES is to serve electrical load. At first glance, it would appear that the simplest methodology for determining the criticality of any element is to remove that element from service and record the resulting load loss. This method is quickly discarded when dealing with a real system though. In a healthy interconnection, the loss of any single element should not lead to the loss of load (that is not radially connected to that element) or to operational limit violations (defined in terms of thermal line loading and bus voltage bands). This is known as N-1 stability. All U.S. interconnections are required to meet N-1 criteria or face penalties imposed by the North Electric Reliability Corporation (NERC) [72].

As such, there should be no transformer, or any other single element, which can cause a large-scale blackout by its loss alone. A set of transformers is necessary. With the number of extra-high voltage substations, simulating the loss of transformers throughout the interconnection requires a defined workflow. In the WECC system there are over 90 substations on the 500 kV system. Combinatorial math quickly surpasses billions of possible scenarios. (Simply using $\binom{n}{7}$ yields over one billion unique possibilities.) In light of this, it is necessary to start by ranking the

criticality of each substation and transformer relative to the others. Combinatorial event scenarios are then informed by this ranking.

A python script is created to identify and remove all large power (500 kV connected) transformers by substation. Helper functions written for this script that may be useful in other scripting situations are available in Appendix C. The script to identify substation bus lists, defined as all buses connected by zero-impedance branches (bus ties) or transformers, is presented in Appendix D. The resulting power flow solutions are recorded for analysis after problematic cases are addressed manually. The two traditional steady state diagnostics, bus voltage levels and transmission line power flows (which are practical translations of equipment thermal limits), are chosen to guide ranking metrics. Due to the mostly decoupled nature of real and reactive power flow, each metric leads to a different methodology. Line flow/thermal limits are represented by incremental thermal transfer capacity analysis. Bus voltage stress is quantified using reactive power generation headroom.

6.2.1 Incremental Thermal Transfer Capacity

While examining the loss of load due to the loss of each transformer is overly simplistic and ultimately unworkable, the idea can be extended into a useful methodology. Instead of simply using the current operating point, a calculation of the additional load that can be supported by the system under a given topology and generation commitment is a natural metric for determining system stress and existing reliability margin. To estimate the load capacity of the system due to thermal limitations, an incremental load calculation is performed using DC linearized power flow analysis. The AC power flow base case solution for the system must be established prior to conducting this analysis.

DC linearization relies on the widely used approximation that for most circuits $X_{ij} \gg R_{ij}$ and the angle between two connected buses is small. These assumptions simplify the power flow from bus i to bus j to

$$\mathrm{P_{ij}} = \frac{\theta_\mathrm{i} - \theta_\mathrm{j}}{\mathrm{X_{ij}}} \tag{6.1}$$

where

θ_i is the voltage phase angle at bus i;

θ_j is the voltage phase angle at bus j; and

X_{ij} is the reactance between bus i and bus j.

and the power injection at a given bus in an N bus system is given by

$$P_i = \sum_{ij}^{N} \frac{\theta_i - \theta_j}{X_{ij}} \tag{6.2}$$

or for the full system

$$\boldsymbol{P = B\theta} \tag{6.3}$$

where $\boldsymbol{B}$ is the sparse admittance matrix of the system.

For small changes from a known nonlinear AC solution, ignoring reactive power and bus voltage in this way produces only negligible solution error [73].

The distribution factor technique expands DC linearization to find the limiting solution of a base case. Sensitivity analysis of the elements under review provides the basis for linear projection [74]. This is illustrated in Figure 6.1.

Applied to this problem, this technique is used to perform the equivalent of a generic N-1 study where each single element connected at a designated voltage level or above is removed in turn. All load across the system, excluding buses with connected generators, is scaled up

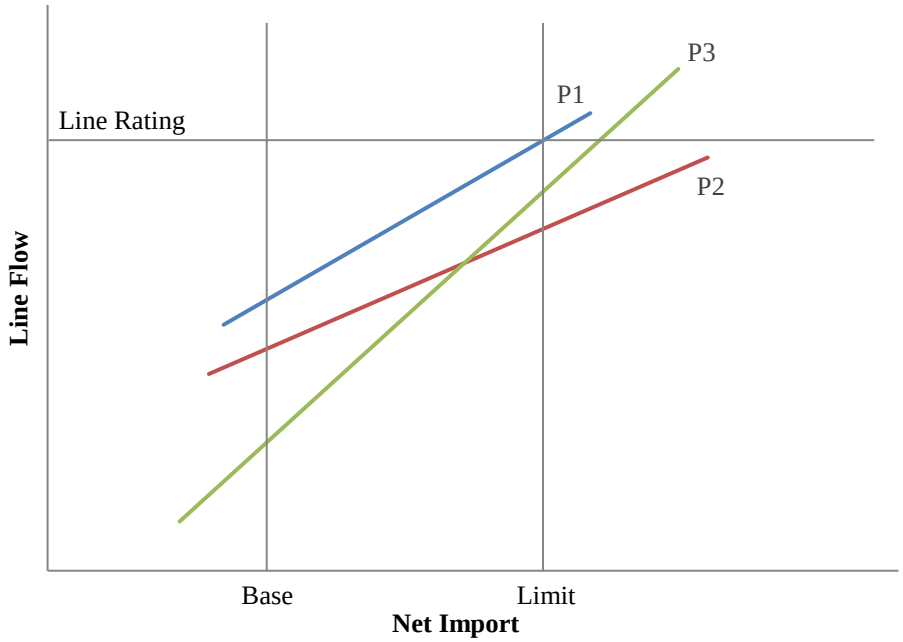

Figure 6.1. Linear projection technique

uniformly. (Note that generator buses are excluded since topology is not a factor in the amount of load that may be served directly at the generator terminals.) This additional load is compensated for by uniformly scaling generation across the system in proportion to the available capacity margin, also referred to as headroom, of each unit. Thermal branch ratings, expressed in terms of MVA flow, are assessed after each scaling solution step. The minimum additional load that leads to any transmission line or transformer surpassing its rated MVA limit is recorded as the incremental load capability of the system.

To rank the criticality of LPTs in relation to one another, the incremental load calculation is repeated over a set of scenarios where each individual scenario covers the loss of a single LPT. This can be extended to the scenarios for the loss of LPTs at entire substations in the WECC system or even more complex multi-contingency scenarios, as necessary. Each scenario (representing the impact of losing that given LPT, substation, etc.) is then ranked relative to the entire set with lower or more negative incremental load capability values representing more critical operating states and thus, more critical scenarios.

PSS®E Implementation

Performing this analysis in PSS®E relies on two main functions: DFAX and TLTG.

DFAX, the distribution factor file setup activity, reads subsystem definitions, contingency sets, and monitored elements lists into a single file as preparation for AC contingency analysis or several other available study activities [75].

In preparation for this incremental transfer capacity analysis, at least two subsystems should be created:

- A subsystem containing all buses with generation
- A subsystem containing all buses with load but not generation

These subsystems are used to conduct load and generation scaling steps.

Contingency sets can be defined to automatically include each single branch elements (transmission lines and two-winding transformers) using a third subsystem definition. A more complex definition set may be used if desired.

The monitored elements should include all branches (transmission lines and two-winding transformers) with a rated voltage matching the network fed by the low side of the LPTs under test. Note that as radial connections, generator step-up units (GSUs) should not be considered

when choosing this voltage level. As with the contingency descriptions, monitored element data can be input using individual entries or defined more simply using an additional voltage-based subsystem.

When assessing the criticality of LPTs in a given system, the subsystem, contingency, and monitored element files created for the base case will apply to all scenarios under study as well.

TLTG, the transmission transfer limit analysis activity, offers a distribution factor technique based on DC linearized network theory for MVA flow (thermal) sensitivity analysis [76].

The distribution factor file created using DFAX and several study parameters (which typically can be left as their default values) must be passed to the engine to run the activity. The result is a text report that lists the increased transfer capability of the generation and load subsystems (as defined in DFAX) along with the most limiting element and contingency for that value. TLTG accepts only a single case for analysis and so must be repeated for each scenario.

Python Implementation

Repeatedly running and recording TLTG activity reports through the PSS®E graphic user interface (GUI) is typically not the most efficient use of an engineer or researcher's time. A simple Python function can optimize this process through the application of the Siemens psspy module, which comes packaged with all new installations of PSS®E.

```
def create_tltg_report(sub, con, mon, report):
    dfx = 'temp.dfx'
    psspy.dfax([1,1], sub, con, mon, dfx)
    psspy.report_output(2, report, [2, 0])
    psspy.tltg([_i, _i, _i, _i, _i, _i, _i, _i, _i, _i, _i,
                _i, _i, _i, _i, _i, _i], [_f, _f, _f, _f,
                _f, _f, _f], [Sys1, Sys2, _s, _s, _s, _s,
                _s, _s], dfx)
    psspy.close_report()
    psspy.report_output(1, _s, [_i, _i])
    return
```

where

`sub`, `mon`, and `con` are, respectively, the paths for the substation, monitored elements, and contingency definition files;

`report` is the path at which results are saved; and

`_i`, `_f`, and `_s` are the PSS®E default integer, real, and string values, respectively.

Limitations of this Methodology

There are three limitations of this method that must be addressed. The first is the reliance on the presence of accurate thermal limitations within the base case. If data for thermal limits are not available or those provided are not correct, then the results of this methodology will be inherently flawed. This problem is avoided by ensuring that the base case is an accepted benchmark model.

The second is oversensitivity to the transfer capacity of low importance elements. Engineering judgement is required when interpreting the transmission transfer limit reports. If the most limiting element is a small radial line serving little to no load, it may be appropriate to choose the transfer capability value of the next most limiting entry instead when ranking that scenario.

The third limitation is that this incremental transfer thermal capacity methodology only considers real power flow constraints. Tallying bus voltage or VAR support constraints requires a separate analysis.

6.2.2 Reactive Power Generation Headroom

The effects of real power imbalance are felt throughout an interconnection—a fact leveraged to great effect in automatic generation control (AGC) systems. In contrast, reactive power flow, and thus voltage issues, is localized by nature. As a result, no single element can be monitored to provide a metric of system stress from a voltage perspective. Instead of focusing on a single worst-case element, the interconnection must be taken into account.

This can be accomplished by measuring reactive power generation headroom, or VAR capacity still available for commitment from each unit, across the system. For a system with M units, this can be expressed as

$$Q_{HR} = \sum_{i=1}^{\mathrm{M}} Q_{i,max} - \sum_{i=1}^{\mathrm{M}} Q_{i,gen} \tag{6.4}$$

or

$$Q_{HR} = \sum_{i=1}^{\mathrm{M}} Q_{i,max} - Q_{i,gen} \tag{6.5}$$

where

Q_{HR} is the total reactive power headroom of the system;

$Q_{i,max}$ is the maximum reactive limit of unit i; and

$Q_{i,gen}$ is the current reactive power generation of unit i.

While each generation unit is only capable of providing local support, the total headroom available across the entire system is a decent metric for overall voltage conditions. Scenarios can be ranked with smaller headroom values representing conditions that are more critical.

PSS®E Implementation

The generation set point of each unit in a PSS®E case can be seen from the GUI. The same view provides the maximum MVAR available from each unit. The headroom can either be manually tallied by the user or, as recommended for larger systems, automatically polled using the built-in PSS®E activity AMACHREAL [77]. This activity must be called twice; once to obtain the current reactive power generation of each unit and once to obtain the maximum reactive power generation of each unit. The total system headroom can then be calculated using (6.4).

Python Implementation

Calculating the reactive power generation headroom for a single case is a simple process. Repeating the calculation for the loss of every single LPT becomes tedious. As with the previous methodology, this process can be optimized with the functionality provided by the psspy Python module. The following function implements (6.4) to return the headroom for the current case.

```
def get_Q_headroom():
    ierr, (QGen,) = psspy.amachreal(-1, 1, 'QGEN')
    ierr, (QMax,) = psspy.amachreal(-1, 1, 'QMAX')
    totalQGen = sum(QGen)
    totalQMax = sum(QMax)
    QHeadroom = totalQMax - totalQGen
    return QHeadroom
```

Limitations of this Methodology

This methodology has two main limitations. First, while the potential exists for real power flow to effect the results of this methodology, it is largely decoupled from reactive power flow and bus voltages (leading to the DC linearization assumptions discussed previously). Therefore, neither the incremental transfer capacity metric or the reactive power generation

headroom calculation can provide a single criticality assessment method for LPTs. Both are necessary to fully understand the system.

The second limitation is that a highly localized voltage collapse may potentially go unnoticed by this metric. If voltage is depressed in an electrically remote section of the system, overall reactive power headroom may not appreciably respond. Engineering judgement is required to assess voltage levels of the system and ensure that no such significant voltage depression exists.

6.2.3 Application of Ranking Methodology

In the author's experience, applying either methodology presented here to a benchmarked system model and plotting the resulting ordered criticality index results in a "knee" curve. An illustrative curve for the incremental thermal transfer capacity method is shown in Figure 6.2. One for the reactive power generation headroom method is shown in Figure 6.3. Due to the sensitive nature of this analysis, actual values from the WECC analysis are not used and both graphs are normalized with no specific identifiers given.

Several things can be seen from these graphs. The first and most obvious is that in each the LPTs can be clustered by relative criticality. The most critical lie before the first knee point. Using the thermal-based incremental transfer capability ranking there are then two distinct groupings of LPTs with similar criticality ranks. Looking at the available VAR support headroom in this case produces a more gradual transition, but the results can still be classified by the section of the curve they fall under.

The next statement that can be made from these graphs is that the two ranking systems will not yield identical results. What cannot be directly seen is that any given LPT's score under one ranking system may or may not be similar to that same element's score under the other. Due to the decoupled nature of the methodologies, this should be expected. Determining the criticality of LPTs requires investigating their impact under both methodologies. An LPT that significantly impacts the system under either scheme must be considered crucial.

Flowing from that, the plotted information yields relative rankings. While it may be feasible to study only those LPTs with the highest criticality measurement in further analysis,

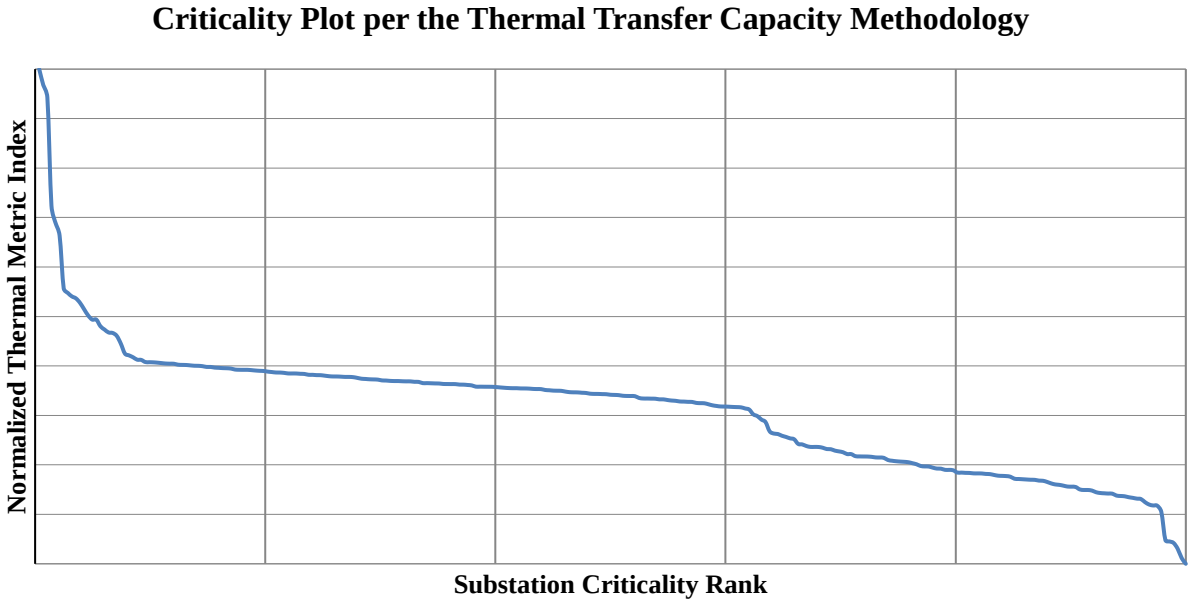

Figure 6.2. Illustrative ordered criticality index plot using thermal ranking

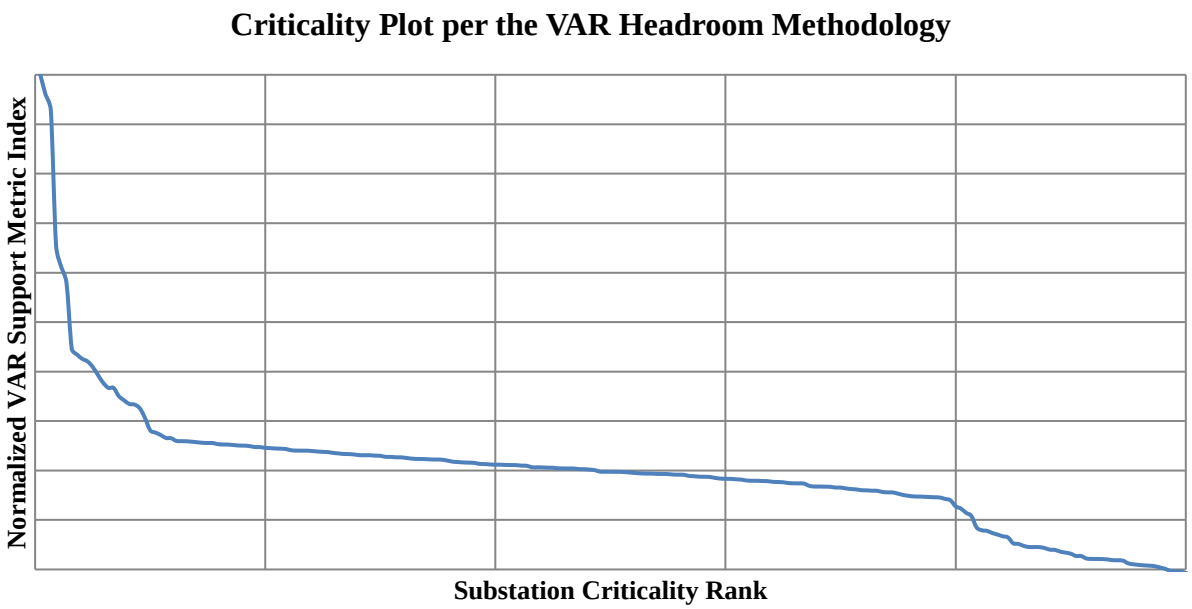

Figure 6.3. Illustrative ordered criticality index plot using VAR support ranking

elements within the lower ranking clusters may also be important enough that they must be considered. This decision requires engineering judgement based on the results of the power flow scenarios. These methodologies do provide direction for such decisions though, and provide quantitative data to facilitate them.

Individual LPTs vs. Full Substation Scenarios

Note that the application of this methodology for the transformer reserve technical review in [71] uses scenarios (and thus rankings) based on full substations instead of individual LPTs. Almost any event that could materially harm an LPT so as to remove it from service would most likely effect the entire substation. Scenarios seeking to quantify immediate repercussions of such an event should remove most, if not all, elements at that substation from service. The transformer reserve analysis investigated the long-term effects of LPT loss. Since lines and buses are comparatively simple to rebuild, only LPTs were removed from service at substations chosen for each scenario. This reflects the long lead time required to manufacture, transport, and connect an LPT.

The resulting rankings are therefore given for each substation instead of each individual LPT in the system. The horizontal axes in Figure 6.2 and Figure 6.3 are labeled according to the same convention for consistency. Curves for individual LPT criticality rankings would possess similar knee shapes.

6.2.4 Combinatorial Scenarios

In relation to the WECC system specifically, it is possible to isolate a subset of crucial transformers with 500 kV primary connections for combinatorial studies. Combinatorial scenarios are constructed based on the sequential loss of all transformers in crucially ranked substations. Modifying the original Python script used to create individual substation scenarios, applying the helper functions found in Appendix C, and adding logic to handle cases that were previously addressed by hand allows these runs to be automated as well so that outages build from highest ranked impact to lowest rank impact until PSS®E reaches a divergent solution. Power flow results for the new system state are recorded after the LPTs at each individual substation are dropped.

Table 6.1. Illustrative results from an example combinatorial outage scenario

Sequence Iteration	Substation Dropped	Solution	Thermal Max (p.u.)	Voltage Max (p.u.)	Voltage Min (p.u.)
1	Station A	Converged	0.9634	1.0831	1.020
2	Station B	Converged	0.9634	1.0874	1.021
3	Station C	Converged	1.0232	1.0852	1.008
4	Station D	Converged	1.0239	1.0863	0.9989
5	Station E	Not Converged	1.0117	1.0993	1.003
5'	Station E	Converged (Manually)	1.0117	1.0992	1.003
6	Station F	Diverged	1.0119	1.747	0.456

Data for an example simulation set are given in Table 6.1. The specifics of how to interpret these data are discussed below. (Note that due to the project NDA, this data is not from the actual WECC model used for this study. Table 6.1 is provided for illustrative purposes only.)

Long-term Emergency Operation Limits

Typically, utilities would determine if an operating state is feasible by referencing predefined bus voltage and thermal line loading limits. These are almost always defined under two categories: normal operation and emergency operation. Normal operation limits cover the restrictions placed upon equipment loading for extended periods in order to maintain the life of each element in the system. Emergency operation limits are higher ratings allowable for short durations (ranging from 15 minutes to four hours, depending on the specific utility). The system cannot operate under emergency rating level states for an extended time without impacting the lifetime performance of stressed elements.

The scenarios envisioned by the FAST Act can certainly be described as emergencies, but the extended lead time required to manufacture, transport, and connect new LPTs for a substation may cover days, weeks, or even months. Given this, short-term emergency ratings are not appropriate metrics to measure system performance against. While counterintuitive at face value, normal ratings are applied since this analysis aims to investigate the long-term status of the post-event system. In consultation with system planners and operators from several utilities, the following criteria are selected to define limit violations:

- Branch thermal constraints (normal operation thermal limits) cannot be met without shedding load; or

- Bus voltages are outside acceptable limits of 95% to 105% of their nominal ratings—or 100% to 110% for 500 kV buses (which are usually run higher on a per unit scale than buses of lower voltage levels).

While in some cases violations only represent a 0.001% deviation beyond these limits, no extra tolerance is considered permissible. This increases confidence in the analysis integrity by removing subjective judgement calls.

Dealing with Non-convergent Power Flow States

During both individual and combinational substation scenarios, certain runs result in PSS®E reporting a non-convergent or divergent state. Manual oversight is required for these since it is possible that the solution engine has overlooked a convergent solution. The process to determine and resolve issues depends on which state the simulation has reached.

A non-convergent solution state is one where total system error is still relatively low, but no convergent solution can be found. If a system is in a non-convergent state after several iterations (40+), there is probably an oscillating control element at play.

The worst offenders are discrete step switched shunt capacitor banks with voltage steps too large for the solver error tolerance. Inside each pair of iterations, the same switched shunt will shift back and forth between the two values, seeking to reach a settling point between the two available steps. In reality, system operators seek to minimize capacitor switching of any kind and automated systems have time constants that prohibit rapid switching. Locking the offending shunt almost always fixes the issue and allows the case to converge within three or four iterations. While the solution may not be optimal in the strictest sense of the word, any additional losses are usually negligible and the converged state is valid. A similar, although less common, issue may occur with transformer taps settings; the resolution method is identical.

A divergent solution state (referred to within PSS®E as a case that has "blown up") typically requires more involvement. In the context of the Strategic Transformer Reserve analysis, almost all divergent solutions are caused by areas of load that become mostly isolated or electrically distant from reactive power sources after the loss of the scenario's LPTs. Effectively, this creates pseudo-islands without significant voltage support. Many of these cases can still be resolved by returning to the last converged solution state and removing the pseudo-island from service. After the LPTs are removed and a valid equilibrium is reached, the pseudo-

island is then brought back into services a few buses at a time. This allows the solver to gradually adjust to the new topology instead of shocking the system with the new reactive power flow pattern all at once. The final solution is valid, the iterative mathematics underlying the Newton-Raphson power flow equations just need a little more help than the actual system.

It is possible for a situation to arise where not every connected load can be served without causing voltage collapse. When this occurs, the minimum level of load possible to resolve the issue is removed from service. The megawatt total of the lost load should be recorded and factored into scenario cruciality assessment.

This process is illustrated in Figure 6.4 through Figure 6.10 using a simple one line diagram. First, the LPTs at the top of the diagram are removed from service (Figure 6.5). This separates the load center from the strong source. Even though another source is available, the result is a divergent solution state due to voltage collapse (Figure 6.6).

After resetting with the base case, removing the entire load center form service (Figure 6.7) and bringing the buses back online in stages (Figure 6.8 and Figure 6.9) allows the solver to calculate an alternate reactive power flow using the remaining path to the system. This yields a valid solution even when only the LPTs of interest remain the only elements out of service (Figure 6.10).

Interpreting Combinatorial Scenarios

The results of the example combinatorial run in Table 6.1 (page 64) show that the cumulative loss of the first four stations (Station A through Station D) results in a convergent solution. Losing the fifth station (Station E) as well requires manual intervention to reach a convergent solution. The additional loss of the sixth station (Station F) results in a divergent solution. It is possible that a solution exists for this last step, but both the thermal and voltage measurements in previous iterations show readings outside acceptable limits, so the effort required to reach a convergent state is unwarranted.

Note that by definition, divergent solutions contain unacceptably high numerical error. Thus, thermal and voltage values from divergent states are not valid and cannot be used to make this determination.

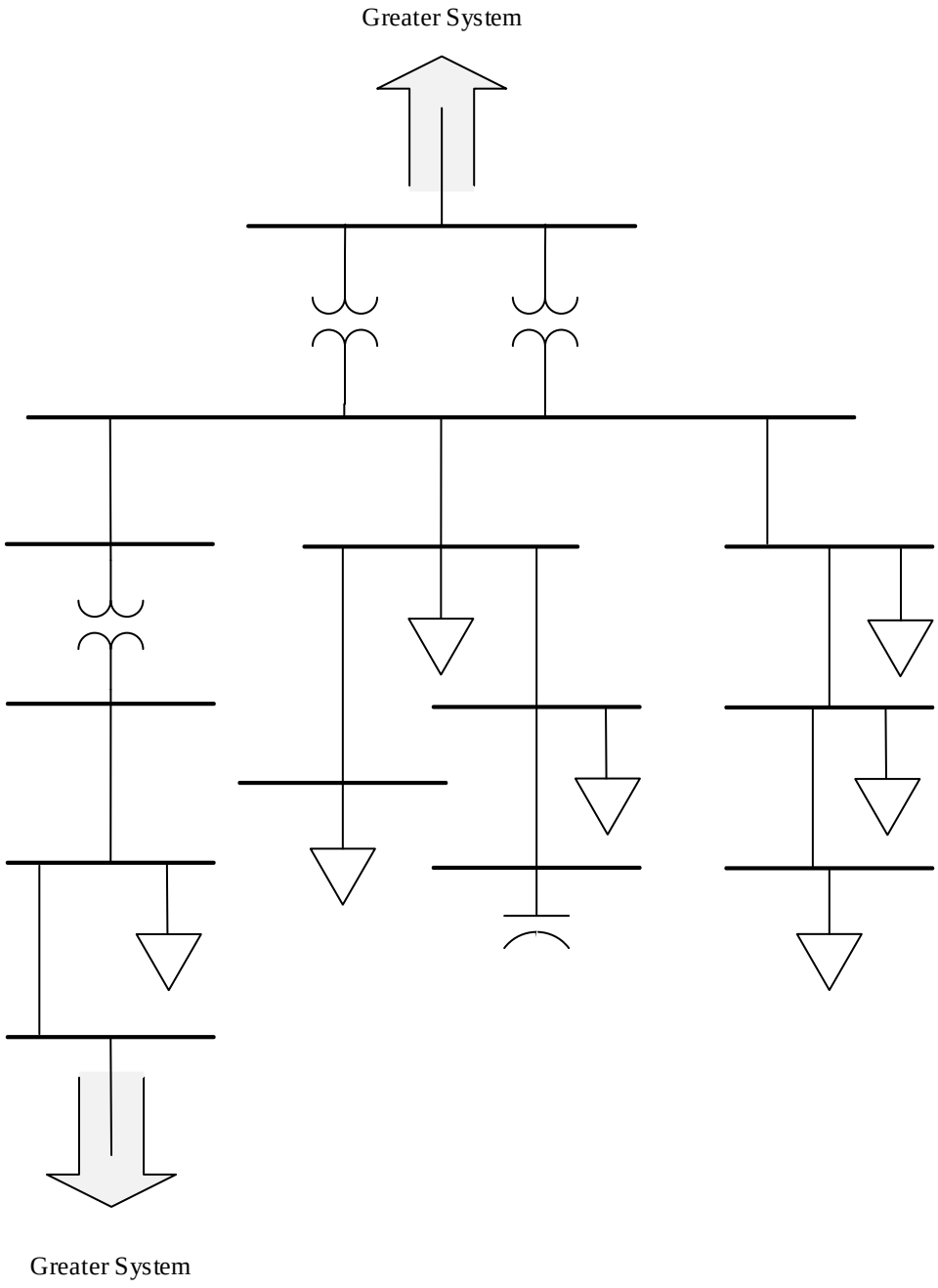

Figure 6.4. Example system one line diagram

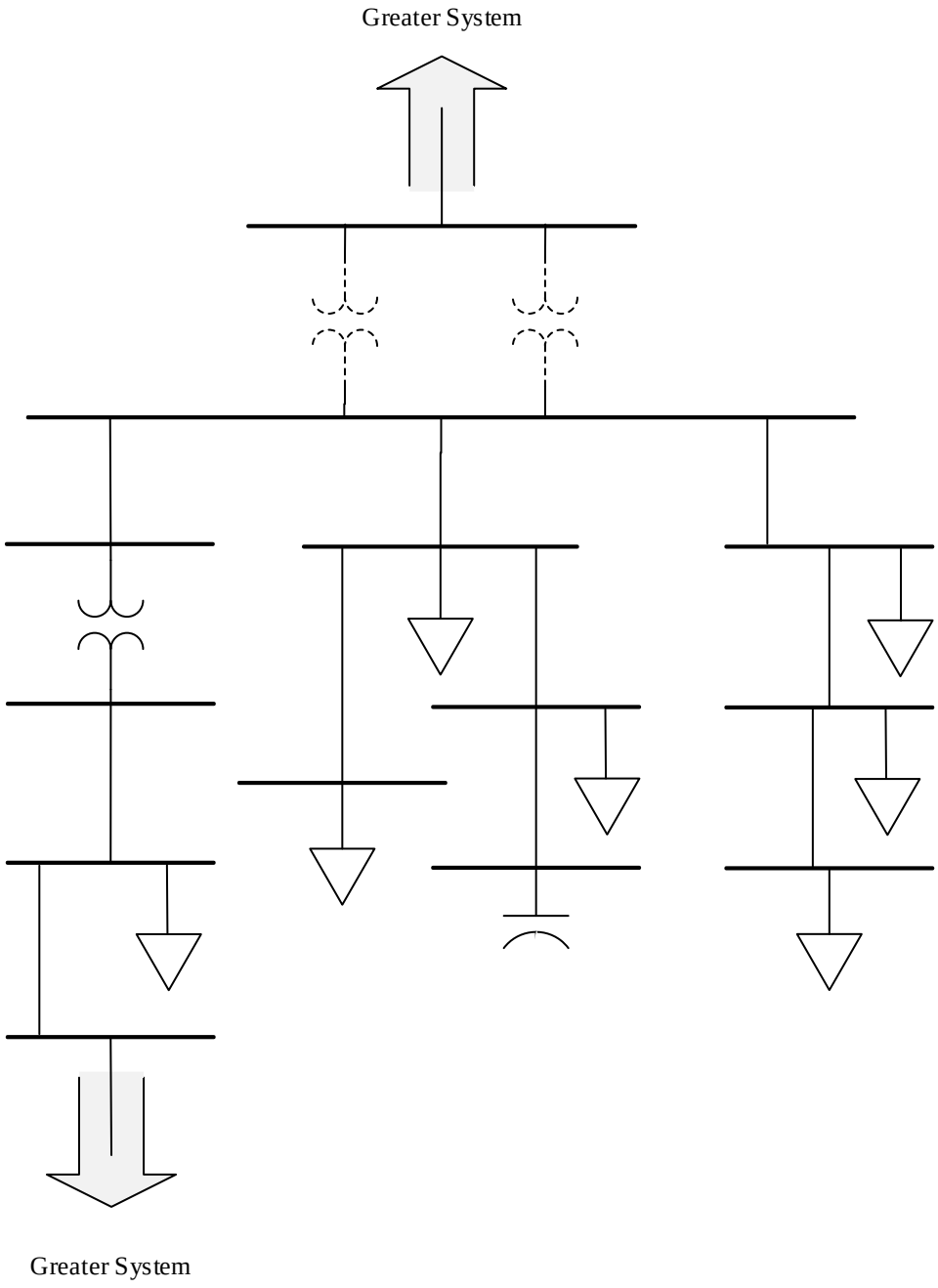

Figure 6.5. LPTs at top removed from service

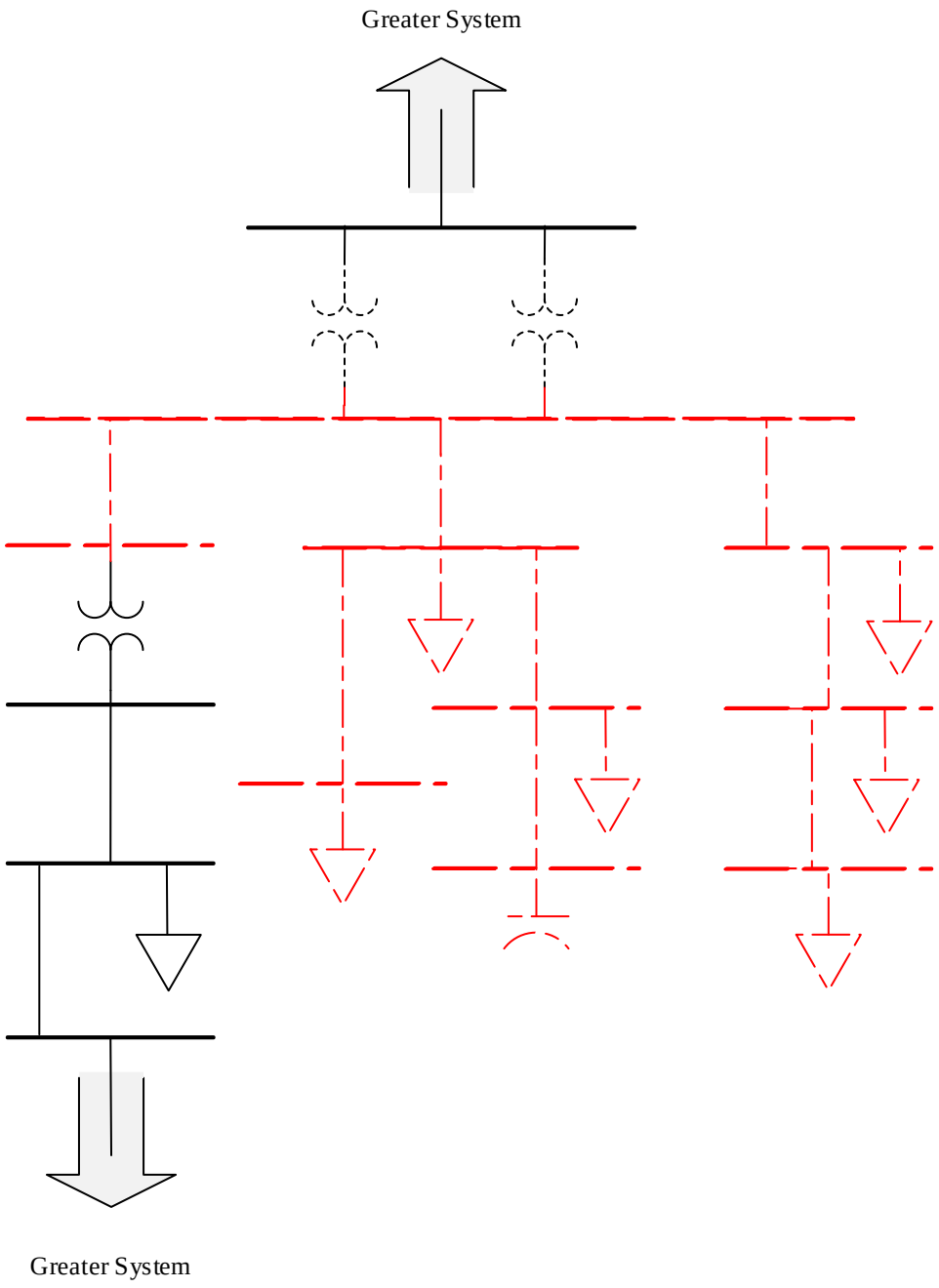

Figure 6.6. Local voltage collapse leads to a divergent solution state

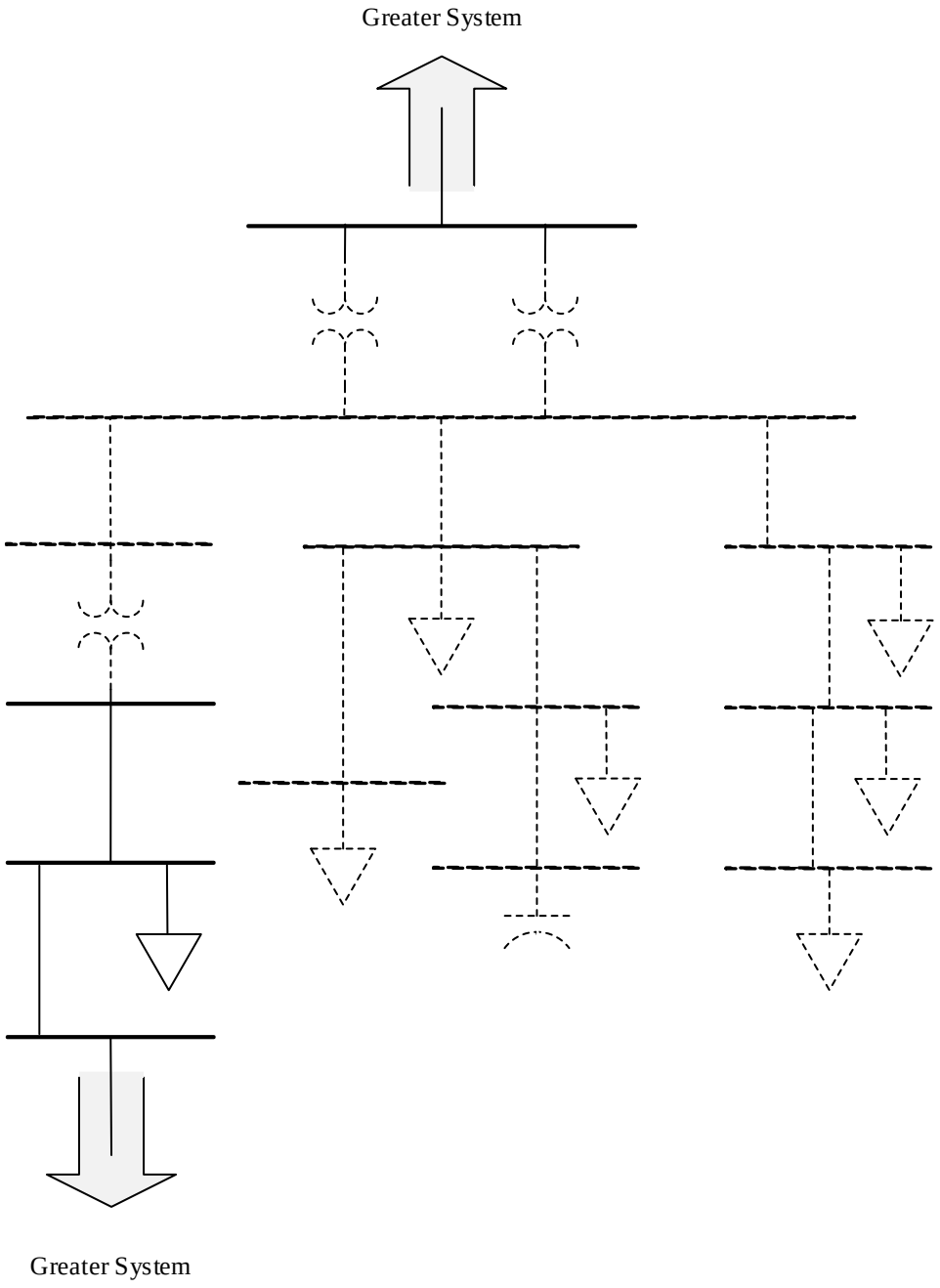

Figure 6.7. Alternative solution process: Begin by removing entire load center from service

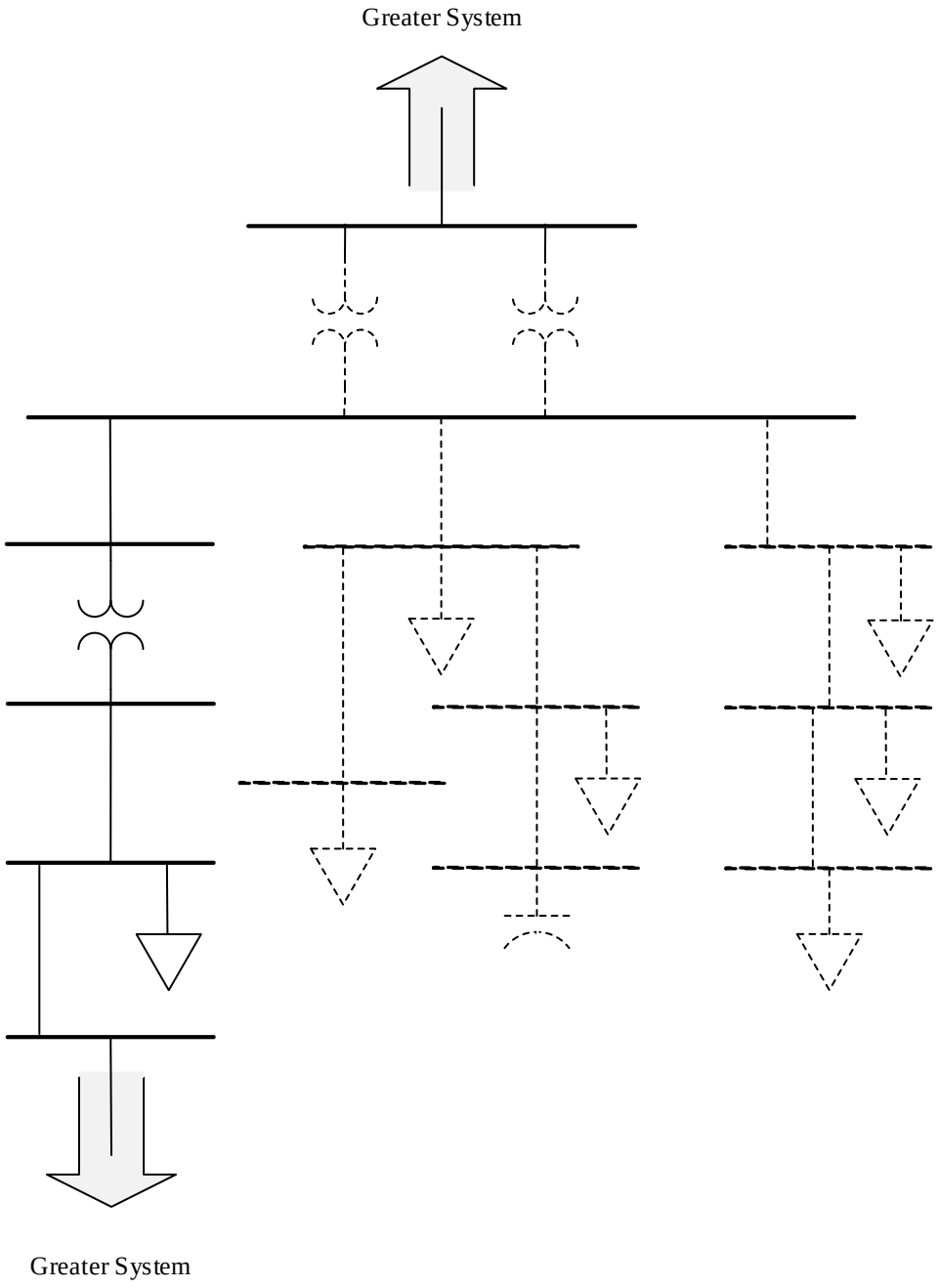

Figure 6.8. Then bring sections back into service in stages

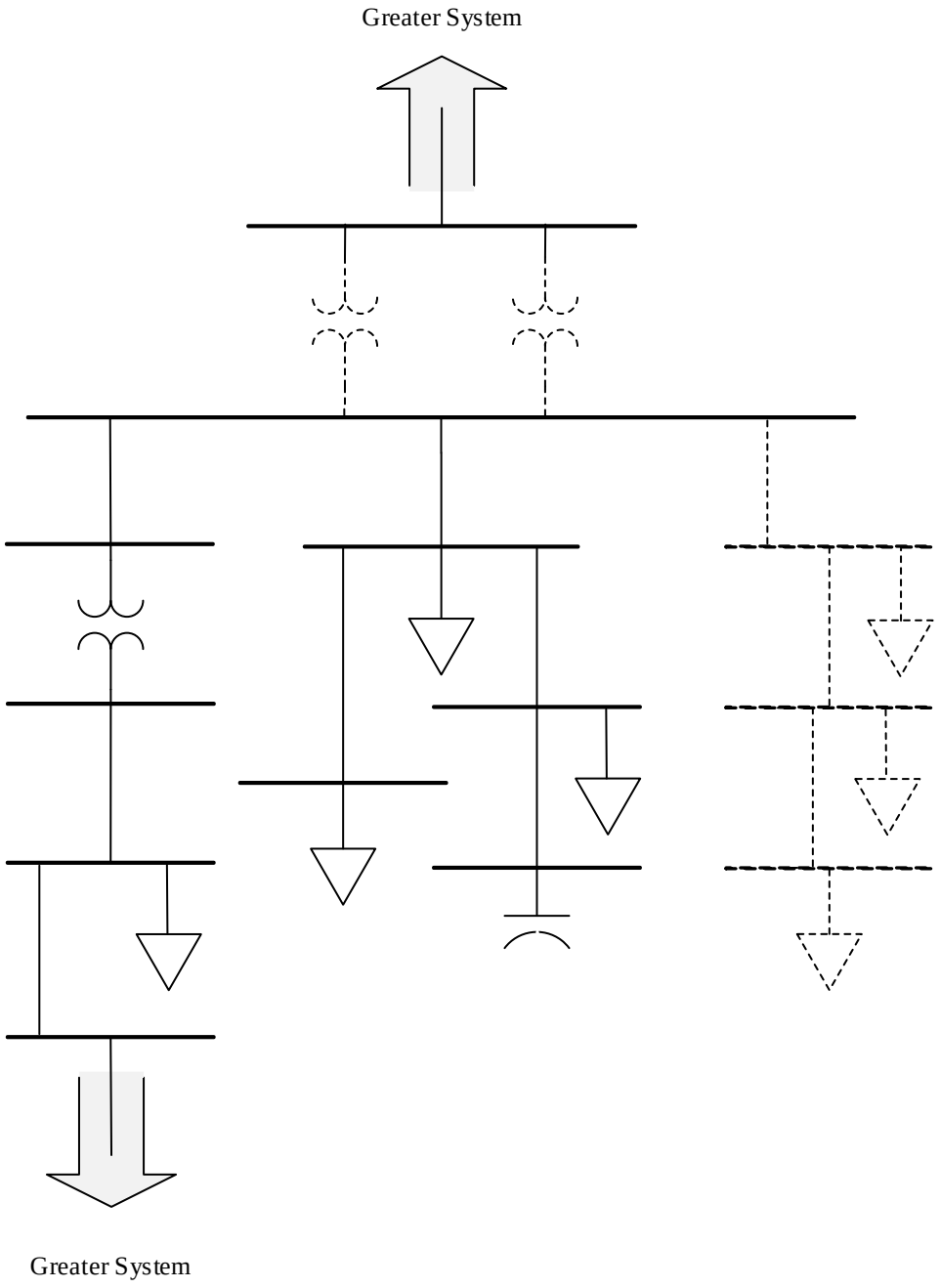

Figure 6.9. This allows the numeric solver to calculate more feasible VAR flow patterns

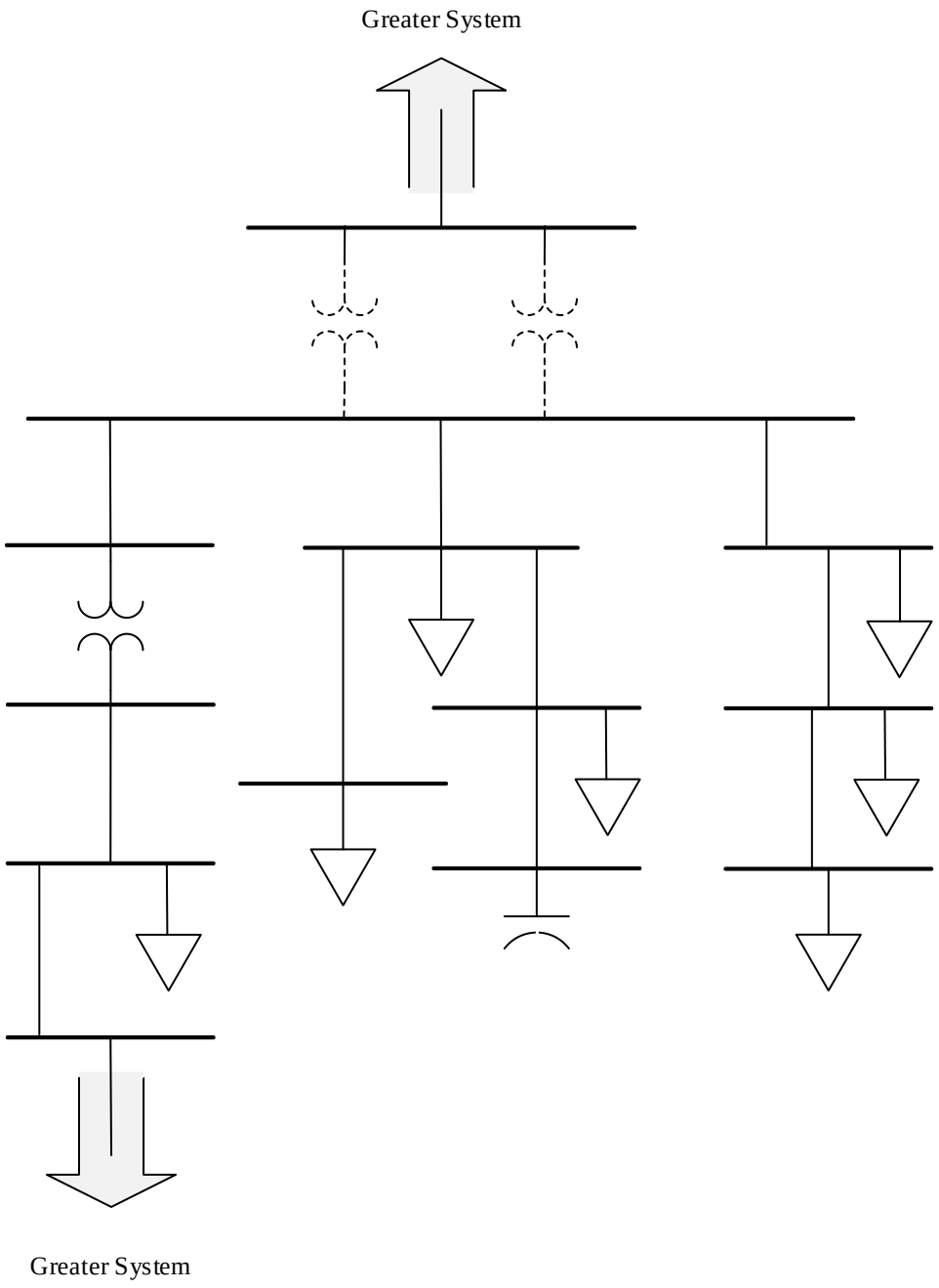

Figure 6.10. The final result is a valid system with only the LPTs under test removed from service

In this case though, at least one branch element exceeded 100% of its thermal rating with the loss of Station C and at least one bus voltage dropped below the 1.0 p.u. rating threshold (assume 500 kV buses) with the subsequent loss of Station D. As the first iteration with unacceptable limit violations, iteration three (loss of Station A through Station C) requires further attention and all successive iterations must be reevaluated.

Under the procedure used for the WECC Strategic Transformer Reserve study, spare transformers should be substituted into the system one at a time until the converged system shows no unacceptable limit violations. Substitution begins with the most critically ranked station (Station A in this example) and works to the least critically ranked (Station C in iteration three). If two transformers are in parallel, as in Figure 6.10, usually only one must be restored to service through the use of a spare transformer in order to gain the benefit of the station. The relative benefit of adding a second spare at either that same substation or the next substation under the criticality ranking is usually heavily weighted toward the latter option.

An example of the sequential process using transformer replacement to alleviate limit violations is presented in Table 6.2. An event that causes the loss of all transformers in Station A through Station F requires four replacement transformers to keep the system within the operational limits defined for this study.

Table 6.2. Illustrative results from an example combinatorial outage scenario with transformer replacement

Sequence Iteration	Substation Dropped	Solution Method	Limit Violations	Cumulative Replacements
1	Station A	Automated	None	0
2	Station B	Automated	None	0
3	Station C	Automated	Thermal	0
3'	Station C	Replacement (1)	None	1
4	Station D	Automated	Voltage	1
4'	Station D	Replacement (1)	None	2
5	Station D	Automated	Not Converged	2
5'	Station E	Manual	None	2
6	Station F	Automated	Diverged	2
6'	Station F	Manual	Thermal & Voltage	2
6"	Station F	Replacement (2)	None	4

Localized Event Scenarios

This same process can be applied to determine the impact of geographically defined events, e.g., earthquakes or hurricanes. Once the footprint of the scenario is defined, substations inside that geographical boundary are determined. These are used as the sequential substations be removed instead of those with the most critical ranking in the interconnection. As replacement transformers are required, their placement should still be directed to substations with higher criticality ranking.

6.2.5 Spare Transformer Identification

After the number of required spare transformers is determined, the number of existing spare transformers must be known in order to identify any shortfall that the Strategic Transformer Reserve should meet. Spare transformers stored on-site at the substation under study are considered to also be lost, and cannot count toward system restoration. Since most transformers that perfectly match operational units are stored in the same switchyard, finding appropriately designed spares became an important point of study.

ORNL surveyed utilities across the nation to obtain an understanding of existing space transformer practices and the size of replacement caches. Survey responses show a high number of spare transformers. The total is discounted though since many utilities share pools of mobile replacement units (and each member utility would report the pool, leading to counting each transformer multiple times). The total is further limited due to the problem statement requiring spares to be located off-site.

Conversely, the complete pool of potential spares grows significantly when existing operational units are considered. While transformers at substations with high criticality rankings should not be removed, a single transformer from a parallel set inside a substation with a low ranking can usually be taken out of service and relocated without significant impact to the original location. Reliability margin is decreased, but under the envisioned scenarios, this decrease is negligible.

Suitable substitution is defined as a donor (replacement) transformer with:

- Identical rated voltage on the primary and secondary connections;
- An MVA rating greater than the original unit's operational MVA loading; and

- A reactance between 100% and 120% of the original unit's reactance.

These requirements were submitted to a panel of experienced industry leaders before their adoption [71].

A Python script was written to locate suitable replacement transformers, considering both two winding and three winding units, for any given PSS®E subsystem. This script is presented in Appendix E. The results of this scripted analysis and the utility surveys provided a complete picture of potential spare and donor transformers for the Strategic Transformer Reserve technical analysis team to consider.

6.3 Substation Pair Analysis

To validate this ranking methodology, analysis is conducted using the 9,241 bus pan-European (EU) fictitious data-set publically distributed with installations of MATPOWER (case9241pegase.m) [78], [79]. Python scripts are used to conduct a full ranking for the loss of all transformers by each substation. The analysis is then rerun with every possible combination of substation pairs is then removed. Due to the large number of simulations involved, divergent cases are not manually resolved as described in Chapter 6.2.4, but instead ranked as most crucial.

6.3.1 European Analysis Results

The script presented in Appendix D is used to group buses connected by zero-impedance branches (bus ties) and transformers into substations sets. In total, the EU case contains 81 such substations with bus voltage levels of at least 400 kV. High voltage (also defined here as at least 400 kV on the primary winding) transformers associated with each of the 81 substations sets are removed in turn, creating 81 initial scenarios for analysis. Incremental thermal transfer capacity and VAR generation headroom rankings for these scenarios are shown in Figure 6.11 and Figure 6.12, respectively. The single data point in each marked with a red diamond represents a divergent system solution. The specific metric values shown for this point are not necessarily valid, but chosen to mark the most critical ranking while preserving a sense of scale in the plots.

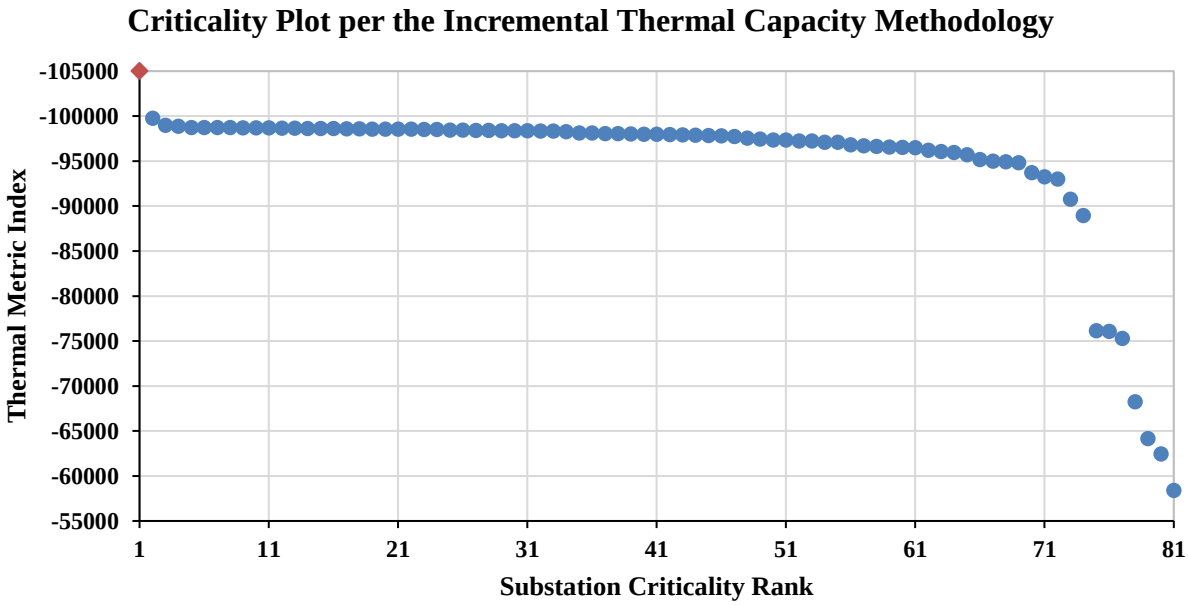

Figure 6.11. Ordered thermal criticality index ranking for high voltage EU substations

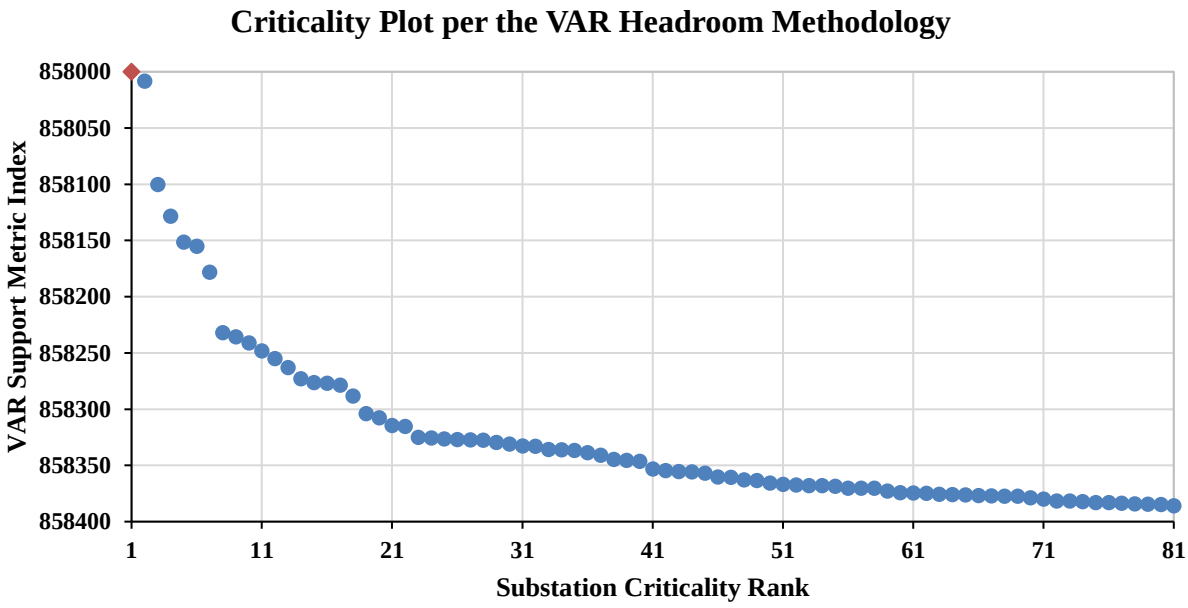

Figure 6.12. Ordered VAR support criticality index ranking high voltage EU substations

Table 6.3. Summary of EU paired substation scenario convergence

Interconnection Summary	**EU**	
Number of Substations	81	
Maximum Substation Voltage	750 kV	
Minimum Substation Voltage	400 kV	
Total Substation Pairs	3240	100.00%
Converged Scenarios	3157	97.44%
Blown Up Scenarios	83	2.56%

With 81 substations, there are 3,240 possible pairs to consider. (There are 85,320 possible triads, which cleanly illustrates why a ranking methodology is important to pare down scenarios for the Strategic Transformer Reserve analysis.) Summary results for scenario convergence are presented in Table 6.3. Out of the 83 divergent solutions, 79 contain a single substation—the one found most critical in the individual substation rankings using both metrics.

To further the comparison with the individual rankings, thermal and VAR support indices are calculated for each scenario. Figure 6.13 and Figure 6.14 each contain a series of box plots created from the thermal and VAR support results, respectively. Each box plot contains the results of all pairs including an individual substation, ordered using the given individual substations' rankings. Thus, in Figure 6.13 the first box plot is created from the thermal metric results of all 80 substation pair scenarios that include the substation with the worst individual thermal metric ranking. The second box plot is created from the thermal metric results of all 80 substation pair scenarios that include the substation with the second worst individual ranking. This continues for all 81 substations. Figure 6.14 follows the same design, but uses the VAR support metric to both create and order the box plots.

For each box, the red central line marks the median, the lower edge falls at the 25th percentile, the upper edge at the 75th percentile, whiskers extend to 2.7 standard deviations, and extreme values are marked with red crosshairs. For either metric, following the median points across each substation box plot series results in a curve shape similar to what is seen in the appropriate individual substation criticality plot (either Figure 6.11 or Figure 6.12). This provides validation for the use of both metrics in ranking individual substations in order to design combinatorial scenarios.

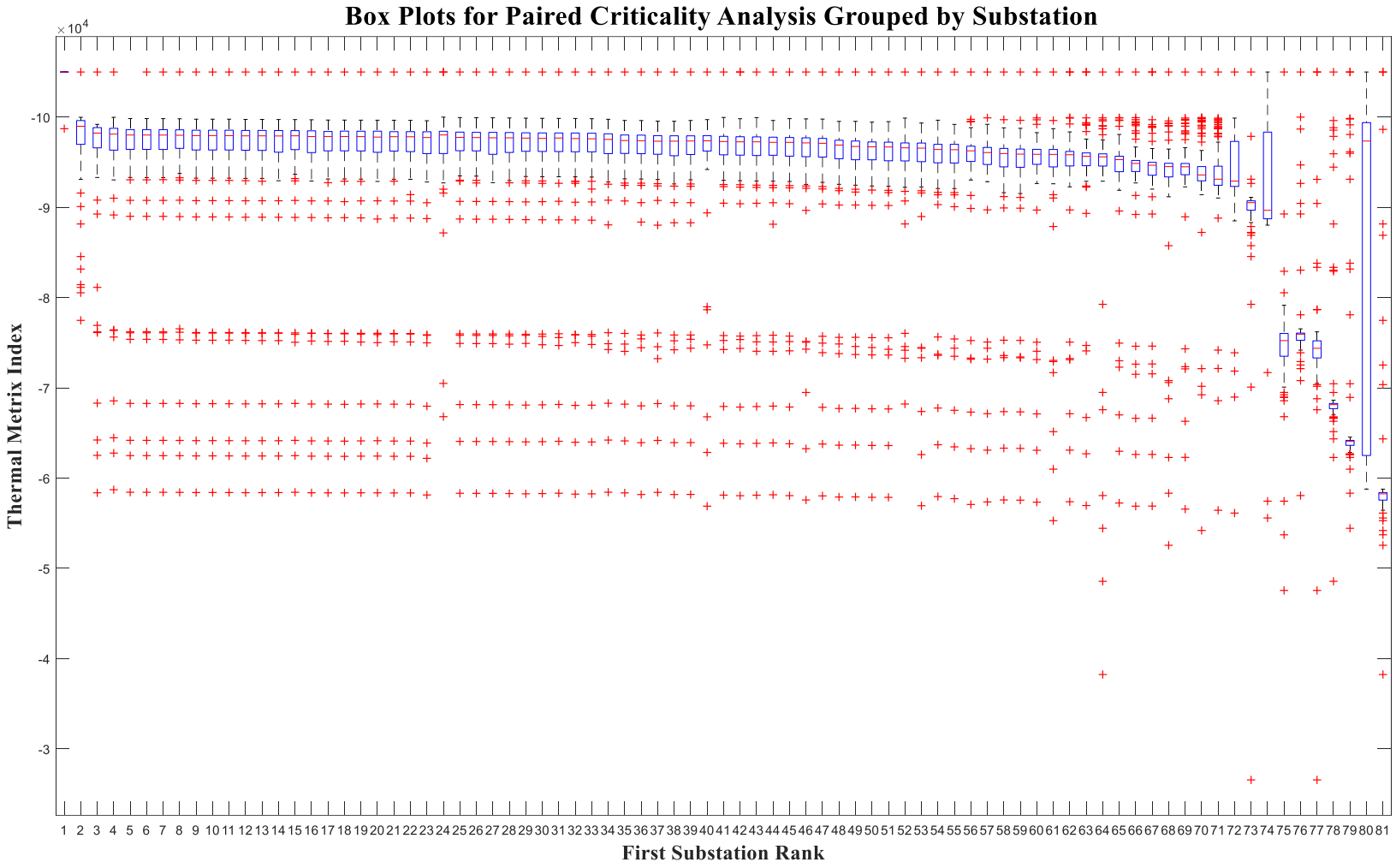

Figure 6.13. Thermal analysis box plots for paired high voltage EU substations ordered by single substation rank

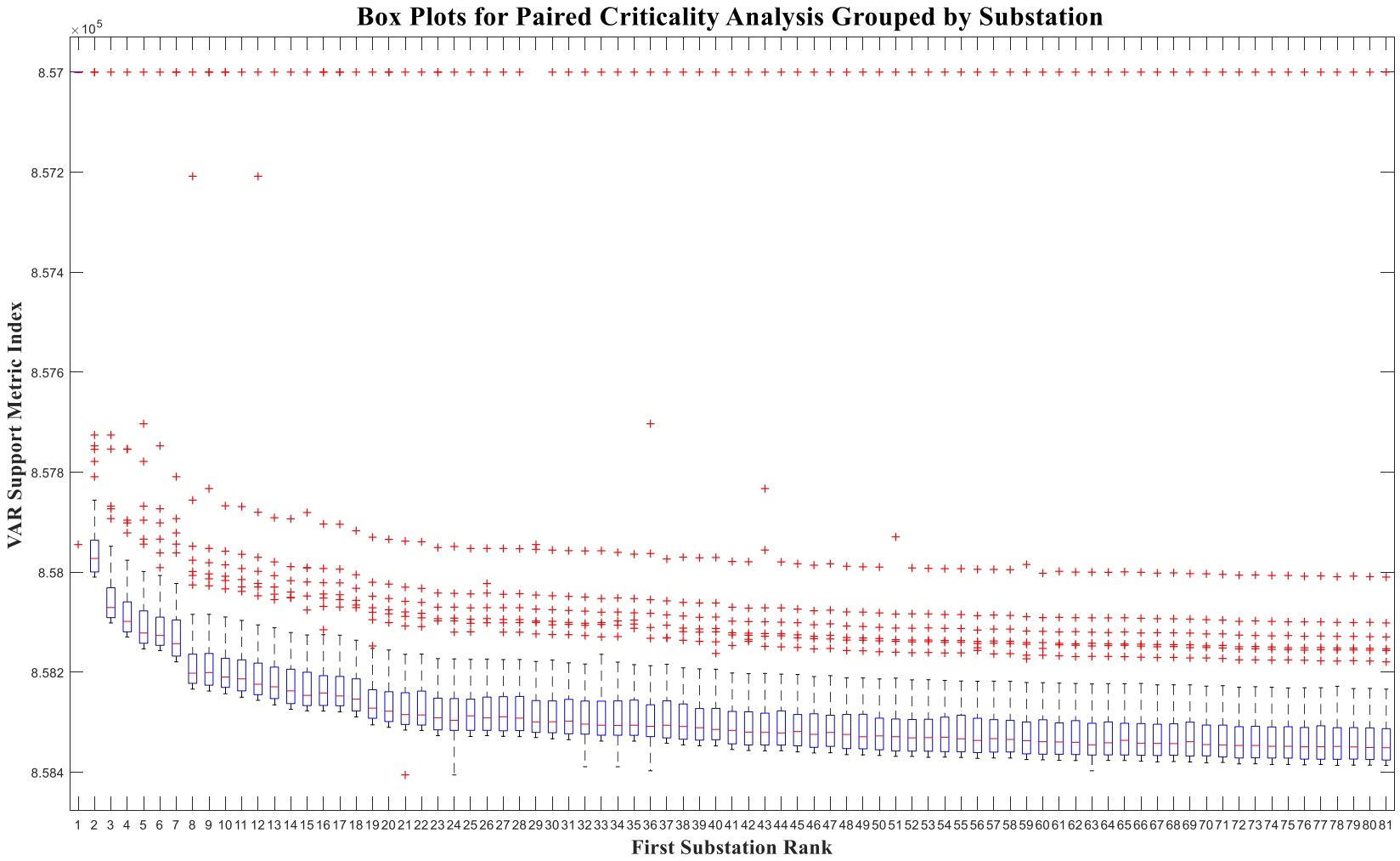

Figure 6.14. VAR support analysis box plots for paired high voltage EU substations ordered by single substation rank

Table 6.4. Summary of WECC and EI paired substation scenario convergence

Interconnection Summary	**WECC**		**EI**	
Number of Substations	292		361	
Maximum Substation Voltage	500 kV		765 kV	
Minimum Substation Voltage	345 kV		500 kV	
Total Substation Pairs	42486	100.00%	64980	100.00%
Converged Scenarios	38791	91.30%	51069	78.59%
Unconverged Scenarios	528	1.24%	1365	2.10%
Blown Up Scenarios	3167	7.45%	12546	19.31%

6.3.2 Comparison with Other Systems

Paired substation analysis is also conducted for the WECC and EI systems. In WECC, substations from 345 kV and up are considered. The cutoff voltage for the EI is set at 500 kV. Even with full Python automation, over a fortnight of simulation runtime was required. Including voltage levels down to 345 kV in the EI would have more than doubled this. A summary of scenario convergence information is provided in Table 6.4.

As with the previous analysis, scenarios that do not converge may not represent dispatch and demand patterns with no true physical solution, but system states that are difficult for the numeric solver to shift between given the specific optimization algorithm used. Unfortunately, the sheer number of scenarios prohibits manual investigation into each case per the methodology laid out in Chapter 6.2.4.

The higher percentage of unconverged and blown up cases in the U.S. analysis is fed by the overall complexity of the benchmarked U.S. models compared to the publically available EU case. This is evident both in the system as a whole, e.g., significant swathes of the EU system are aggregated for the model while the U.S. cases are fairly detailed, and from examining individual substation composition, e.g., there are no three winding transformers and few parallel transformers in the EU case, both are common in the U.S. cases. Blown up scenarios do not correlate with distance (geographic or electric) between affected substation pairs. Instead, as with the EU case, a short list of critical substations accounts for almost the entirety of these cases in both systems.

The WECC and EU analysis both return network transformers as the majority of critical points. Critical units in the EI are split almost evenly between network transformers and GSUs. This is like a reflection of network topology. The EI is heavily meshed and the loss of any given unit does not require major power flow shifts as a result. In contrast, the EU has fewer major high voltage connections and a ring around the western states with a line through the middle can approximate the WECC high voltage system. The loss of any intertie in these systems causes a more dramatic power flow shift and carries a greater risk to system reliability.

6.4 Further Combinatorial Studies

Under the scope of the FAST Act technical analysis, additional sequential studies are created based on proximity to fourteen locations, chosen for either their status as metropolitan centers or grid connection points. In each case, a focal point is chosen and LPTs are dropped from each substation in order from closest to furthest until the power flow solution diverges. While divergence of the load flow solution is not a perfect measure of true system issues, it does serve as a decent metric of developing problems. It is possible for the loss of LPTs at a single substation to lead to a divergent solution but with the methodology detailed in Chapter 6.2.4, it is possible to manually lead the algorithm to viable convergent solution states.

Figure 6.15 through Figure 6.28 present maps for each case. A red circle designates the final impact radius as measured from the central focal point for each case (marked with crosshairs) where the case ceases to converge. 500 kV substations are represented with green dots, 345 kV substations with blue dots. The loss of all LPTs within the circle is sustainable. The additional loss of LPTs at the substation (singular in all cases) located on the circle is not. Note that water features are plotted using low-resolution shape files, so boundary lines are not fully precise.

Results for all cases are summarized in **Error! Reference source not found.**. With s urvivable impact zones ranging from 13 to 200 miles containing anywhere from two to 19 individual high voltage substations, the data clearly show that no single scale or event may be utilized to assess the entire interconnection.

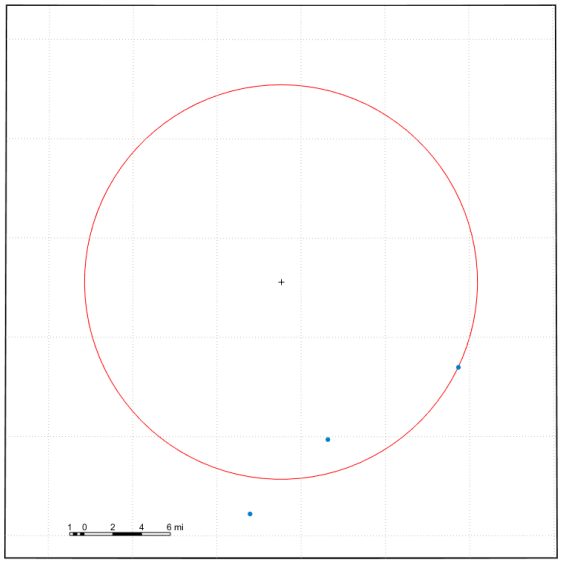

Figure 6.15. Map of Case A impact zone

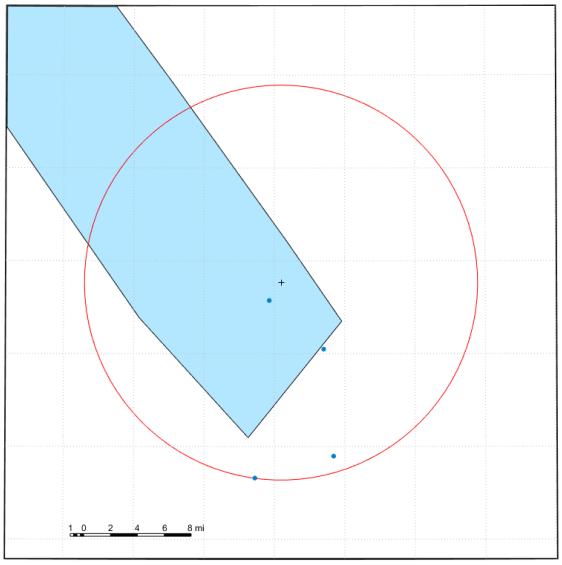

Figure 6.16. Map of Case B impact zone

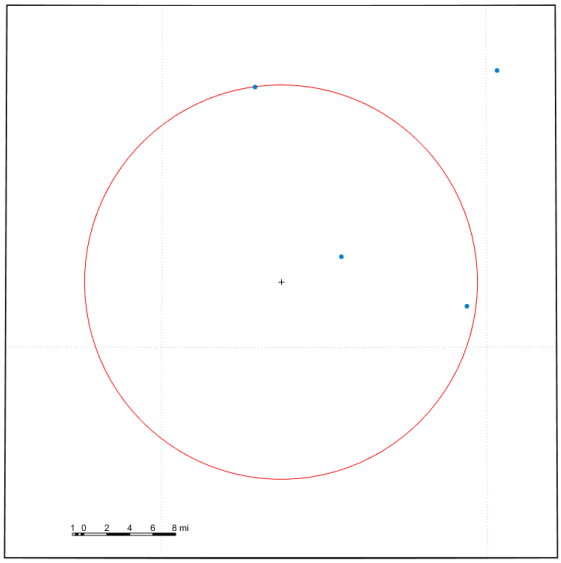

Figure 6.17. Map of Case C impact zone

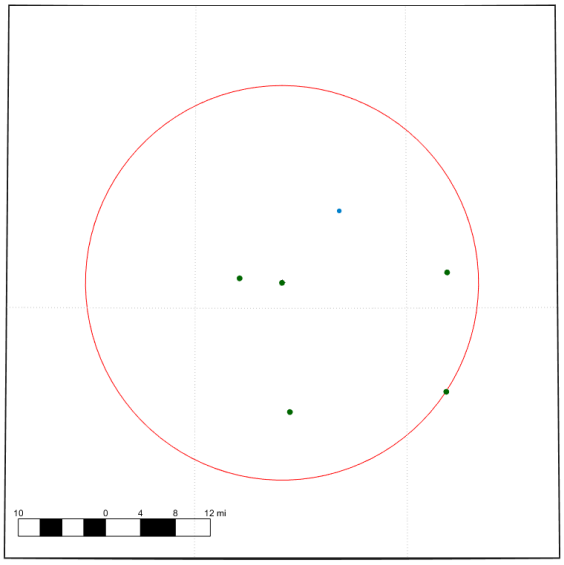

Figure 6.18. Map of Case D impact zone

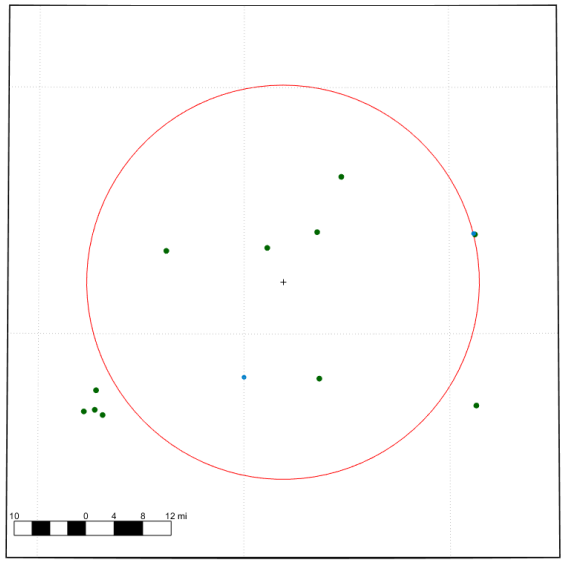

Figure 6.19. Map of Case E impact zone

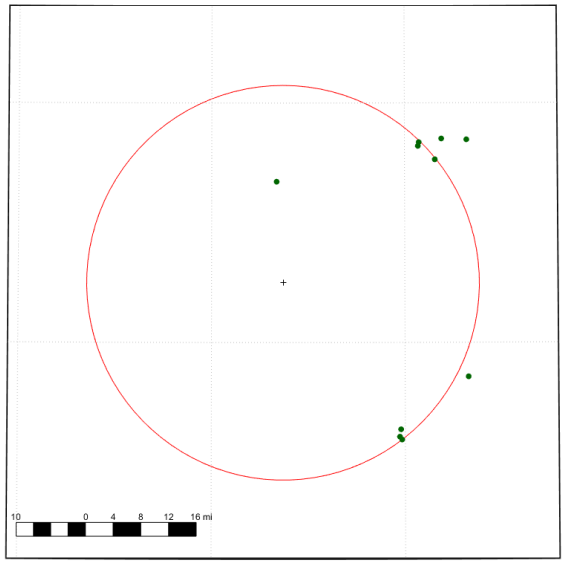

Figure 6.20. Map of Case F impact zone

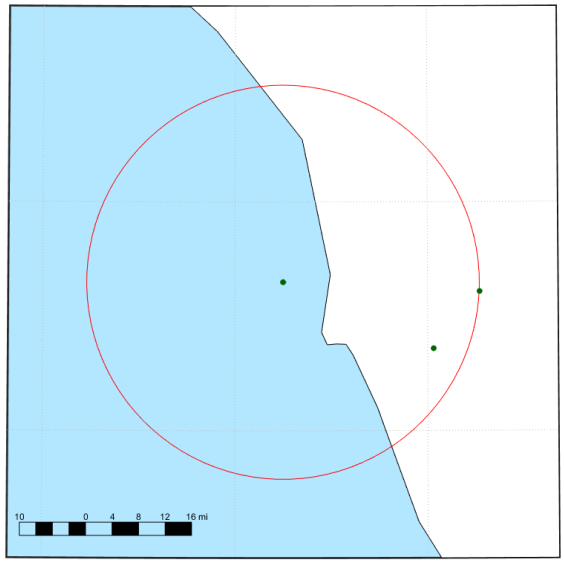

Figure 6.21. Map of Case G impact zone

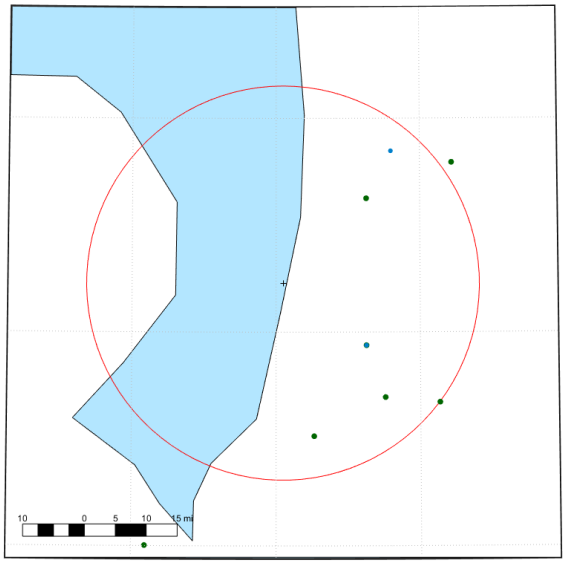

Figure 6.22. Map of Case H impact zone

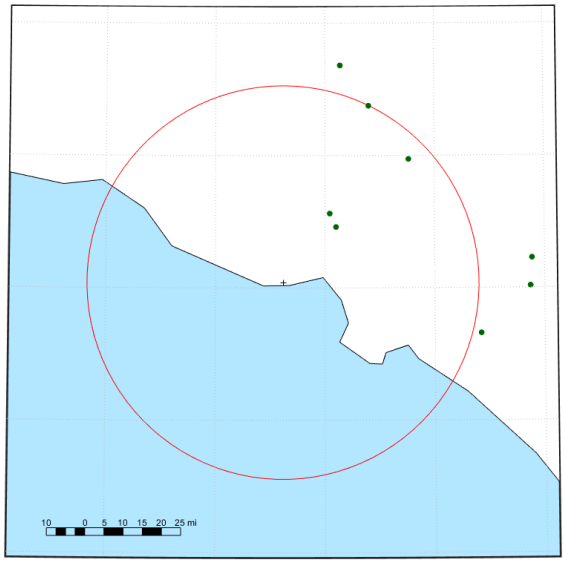

Figure 6.23. Map of Case I impact zone

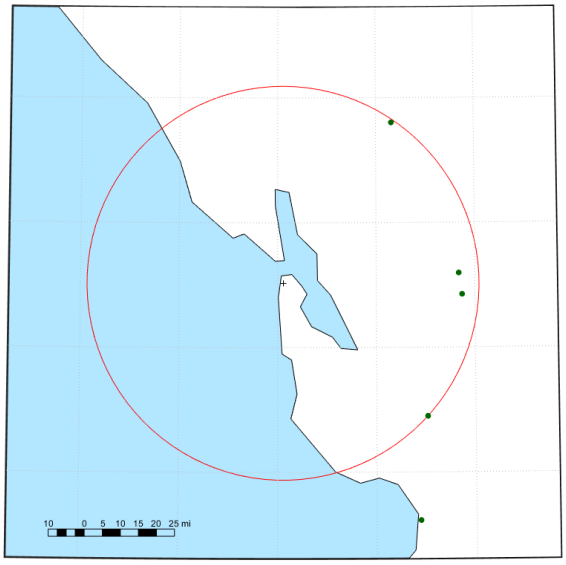

Figure 6.24. Map of Case J impact zone

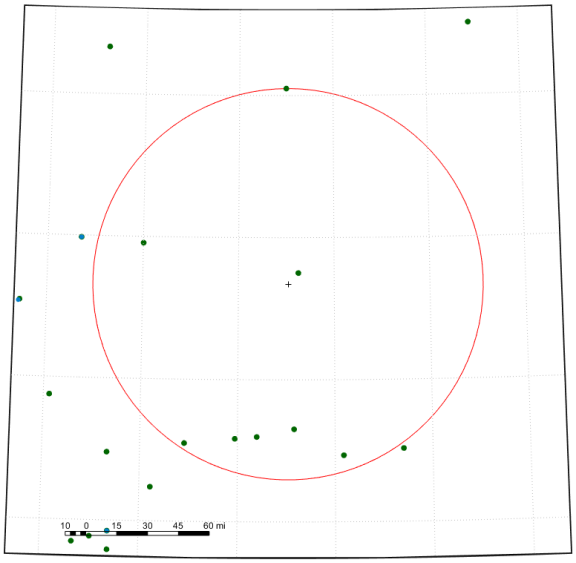

Figure 6.25. Map of Case K impact zone

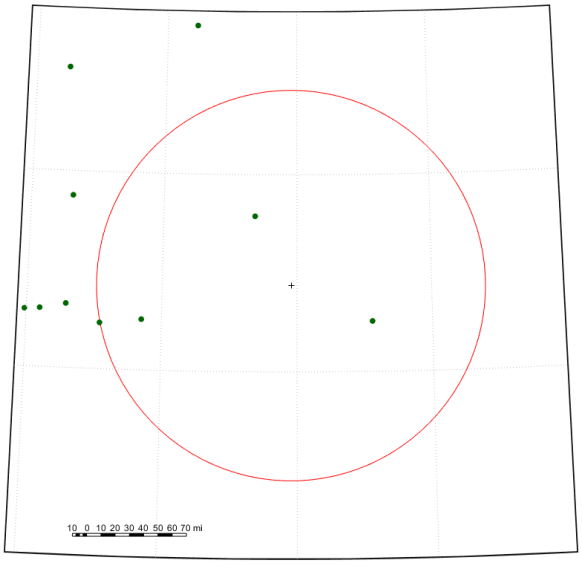

Figure 6.26. Map of Case L impact zone

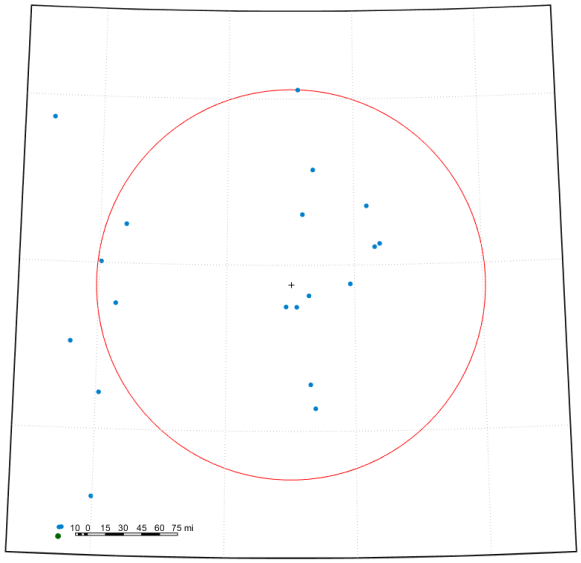

Figure 6.27. Map of Case M impact zone

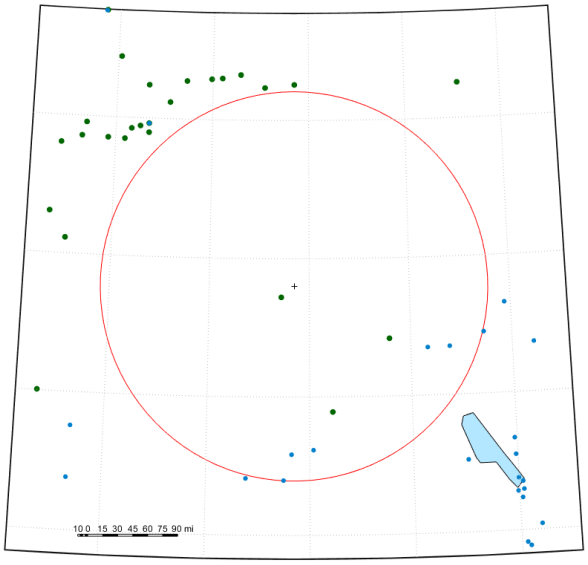

Figure 6.28. Map of Case N impact zone

Table 6.5. Proximity-based impact study results

Case	Final Radius (miles)	Substations Impacted		
		Total	500 kV	345 kV
Case A	13.7	2	0	2
Case B	14.7	4	0	4
Case C	17.1	3	0	3
Case D	22.6	6	5	1
Case E	27.6	6	4	2
Case F	28.4	8	8	0
Case G	29.7	3	3	0
Case H	31.9	9	6	3
Case I	51.2	4	4	0
Case J	54.4	4	4	0
Case K	95.1	8	8	0
Case L	136.8	4	4	0
Case M	162.0	19	0	19
Case N	194.4	8	3	5

6.5 Findings and Conclusions

The methodology presented here for ranking crucial substations and designing sequential or geography-based scenarios revealed a finite number of crucial substations that require spare transformers in the event of an interconnection-wide catastrophic event. The vast majority of transformers do not qualify as crucial. Only a small fraction—less than 10% of the total in-service fleet—receive this designation. More than 90% of these crucial transformers can be matched with donor transformers from other substation if necessary. Additional replacement options are provided by existing centrally located spare pools. Furthermore, utilities continue to improve spare transformer inventory and substation defenses as directed by NERC CIP-014 [80].

The metrics defined here are useful for broader power system resiliency analysis covering any set of elements. While both metrics must be compared to a baseline specific to the system in question as opposed to a universal constant, the analysis for individual elements accurately predicts worst-case combinatorial scenarios.

Further discussion of the findings relating to the technical analysis performed in response to the FAST Act along with analysis of topics handled by team members other than this author

such as reserve location planning and transportation logistics are discussed in the final technical report to the DOE [71].

CHAPTER 7: CONCLUSIONS AND RECOMMENDATIONS

Advancements in technology and computing have opened up areas of inquiry that were not previously accessible. Wide-area analysis can now be conducted for power system topics previously studied in highly equivalized models. This work covered two such topics.

The first was the changes in the dynamic response of the Eastern Interconnection as coal-fired plants retire. As stalwart synchronous generation with large inertia constants, the loss of traditional coal carries the potential to weaken the grid. Replacing these units with natural gas, per federal filings in 2012 anticipating the 2017 grid does show this effect, but at a slight enough difference to be considered as a non-issue.

Replacing traditional synchronous generation with non-synchronous sources, e.g., solar photovoltaics and wind turbines, is a different story. The loss of generator controls inherent to present day renewable installations exacerbates dynamic response degradation. As renewable sources replace coal units, inertia should be added to the system, either organically or artificially, to account for retiring synchronous generators. Stability standards should also require renewable units to provide control actions as the share of system demand they meet increases. Losing turbine governor and voltage exciter controls causes just as significant an impact as the loss of system inertia.

The second topic was the methodology required to assess high-impact events with the potential to effect an entire interconnection. The need for such methodology was clearly demonstrated with the development of the GMD model for DVP's transmission network. The results of that analysis clearly show that the traditional equivalisation of systems down to a single generator, step-up transformer, and infinite bus (representing the rest of the system) cannot accurately capture the interaction of harmonic currents injected due to transformer saturation across a large area. Assessing the impact of solar flares and other geomagnetic events requires wide-area models and analysis. In Virginia, given a hundred year solar storm, the bus voltage THD across the system is high enough to notice, but low enough not to be a major concern.

The need to advance existing techniques was then shown, specifically when discussing HEMP E1. At this time, un-classified HEMP models do not provide a complete enough picture to determine what the result of a given detonation will be. Even knowing the area of effect,

potential impacts from distribution flashover can range from a small loss of load to wide-area cascading failures.

Finally, an event agnostic methodology for interconnection-wide security assessments was developed. Two metrics were presented, the first reliant on real power concerns, the second on voltage support capability. Together these allow criticality ranking of any individual or combinations of elements in a system, providing a framework for identifying lapses in backup equipment. The process for this is presented in generic form, but was conducted specifically for large power transformers per the mandate of the FAST Act. These metrics function as a measure of system resiliency against any given event. Result patterns are consistent in both industry benchmarked EI and WECC model as well as the EU case provided by MATPOWER.

7.1 Future Work

Further investigation into dynamic response implications of transitioning from traditional synchronous generators to non-synchronous renewable sources requires wind turbine and solar photovoltaic models that do not introduce numerical instability into dynamic power system solvers. This is a known issue for PSS®E simulations of high-density renewable scenarios. A solution to this problem would allow for greater simulation fidelity.

Dominion's service territory is located further south than most solar flares reach. Repeating the wide-area analysis methodology used to assess Virginia with a system in New England or Canada may produce interesting results and discussion.

As ORNL refined HEMP models, electric power grid impact analysis should be revised. Further detail on the waveform produced by the initial detonation and the inclusion of system protection in grid simulations are both desirable.

The two security assessment metrics, incremental transfer capability and VAR generation headroom, act as measures of system resiliency. The methodology presented here can be extended to elements beyond large power transformers as well as more complex event scenarios. The scripting tools created during this project may be further developed to this end.

REFERENCES

[1] H. Saadat, “The power system and electric power generation,” in Power System Analysis, 3rd ed. Alexandria, VA: PSA Publishing, LLC, 2010, ch. 1, pp. 1-52.
[2] M. Amin, “North America’s electricity infrastructure: are we ready for more perfect storms?,” *IEEE Security & Privacy*, vol. 1, no. 5, pp. 19-25, 2003.
[3] NERC, “Key players,” North American Electric Reliability Corporation, Atlanta, GA, 2016. Available: http://www.nerc.com/AboutNERC/keyplayers/Pages/default.aspx [Accessed Sep. 2, 2016].
[4] NERC, “Bulk electric system (BES) definition, notification, and exception process,” North American Electric Reliability Corporation, Atlanta, GA, 2016. Available: http://www.nerc.com/pa/RAPA/Pages/BES.aspx [Accessed Sep. 2, 2016].
[5] ReliabilityFirst, “MMWG,” ReliabilityFirst Corporation, Cleveland, OH, Aug. 2016. Available: https://rfirst.org/reliability/easterninterconnectionreliabilityassessmentgroup/mmwg/Pages/default.aspx [Accessed Sep. 2, 2016].
[6] EIA, “U.S. energy outlook 2016,” U.S. Department of Energy, Jun. 2016, data table A9. Available: http://www.eia.gov/forecasts/aeo/data/browser/#/?id=9-AEO2016&cases=ref2016~ref_no_cpp&sourcekey=0 [Accessed Aug. 29, 2016].
[7] H. Saadat, “Power flow analysis,” in *Power System Analysis*, 3rd ed. Alexandria, VA: PSA Publishing, LLC, 2010, ch. 6, pp. 228-295.
[8] H. Saadat, “Power system control,” in *Power System Analysis*, 3rd ed. Alexandria, VA: PSA Publishing, LLC, 2010, ch. 12, pp. 566-624.
[9] P. N. Markham, “Data mining and machine learning applications of wide-area measurement data in electric power systems,” Ph.D. dissertation, EECS, UTK, Knoxville, TN, 2012.
[10] J. J. Conti *et al.*, “Annual energy outlook 2012,” U.S. Department of Energy, Nov. 2012.
[11] EPA, “Cross-state air pollution rule (CSAPR),” U.S. Environmental Protection Agency, Feb. 2016. Available: https://www3.epa.gov/airtransport/CSAPR/ [Accessed Aug. 29, 2016].
[12] EPA, “Basic information about mercury and air toxic standards,” U.S. Environmental Protection Agency, Jun. 2016. Available: https://www.epa.gov/mats/basic-information-about-mercury-and-air-toxics-standards [Accessed Aug. 29, 2016].
[13] Supreme Court of the United States, “Massachusetts et al. v. Environmental Protection Agency et al.,” Oct. 2006. Available: https://www.supremecourt.gov/opinions/06pdf/05-1120.pdf [Accessed Aug. 29, 2016].
[14] EPA, “Carbon pollution emission guidelines for existing stationary sources: electric utility generating units,” Federal Register, vol. 80, no. 205, book 2, pp. 64,661-65,120, Oct. 2015.
[15] Supreme Court of the United States, “Order list: 577 U.S.,” Feb. 2016.

[16] “Clean Power Plan case resources,” Environmental Defense Fund, 2016. Available: https://www.edf.org/climate/clean-power-plan-case-resources [Accessed Aug. 29, 2016].
[17] C. Davenport, “Fighting Obama’s climate plan, but quietly preparing to comply,” The New York Times, Jul. 19, 2016. Available: http://www.nytimes.com/2016/07/20/us/obama-clean-power-plan.html [Accessed Aug. 29, 2016].
[18] EIA "Annual Electric Generator Report," U.S. Energy Information Administration., Available: http://www.eia.gov/cneaf/electricity/page/eia860.html [Accessed Aug. 29, 2016].
[19] "U.S. Commercial Nuclear Power Reactors," U.S N.R. Agency, Washington, D.C.
[20] "2008–2017 Regional & National Peak Demand and Energy Forecasts Bandwidths," North American Electric Reliability Corporation, Princeton, NJ, August 2008.
[21] “The nuclear renaissance,” World Nuclear Organization, Sep. 2015. Available: http://www.world-nuclear.org/information-library/current-and-future-generation/the-nuclear-renaissance.aspx [Accessed Aug. 29, 2016].
[22] "Expected new nuclear power plant applications," Nuclear Regulatory Commission, Washington, D.C., Oct. 2011.
[23] E. Marcum, "NRC sets meeting on delayed Watts Bar reactor," *Knoxville News-Sentinel*, Apr. 6, 2012. Available: http://www.knoxnews.com/news/2012/apr/06/tva-says-watts-bar-construction-to-cost-more/ [Accessed Aug. 29, 2016].
[24] F. Vanek *et al.*, *Energy Systems Engineering*, 2nd ed., USA: McGraw-Hill, 2012, pp. 140-141.
[25] S. Brooks, “TVA dedicates Magnolia combined cycle gas power plant,” *TVA News Release*, Aug. 14, 2012. Available: http://www.tva.com/news/releases/julsep12/magnolia.html. [Accessed Oct. 10, 2012].
[26] G. W. Cauley *et al.*, “Comments of the North American Electric Reliability Corporation following September 23 frequency response technical conference,” NERC, Washington, D.C., Docket Nos. RM06-16-010, RM06-16-011, 2010.
[27] ERAG, “MMWG,” Aug. 2016. Available: https://rfirst.org/reliability/easterninterconnectionreliabilityassessmentgroup/mmwg/Pages/default.aspx [Accessed Aug. 29, 2016].
[28] E. Williams, J. Hensley, and E. Salerno, “AWEA U.S wind industry annual market report year ending 2012,” AWEA, Washington, D.C., 2012.
[29] DOE, “Wind vision: a new era for wind power in the United States,” U.S. Department of Energy, Mar. 2015. Available: http://energy.gov/sites/prod/files/2015/03/f20/wv_full_report.pdf [Accessed Aug. 31, 2016].
[30] “20% wind energy by 2030,” U.S. Department of Energy, Oak Ridge, TN, DOE/GO-102008-2567, 2008.

[31] A. Mullane, G. Lightbody, and R. Yacamini, "Wind-turbine fault ride-through enhancement", *IEEE Trans. on Power Systems*, 20(4): 1929-1937, 2005.

[32] E. Muljadi, C. P. Butterfield, J. Chacon, and H. Romanowitz, "Power quality aspects in a wind power plant", in *IEEE PES General Meeting*, 2006.

[33] A. Causebrook, D. J. Atkinson, and A. G. Jack, "Fault ride-through of large wind farms using series dynamic braking resistors", *IEEE Trans. on Power Systems* 22(3): 966-975, 2007.

[34] A. Abrantes, "Overview of power quality aspects in wind generation", in *North American Power Symposium (NAPS)*, pp. 1-6, 2012.

[35] K. Shanthini, and N. Verappan, "Power quality enhancement of wind generators connected to grid", in *International Conference on Emerging Trends in Electrical Engineering and Energy Management (ICETEEEM)*, pp. 398-403, 2012.

[36] G. Lalor, A. Mullane, and M. O'Malley, "Frequency control and wind turbine technologies," *IEEE Trans. on Power Systems*, vol. 20, no. 4, pp. 1905-1913, Nov. 2005.

[37] J. Villena-Lapaz, A. Vigueras-Rodriguez, E. Gomez-Lazaro, A. Molina-Garcia, and J. A. Fuentes-Monerno, "Evaluation of frequency response of variable speed wind farms for reducing stability problems in weak grids", in *Power Electronics and Machines in Wind Applications (PEMWA)*, pp. 1-5, 2011.

[38] L. Ruttledge, N. W. Miller, J. O'Sullivan, and D. Flynn, "Frequency response of power systems with variable-speed wind turbines", *IEEE Trans. on Sustainable Energy*, 3(4): 683-691, 2012.

[39] J. E. S. de Haan, J. Frunt, and W. L. Kling, "Grid frequency response of different sized wind turbines", in *Universities' Power Engineering Conference (UPEC)*, pp. 1-6, 2011.

[40] J. G. Slootweg and W. L. Kling, "The impact of large scale wind power generation on power system oscillations", *Electric Power Systems Research*, 67(1): 9-20, 2003.

[41] N. W. Miller, M. Shao, S. Venkataraman, C. Loutan, and M. Rothleder, "Frequency response of California and WECC under high wind and solar conditions", in *IEEE PES General Meeting*, pp. 1-8, 2012.

[42] P. Mackin, R. Daschmans, B. Williams, B. Haney, R. Hunt, J. Ellis, and J. H. Eto, "Dynamic simulation study of the frequency response of the Western Interconnection with increased wind generation", in *International Conference on System Sciences (HICSS)*, pp. 2222-2229, 2013.

[43] Micah J. Till, Yong Liu, Yilu Liu, Mahendra Patel, and Thomas King, "Frequency response of the Eastern Interconnection due to increased wind generation," *IEEE PESGM 2014*, Washington D.C., vol. 1, no. 5, pp. 27-31, Jul. 2014.

[44] Y. Liu, "Wide-area measurement and applications in power system dynamic modeling and control," Ph.D. dissertation, EECS, UTK, Knoxville, TN, 2013.

[45] H. Saadat, "Stability," in *Power System Analysis*, 3rd ed. Alexandria, VA: PSA Publishing, LLC, 2010, ch. 11, pp. 499-565.

[46] S Lu, Y. Liu, and J. De La Ree, "Harmonics generated from a DC biased transformer," *IEEE Trans. on Power Delivery*, vol. 8, no. 2, pp. 725-731, Apr. 1993.
[47] J. Yao *et al.*, "Harmonics and reactive power of power transformers with DC bias," *APPEEC*, Chengdu, 2010, pp. 1-4.
[48] R. A. Walling and A. N. Khan, "Characteristics of transformer exciting-current during geomagnetic disturbances," *IEEE Trans. on Power Delivery*, vol. 6, no. 4, pp. 1707-1714, Oct. 1991.
[49] E. Bernabeu, "Single-phase transformer harmonics produced during geomagnetic disturbances: theory, modeling, and monitoring," *IEEE Trans. on Power Delivery*, vol. 30, no. 3, pp. 1323-1330, Jun. 2015.
[50] E. Bernabeu, M. Baldwin, and M. J. Till, "Harmonic load flow during geomagnetic disturbances," *Cigre Science & Engineering*, vol. N°3, pp. 5-14, Oct. 2015.
[51] R. D. Christie, "Power systems test case archive," University of Washington, Seattle, WA, Available: http://www2.ee.washington.edu/research/pstca/pf14/pg_tca14bus.htm [Accessed Jan. 23, 2016].
[52] "Modeling and simulation of the propagation of harmonics in electric power networks. I. Concepts, models, and simulation techniques," Power Delivery, IEEE Transactions on, vol. 11, no. 1, pp. 452-465, Jan. 1996.
[53] A. Pulkkinen *et al.*, "Generation of 100-year geomagnetically induced current scenarios," *Space Weather*, vol. 10, no. 4, Apr. 2012.
[54] A. Pulkkinen *et al.*, "Regional-scale high-latitude extreme geoelectric fields pertaining to geomagnetically induced currents," *Earth, Planets and Space*, Jun. 2015.
[55] E. Bernabeu, "Modeling geomagnetically induced currents in Dominion Virginia Power using extreme 100-year geoelectric field scenarios—Part 1," *IEEE Trans. on Power Delivery*, vol. 28, no. 1, pp. 516-523, Jan. 2013.
[56] "TPL-007-1 — transmission system planning performance during geomagnetic disturbances," North American Electric Reliability Corporation, Atlanta, GA, Dec. 2014. Available: http://www.nerc.com/pa/Stand/Pages/Project-2013-03-Geomagnetic-Disturbance-Mitigation.aspx [Accessed Sep. 5, 2016].
[57] C. N. Vittitoe, "Did high-altitude EMP cause the Hawaiian streetlights incident?," Sandia National Laboratories, Albuquerque, N.M., SAND88-0043C, Jan. 1988.
[58] R. Sherman, EMP Engineering and Design Principles, Whippany, NJ: Bell Telephone Laboratories, Technical Publication Dept., 1975
[59] E. Savage, J. Gilbert, and W. Radasky, "The early-time (E1) high-altitude electromagnetic pulse (HEMP) and its impact on the U.S. power grid," Metatech Corporation, Goleta, CA, Meta-R-320, Jan. 2010.
[60] J. S. Foster, Jr. *et al.*, "Report of the commission to assess the threat to the United States from electromagnetic pulse (EMP) attack: volume 1: executive report," Commission to

Assess the Threat to the United States from Electromagnetic Pulse (EMP) Attack, McLean, VA, 2004.

[61] J. S. Foster, Jr. *et al.,* "Report of the commission to assess the threat to the United States from electromagnetic pulse (EMP) attack: critical national infrastructures," Commission to Assess the Threat to the United States from Electromagnetic Pulse (EMP) Attack, McLean, VA, Apr. 2008.

[62] C. L. Longmire, R. M. Hamilton, and J. M. Hahn, "A nominal set of high-altitude EMP environments," ORNL, Oak Ridge, TN, ORNL/Sub/86- 184 1711, Feb. 1987.

[63] P. R. Barnes, B. W. McConnell, and J. W. Van Dyke, "Electromagnetic pulse research on electric power systems: program summary and recommendations," ORNL, Oak Ridge, TN, ORNL-6708, May 1992.

[64] J. R. Legro *et al.*, "Study to assess the effects of electromagnetic pulse on electric power systems phase I - final report," ORNL, Oak Ridge, TN, ORNL/Sub/83-43374/1/V2, Feb. 1986.

[65] F. M. Tesche and P. R. Barnes, "The HEMP response of an overhead power distribution line," *IEEE Trans. on Power Delivery*, vol. 4, no. 3, pp. 1937-1944, Jul 1989.

[66] V. Kruse, P. R. Barnes, and F. M. Tesche, "Flashover vulnerability of transmission and distribution lines to high altitude electromagnetic pulse," *IEEE Trans. on Power Delivery,* vol. 5 no. 2, pp. 1164-1169, Apr. 1990.

[67] P. D. Ewing *et al.*, "Methodologies of assessing the impact of a high-altitude electromagnetic pulse on the electric power grid," ORNL, Oak Ridge, TN, ORNL/TM-2015/777, unpublished.

[68] G. Kou, "Dynamic modeling and renewable integration studies on the U.S. power grids," Ph.D. dissertation, EECS Dept., University of Tennessee, Knoxville, TN, 2016.

[69] United States Congress, *Fixing America's Surface Transportation Act*, 114th Congress, 1st Session, Res. 22, Dec. 2015.

[70] R. Smith, "Assault on California power station raises alarm on potential for terrorism," *The Wall Street Journal*, New York, NY, Feb. 5, 2014.

[71] J. Gracia *et al.*, "Technical assessment of the need for a strategic reserve of large power transformers," ORNL, Oak Ridge, TN, ORNL/TM-2016/755, under review.

[72] "TPL-001-4 — transmission system planning performance requirements," North American Electric Reliability Corporation, Atlanta, GA, Dec. 2014.

[73] "Feasibility studies and interchange transaction analysis" in *Program Application Guide: Volume I*, PSS®E 33.8, Schenectady, NY: Siemens Industry, Inc., 2016, ch. 7.9, pp. 7-32 to 7-35.

[74] "Overview: transmission transfer limit analysis" in *Program Operation Manual*, PSS®E 33.8, Schenectady, NY: Siemens Industry, Inc., 2016, ch. 8.7.1, pp. 8-56 to 8-57.

[75] "Building the distribution factor data file" in *Program Operation Manual*, PSS®E 33.8, Schenectady, NY: Siemens Industry, Inc., 2016, ch. 8.1, pp. 8-1 to 8-23.

[76] "Calculating transmission interchange limits" in *Program Operation Manual*, PSS®E 33.8, Schenectady, NY: Siemens Industry, Inc., 2016, ch. 8.7, pp. 8-56 to 8-70.
[77] "aMachReal" in *PSS®E Application Program Interface (API)*, PSS®E 33.8, Schenectady, NY: Siemens Industry, Inc., 2016, ch. 8.5.3, pp. 8-25 to 8-27.
[78] R. D. Zimmerman *et al.*, "MATPOWER: a MATLAB power system simulation package," Dec. 16, 2016, Available: http://www.pserc.cornell.edu/matpower/ [Accessed: Jan. 25, 2017].
[79] C. Josz *et al.*, "AC power flow data in MATPOWER and QCQP format: iTesla, RTE snapshots, and PEGASE," arXiv, Ithaca, NY, Mar. 20, 2016, Available: http://arxiv.org/abs/1603.01533v3 [Accessed: Jan. 25, 2017].
[80] "CIP-014-02 — physical security," North American Electric Reliability Corporation, Atlanta, GA, May 2015.

APPENDICES

APPENDIX A: FUEL TRANSITION SIMULATION RESULTS

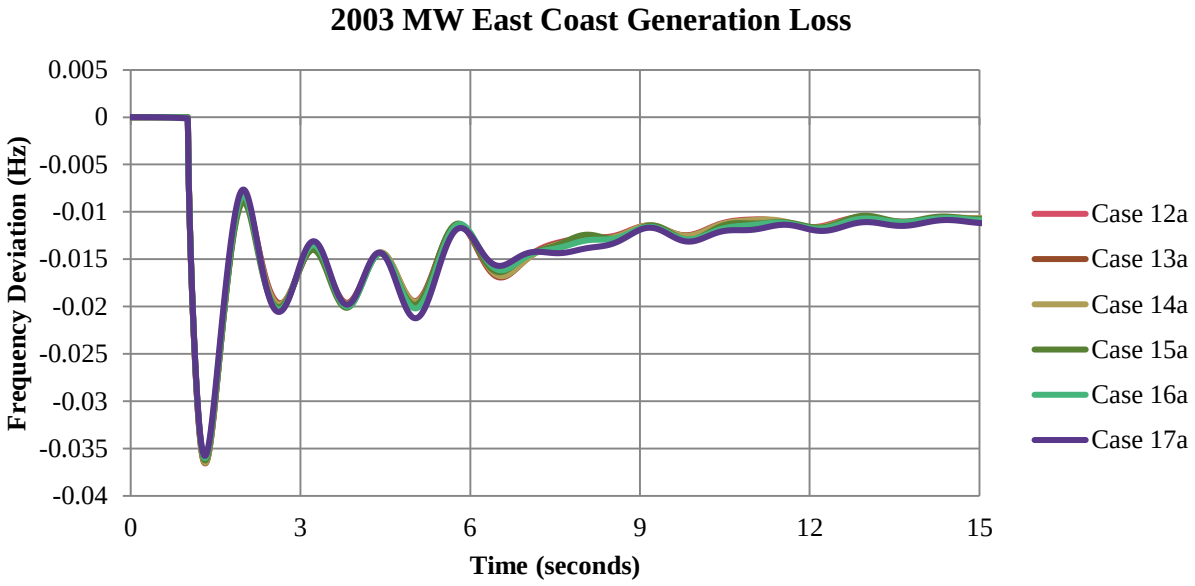

Figure A.1. Base case frequency response for 2003 MW east coast generation loss

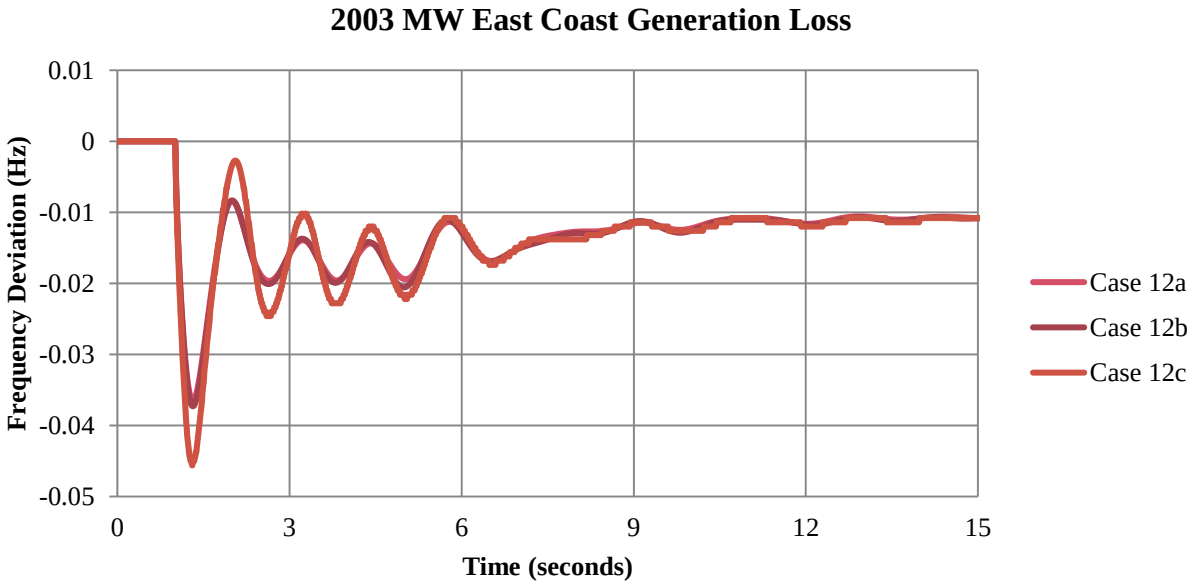

Figure A.2. Year 2012 frequency response for 2003 MW east coast generation loss

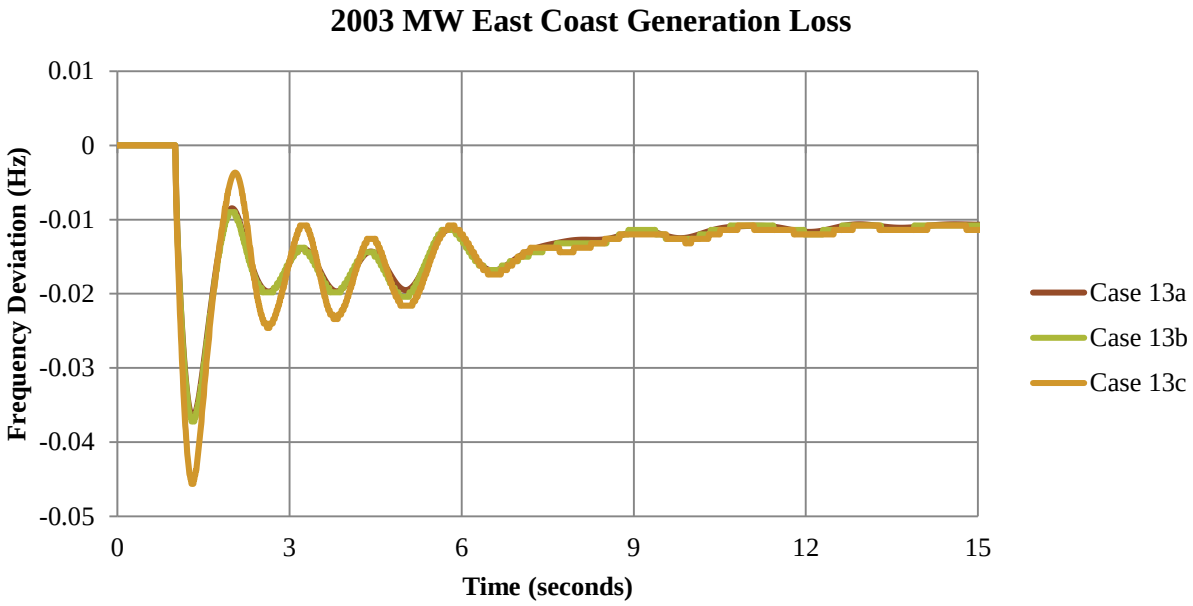

Figure A.3. Year 2013 frequency response for 2003 MW east coast generation loss

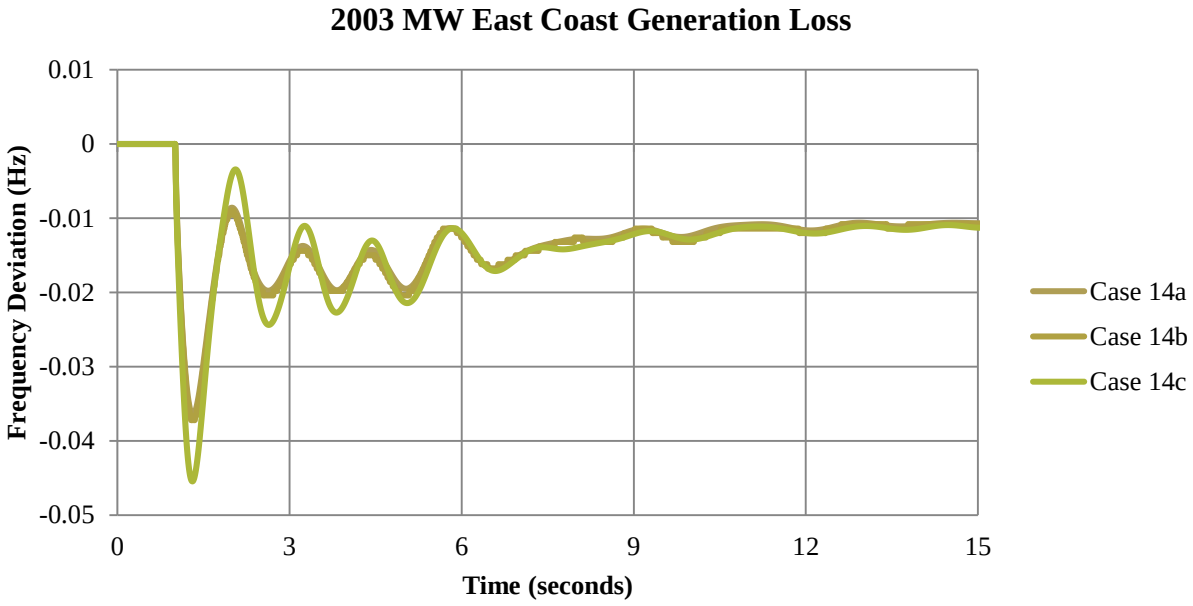

Figure A.4. Year 2014 frequency response for 2003 MW east coast generation loss

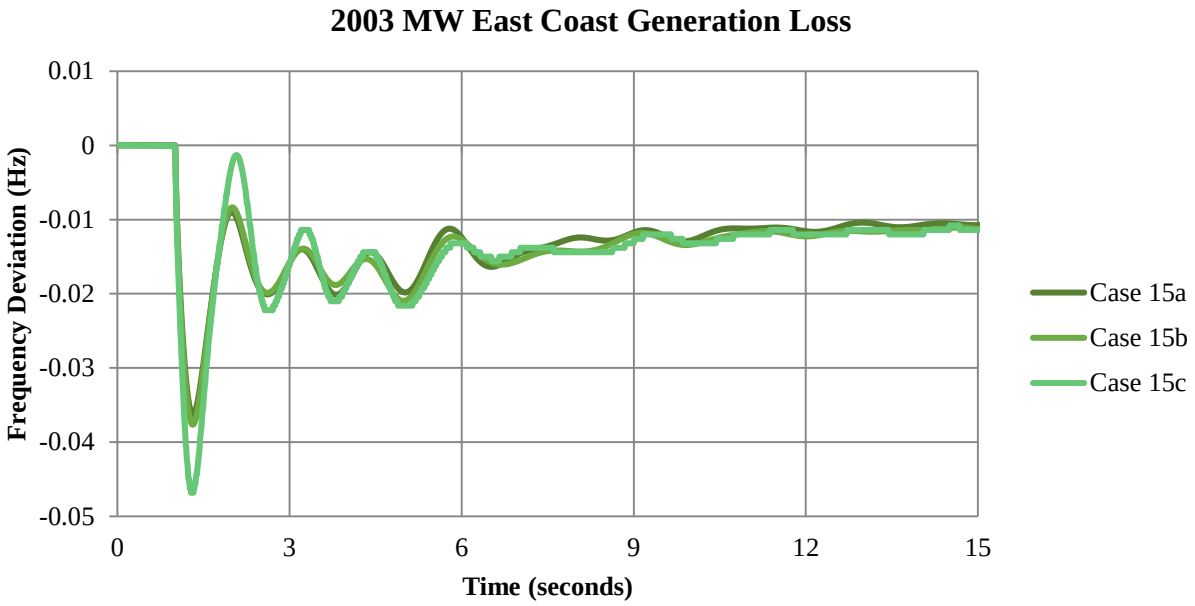

Figure A.5. Year 2015 frequency response for 2003 MW east coast generation loss

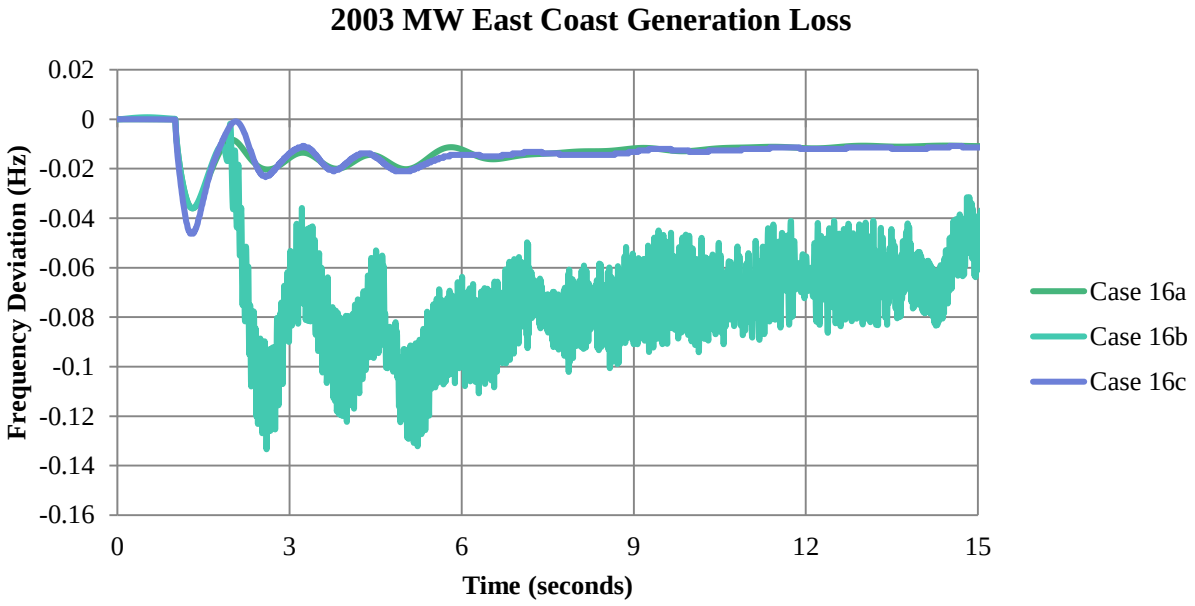

Figure A.6. Year 2016 frequency response for 2003 MW east coast generation loss

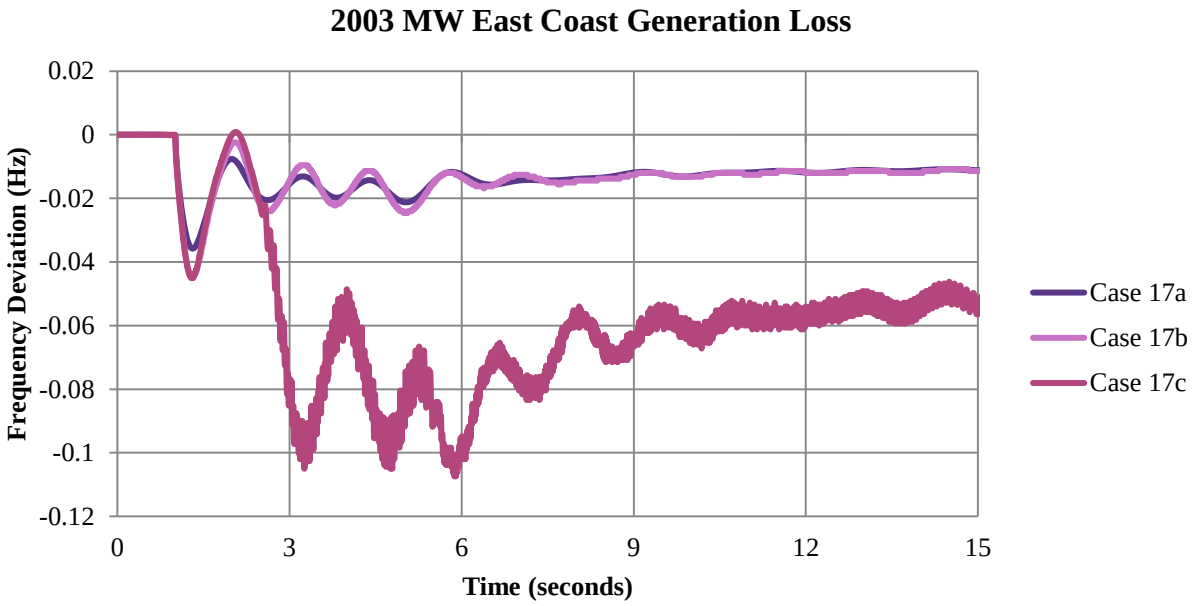

Figure A.7. Year 2017 frequency response for 2003 MW east coast generation loss

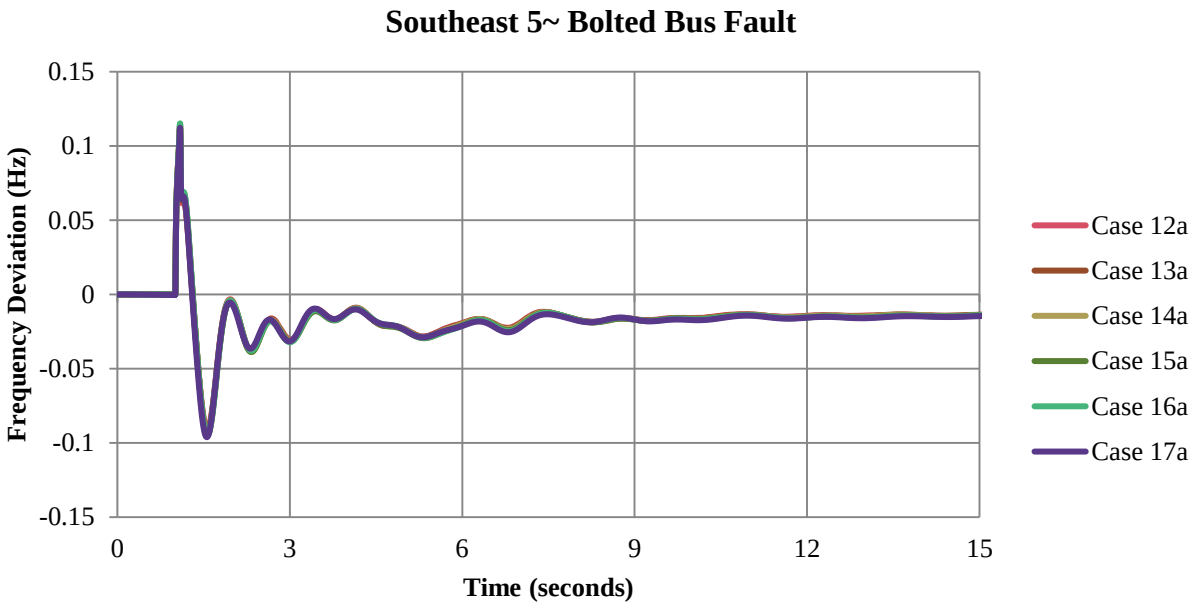

Figure A.8. Base case frequency response for 5~ southeast bolted bus fault

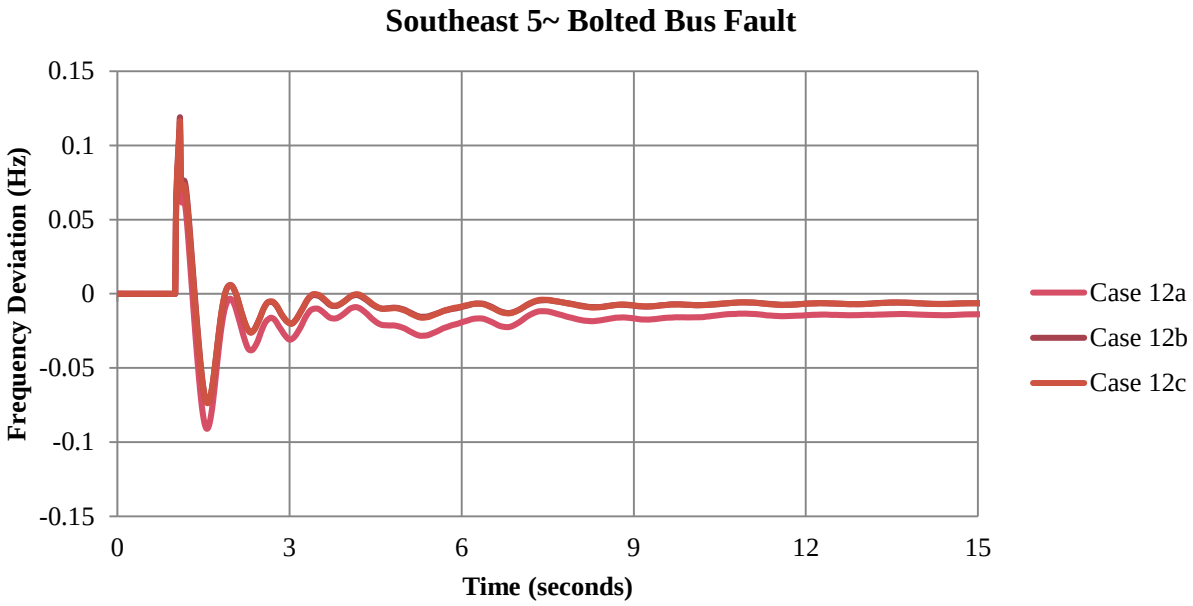

Figure A.9. Year 2012 frequency response for 5~ southeast bolted bus fault

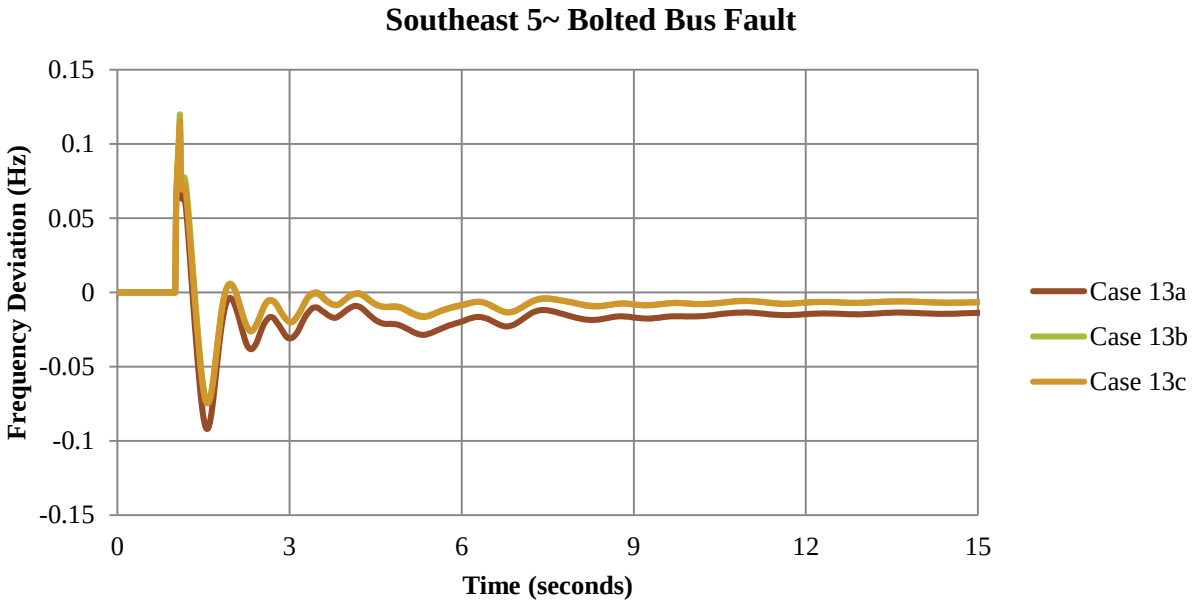

Figure A.10. Year 2013 frequency response for 5~ southeast bolted bus fault

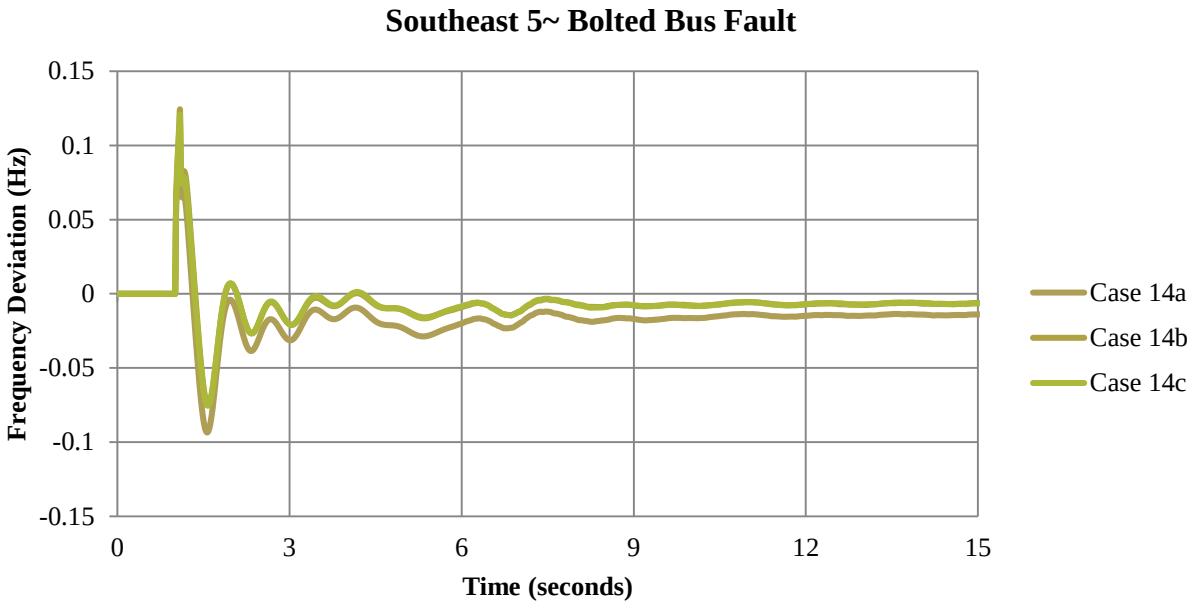

Figure A.11. Year 2014 frequency response for 5~ southeast bolted bus fault

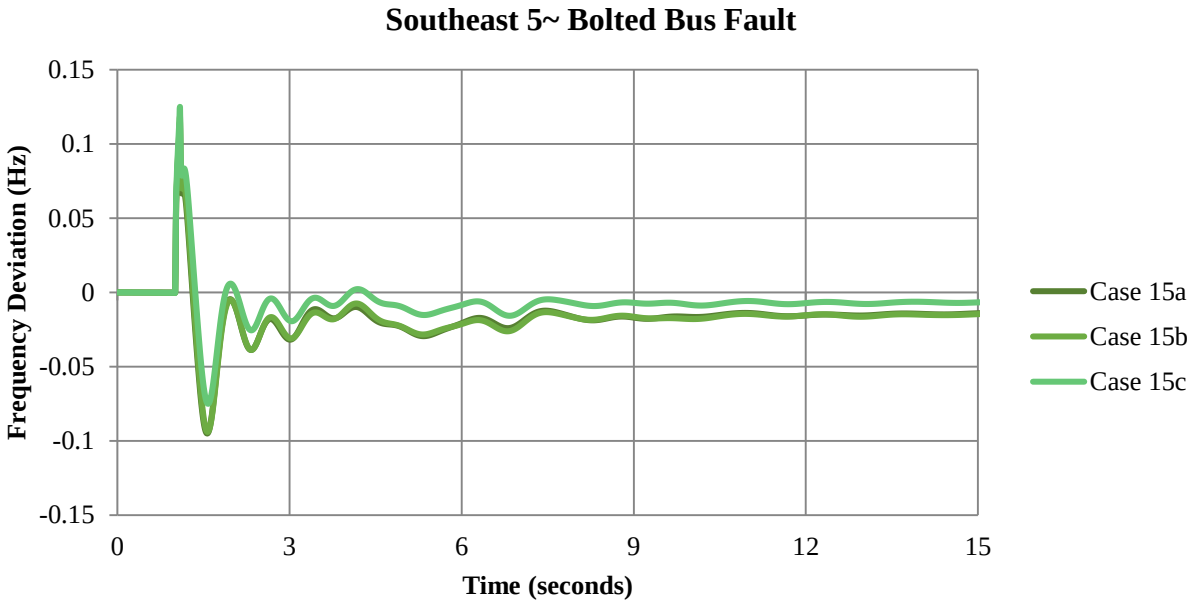

Figure A.12. Year 2015 frequency response for 5~ southeast bolted bus fault

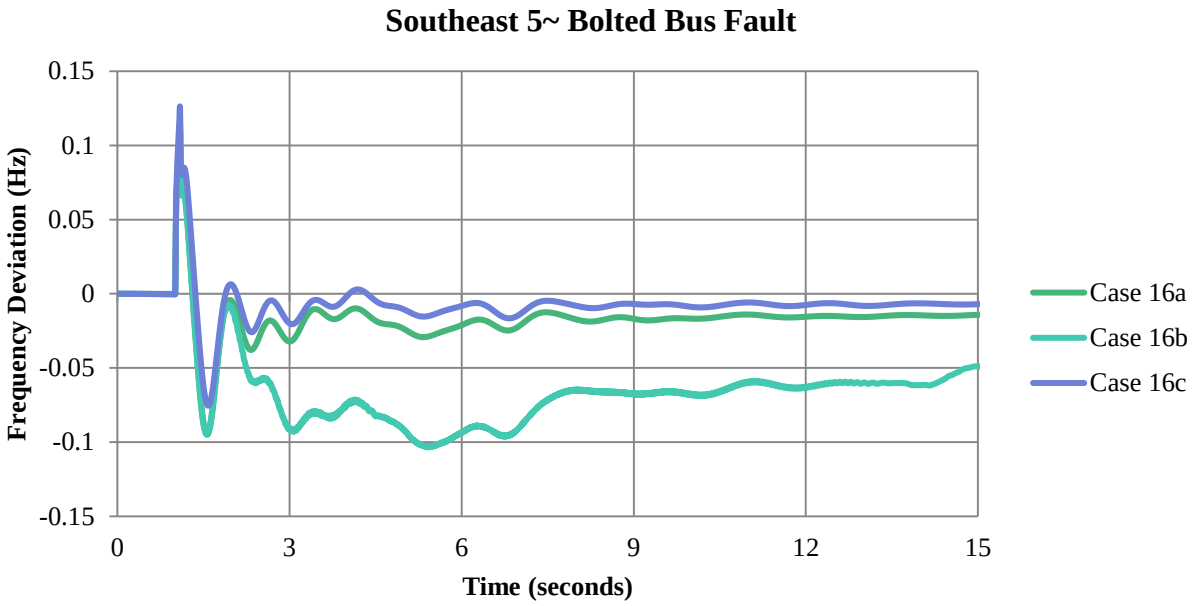

Figure A.13. Year 2016 frequency response for 5~ southeast bolted bus fault

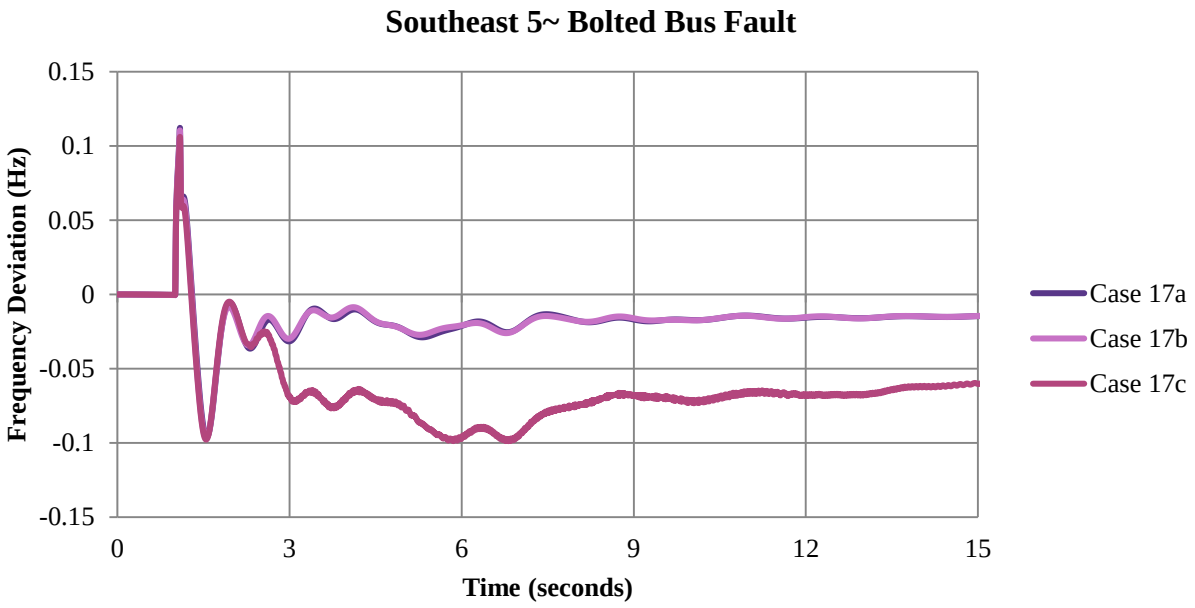

Figure A.14. Year 2017 frequency response for 5~ southeast bolted bus fault

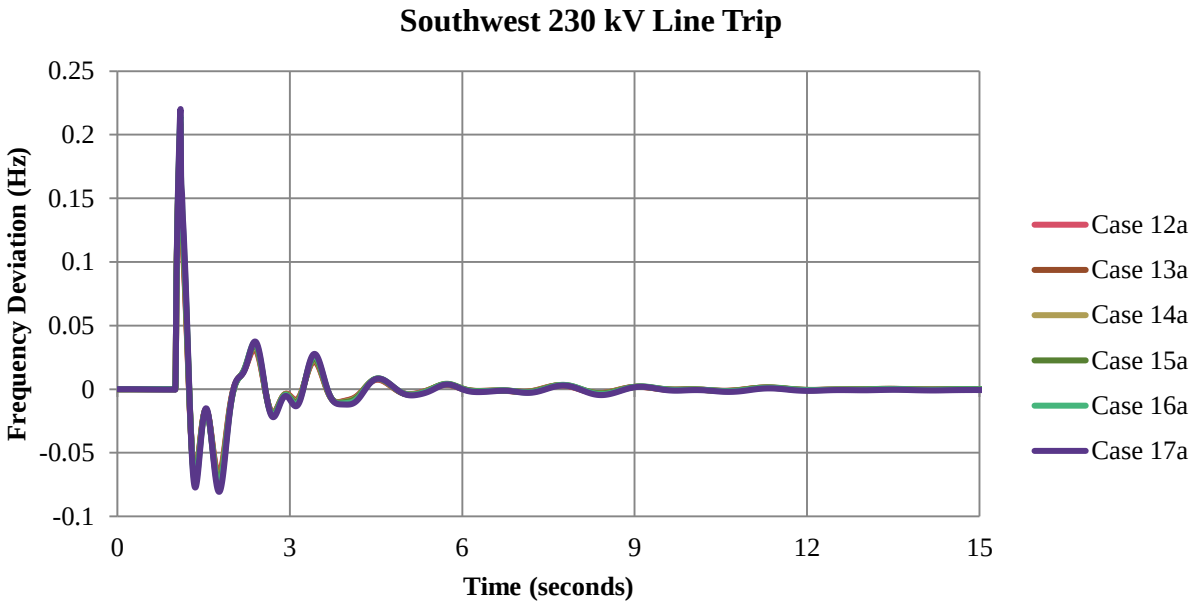

Figure A.15. Base case frequency response for southwest 230 kV line trip

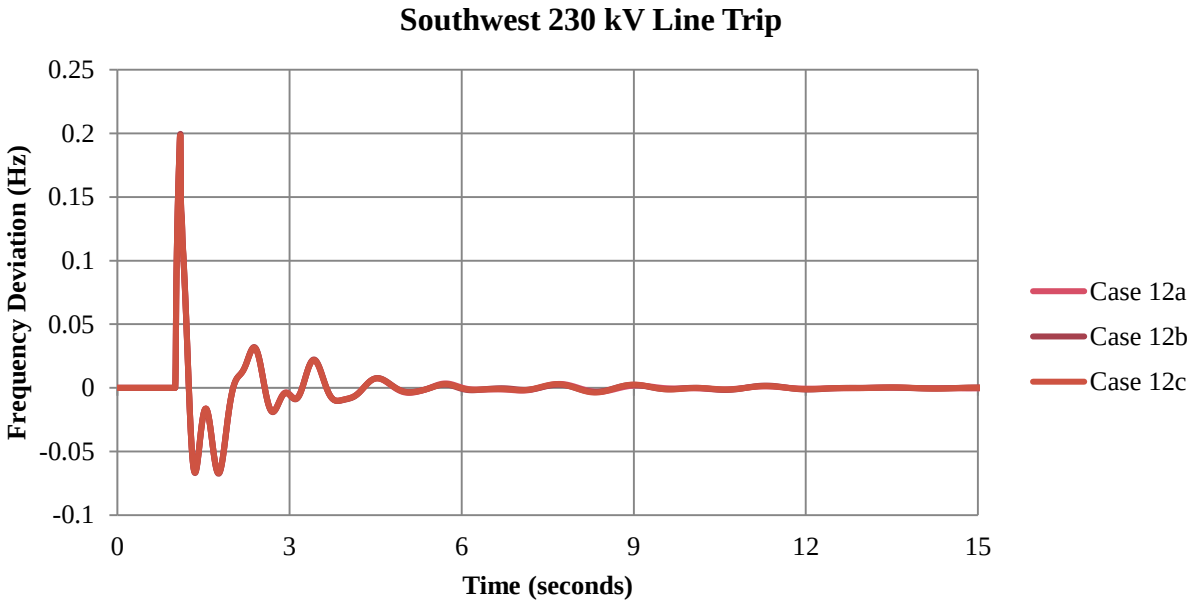

Figure A.16. Year 2012 frequency response for southwest 230 kV line trip

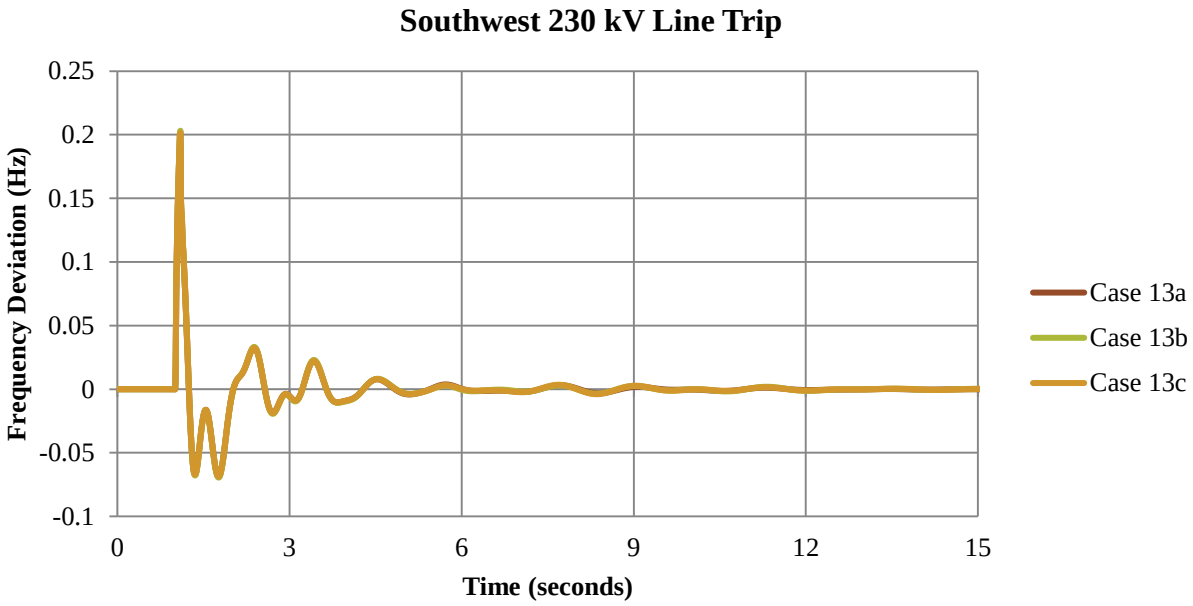

Figure A.17. Year 2013 frequency response for southwest 230 kV line trip

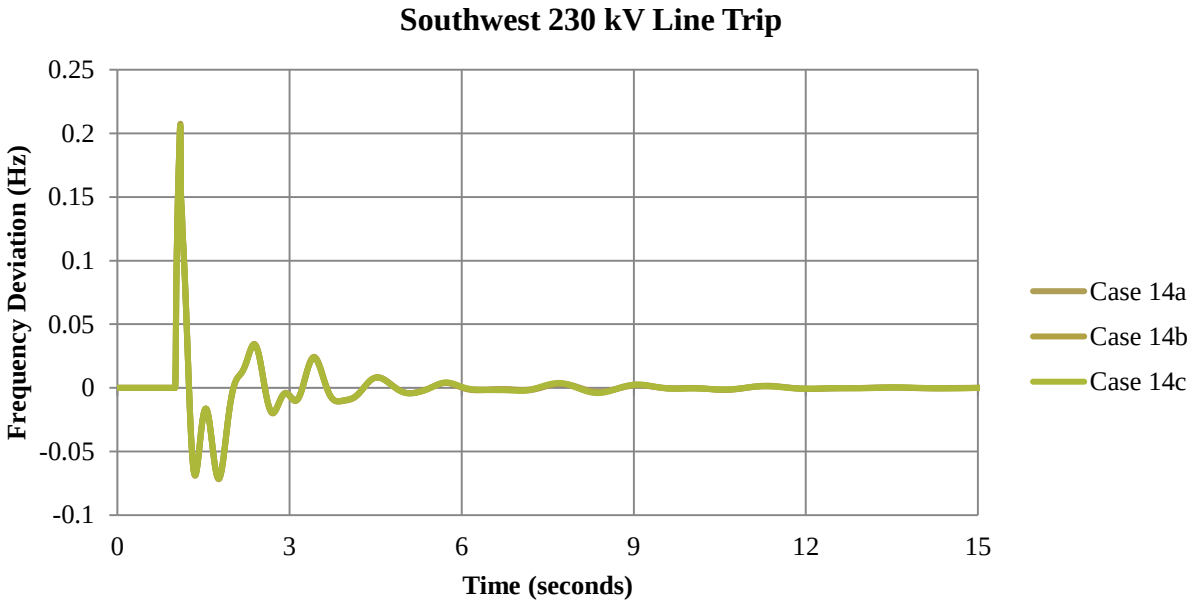

Figure A.18. Year 2014 frequency response for southwest 230 kV line trip

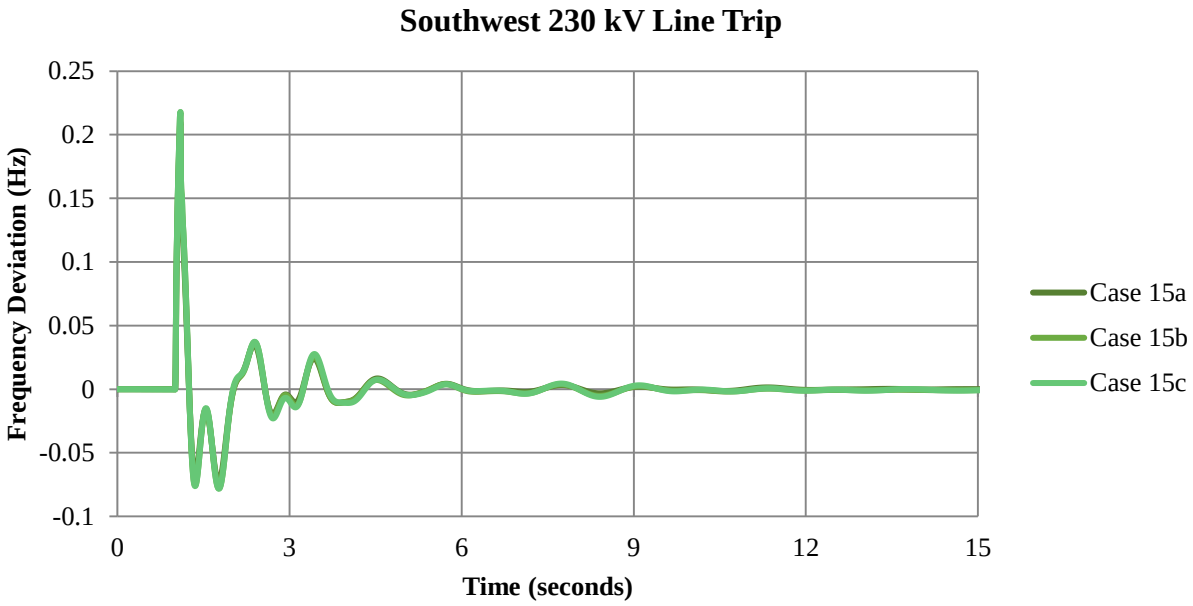

Figure A.19. Year 2015 frequency response for southwest 230 kV line trip

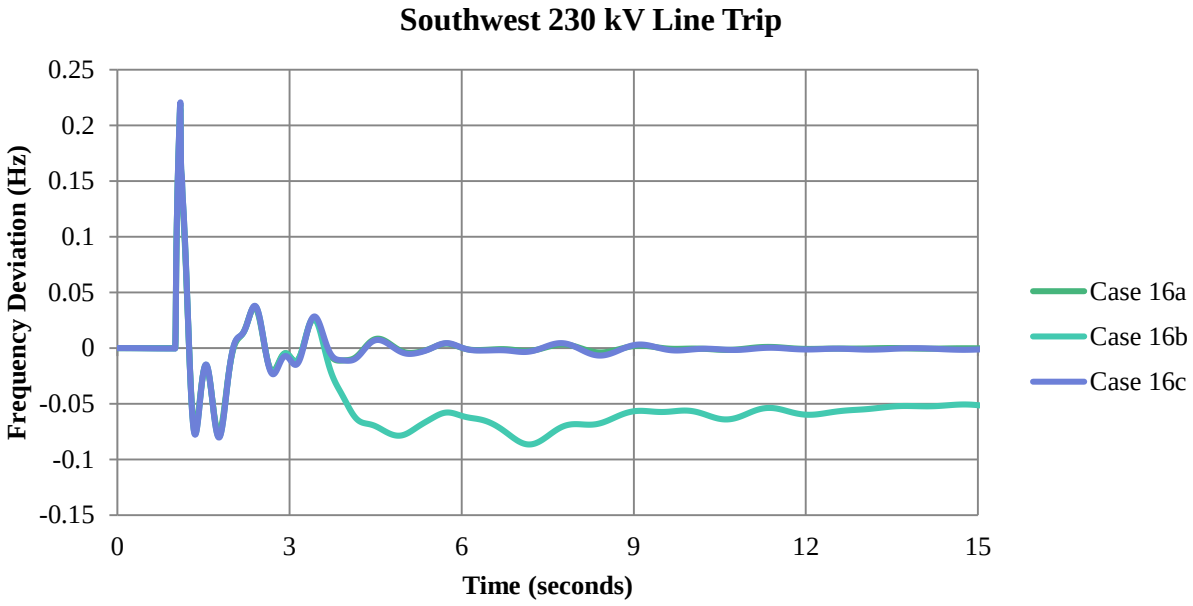

Figure A.20. Year 2016 frequency response for southwest 230 kV line trip

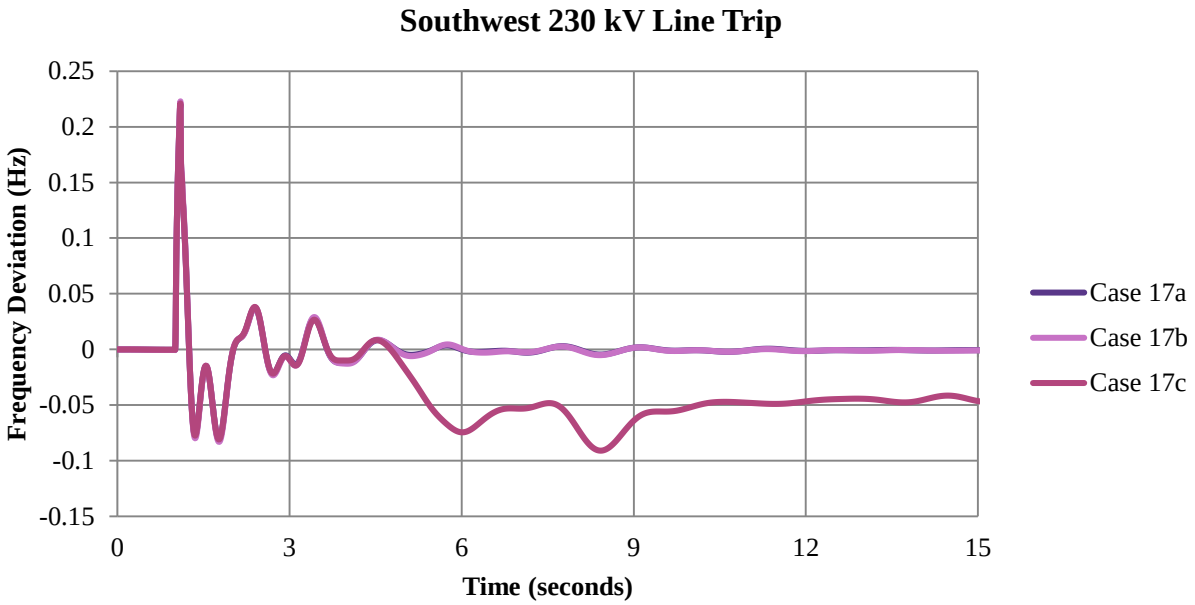

Figure A.21. Year 2017 frequency response for southwest 230 kV line trip

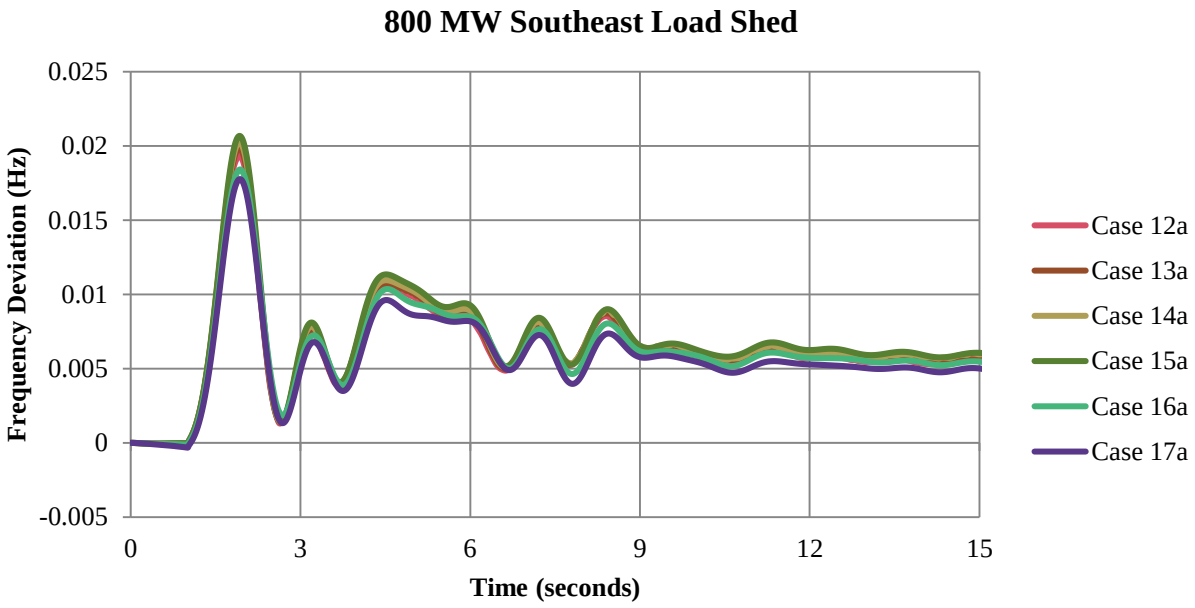

Figure A.22. Base case frequency response for 800 MW southeast load shed

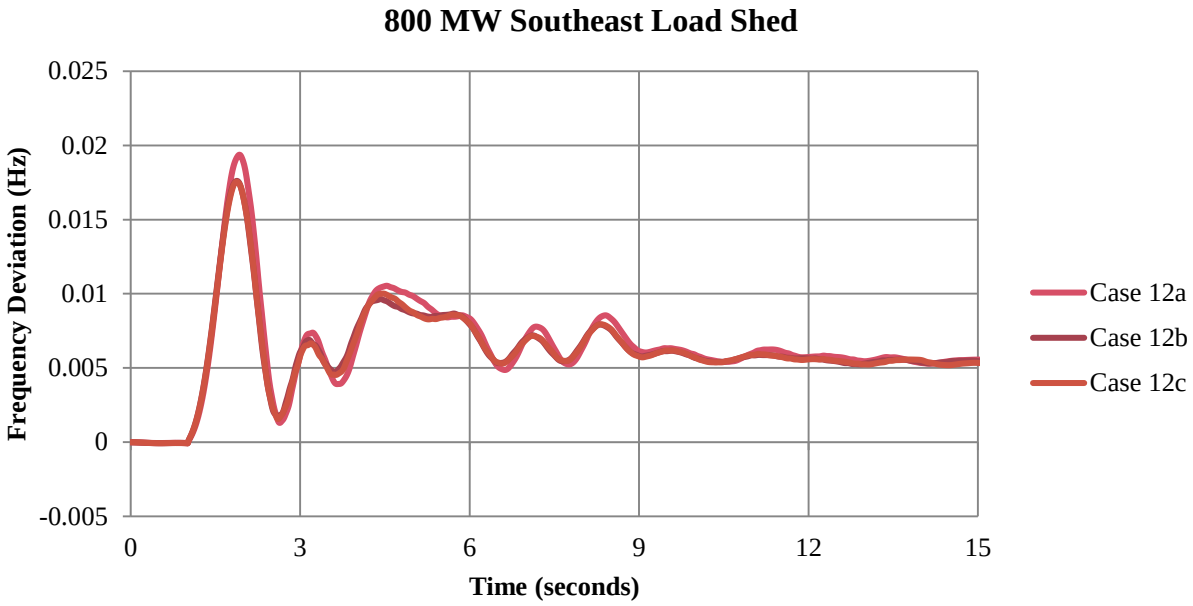

Figure A.23. Year 2012 frequency response for 800 MW southeast load shed

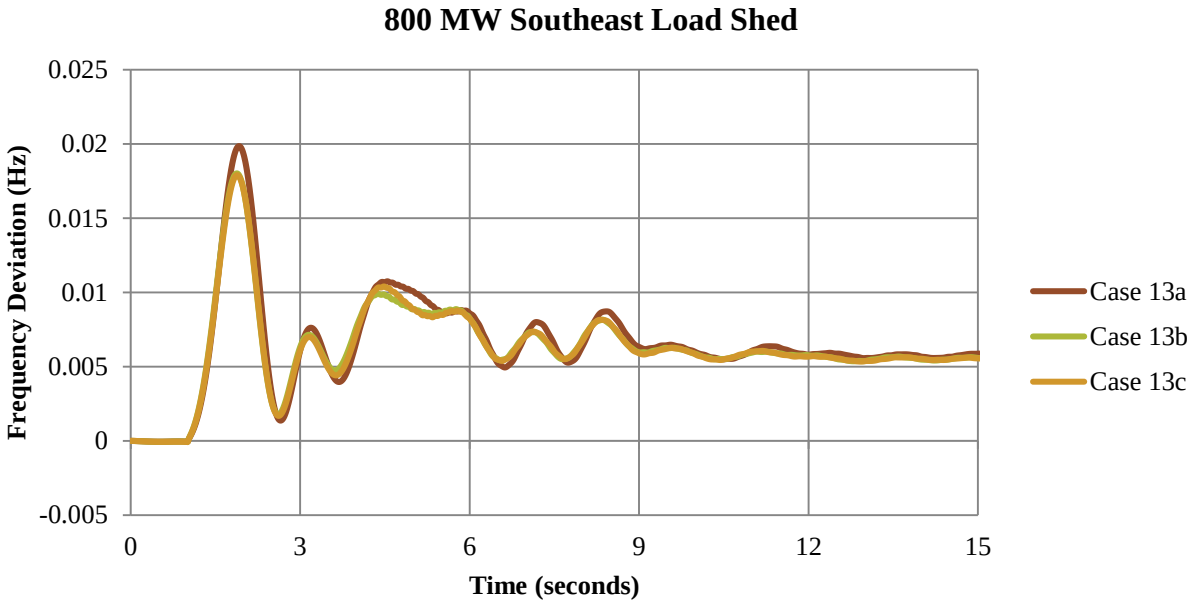

Figure A.24. Year 2012 frequency response for 800 MW southeast load shed

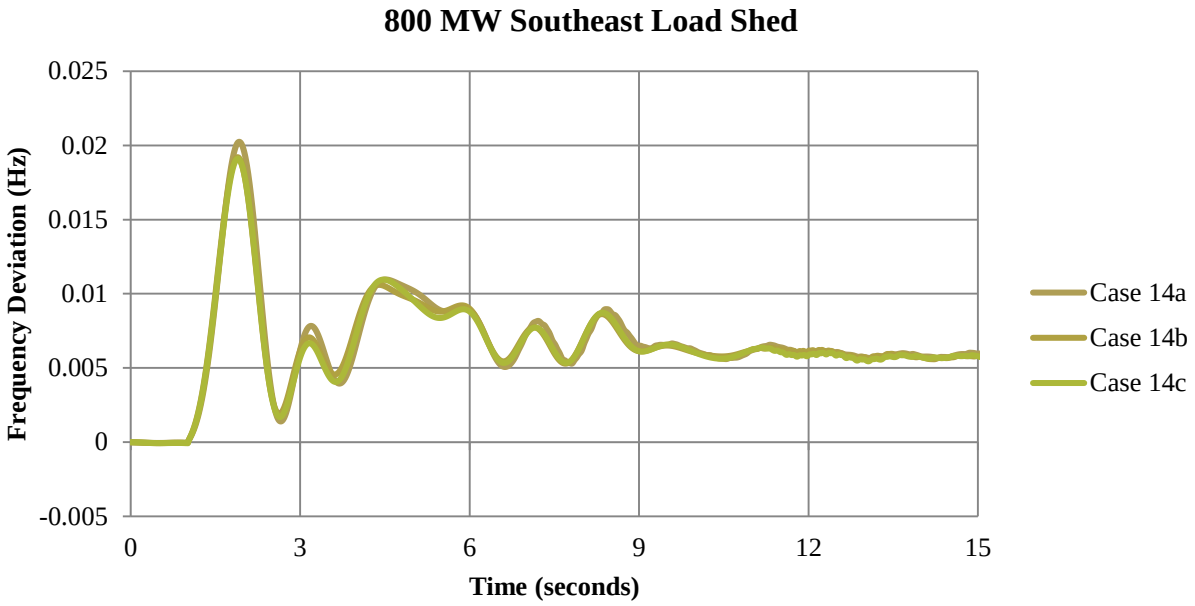

Figure A.25. Year 2014 frequency response for 800 MW southeast load shed

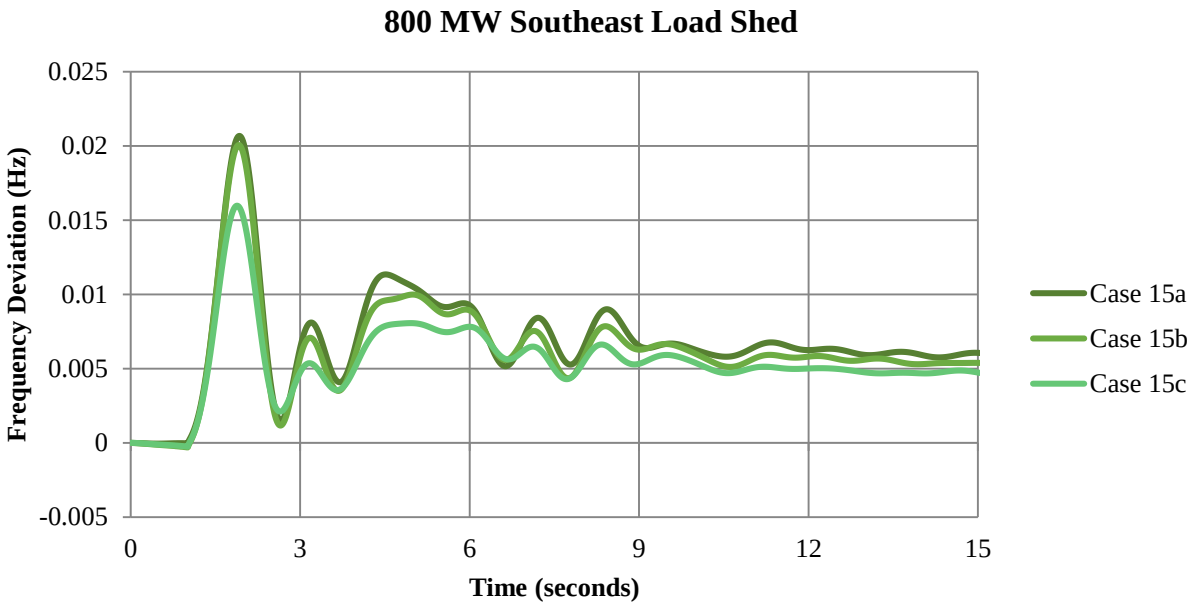

Figure A.26. Year 2015 frequency response for 800 MW southeast load shed

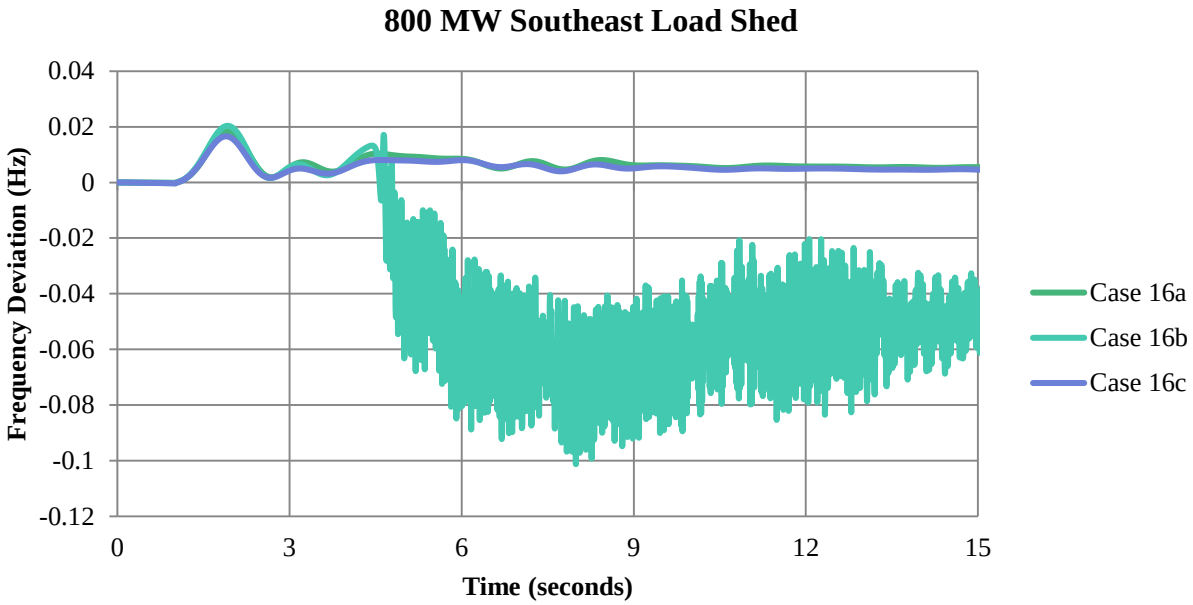

Figure A.27. Year 2016 frequency response for 800 MW southeast load shed

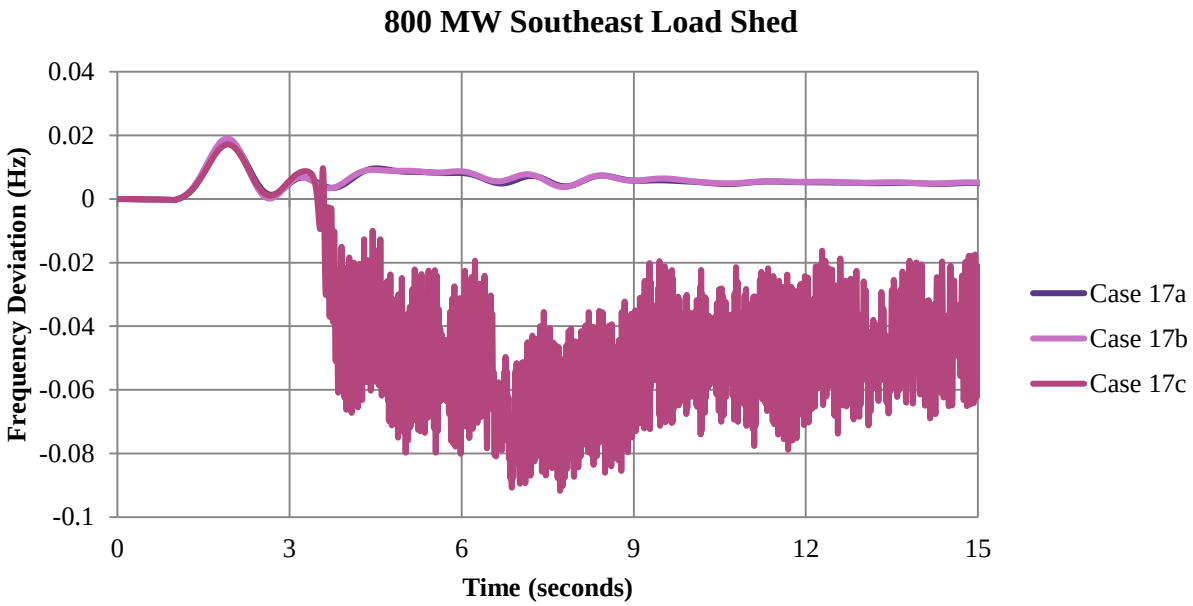

Figure A.28. Year 2017 frequency response for 800 MW southeast load shed

APPENDIX B: LOSS OF INERTIA SIMULATION RESULTS

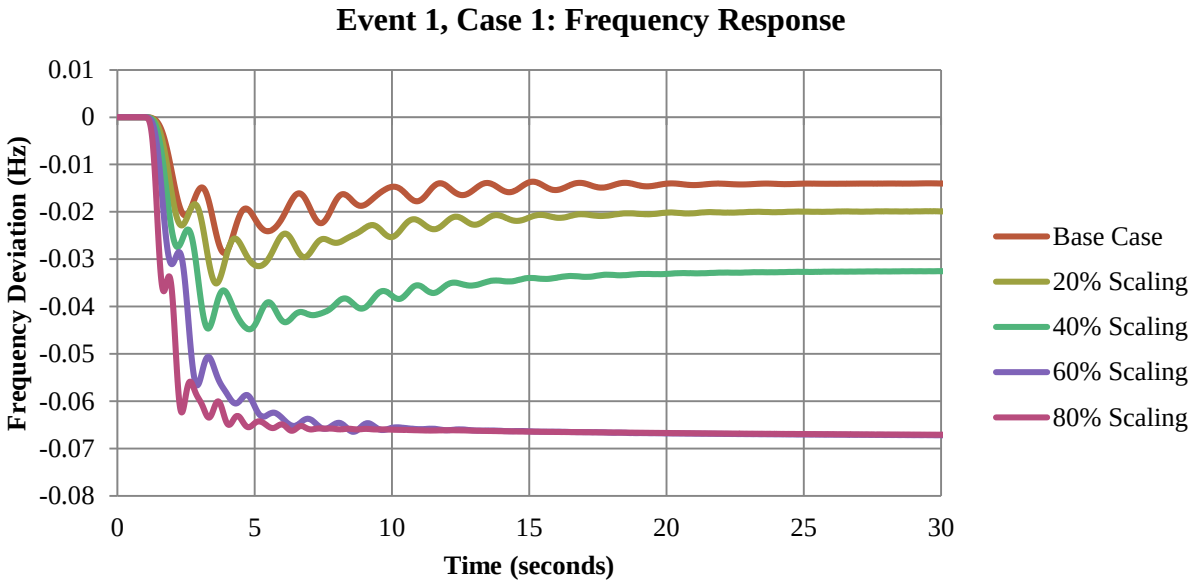

Figure B.1. Event 1, Case 1: Frequency response

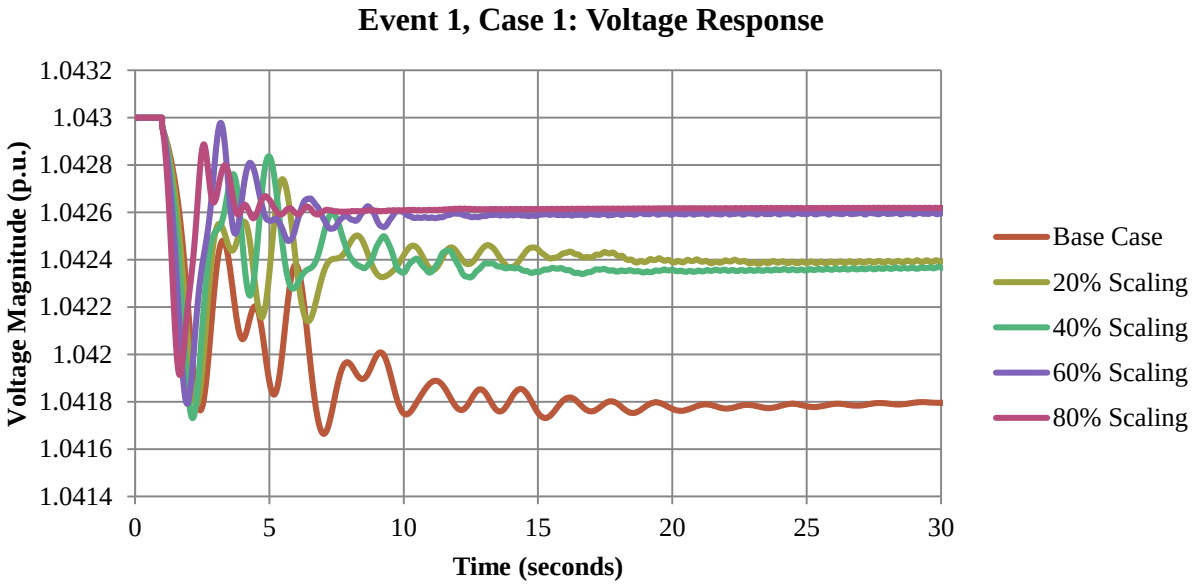

Figure B.2. Event 1, Case 1: Voltage response

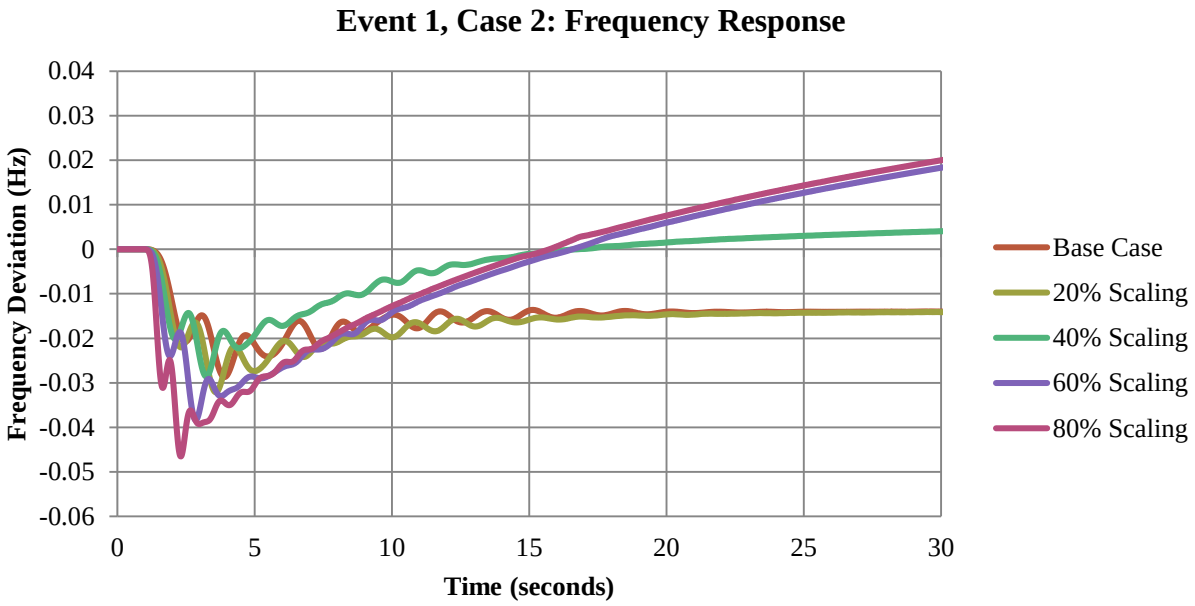

Figure B.3. Event 1, Case 2: Frequency response

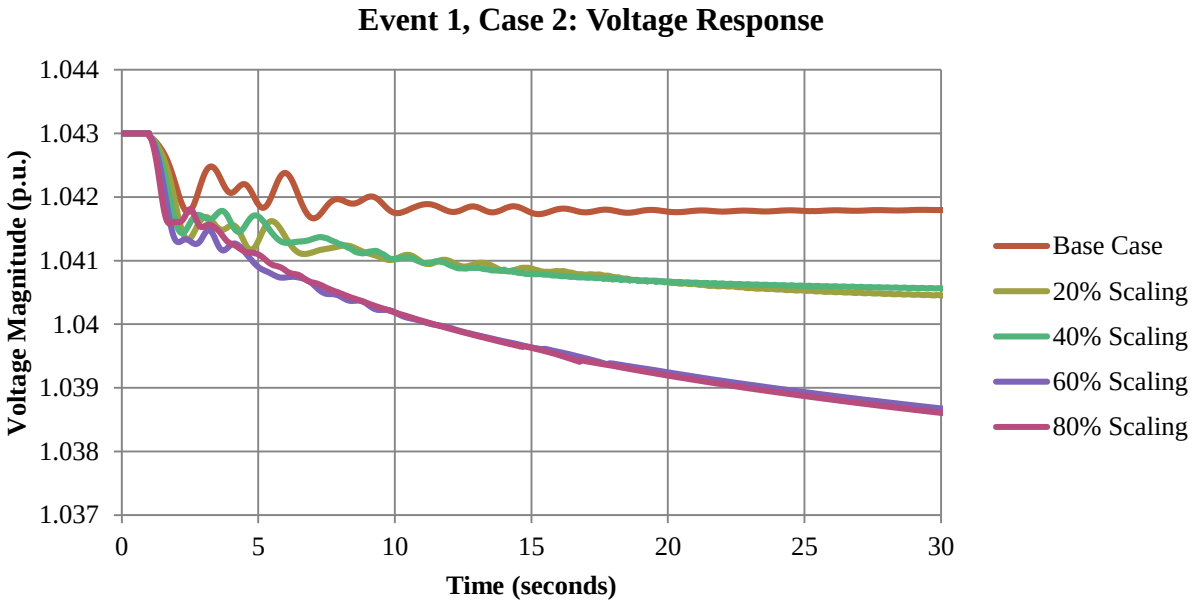

Figure B.4. Event 1, Case 2: Voltage response

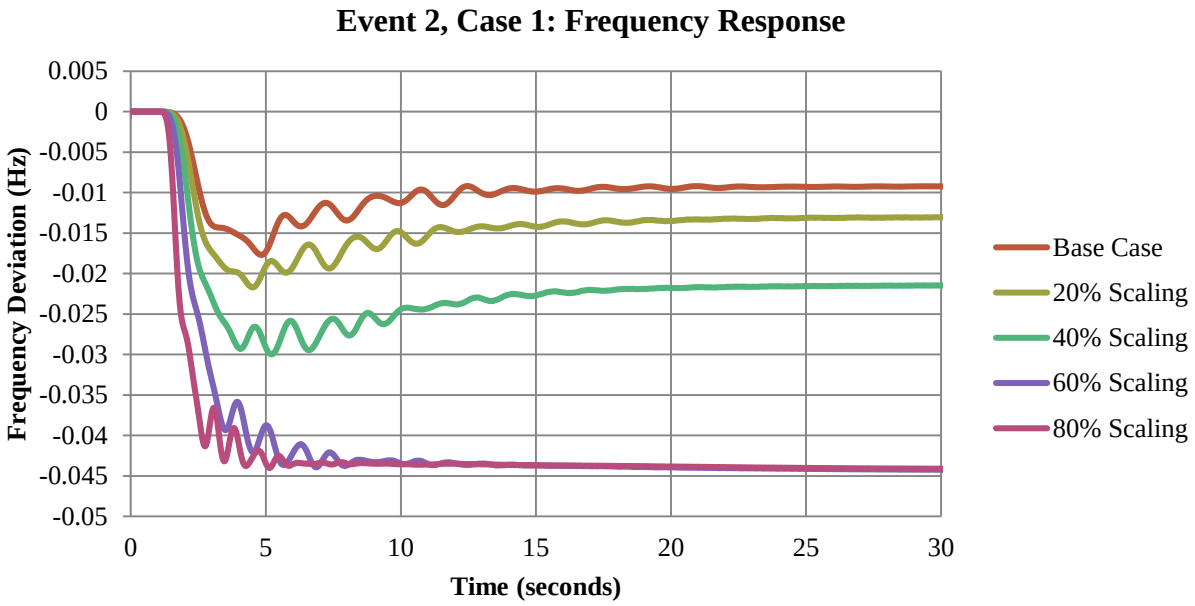

Figure B.5. Event 2, Case 1: Frequency response

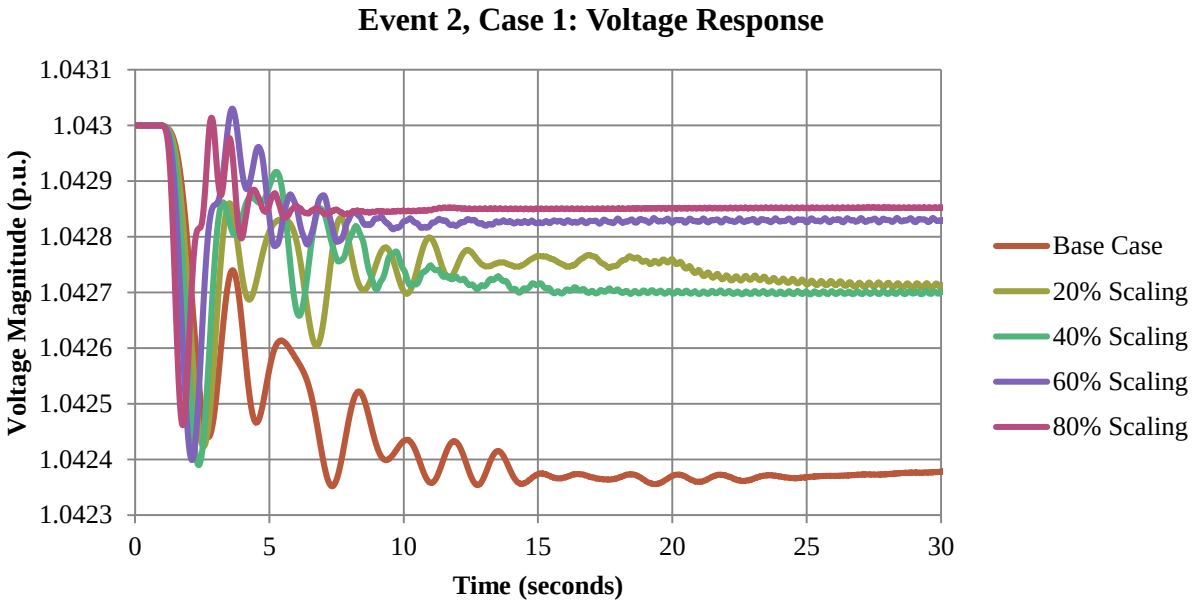

Figure B.6. Event 2, Case 1: Voltage response

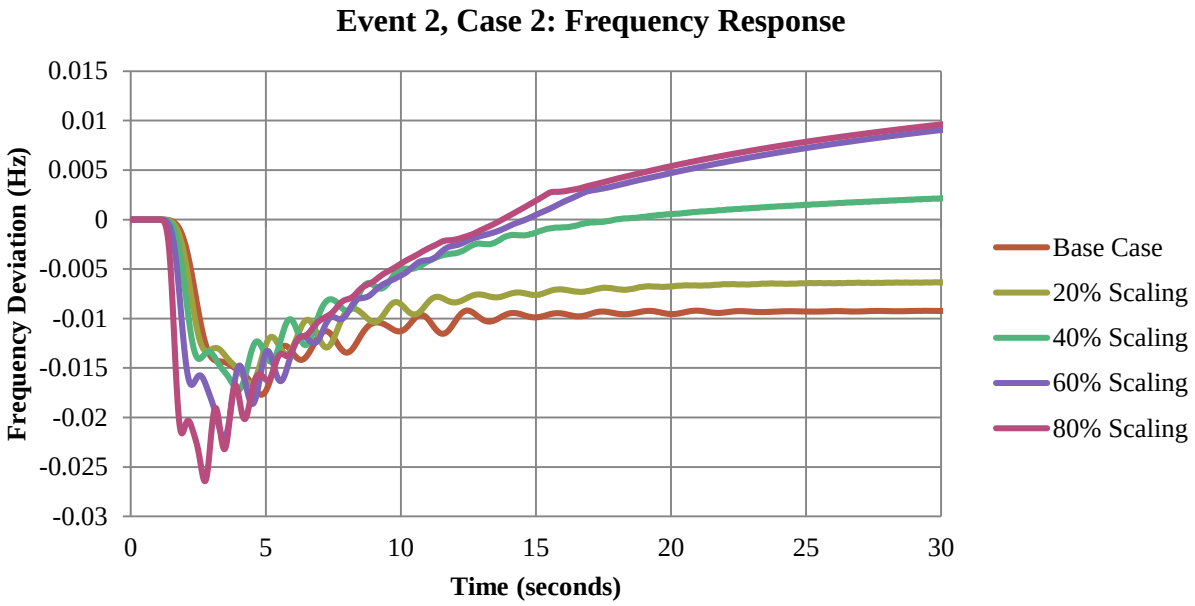

Figure B.7. Event 2, Case 1: Frequency response

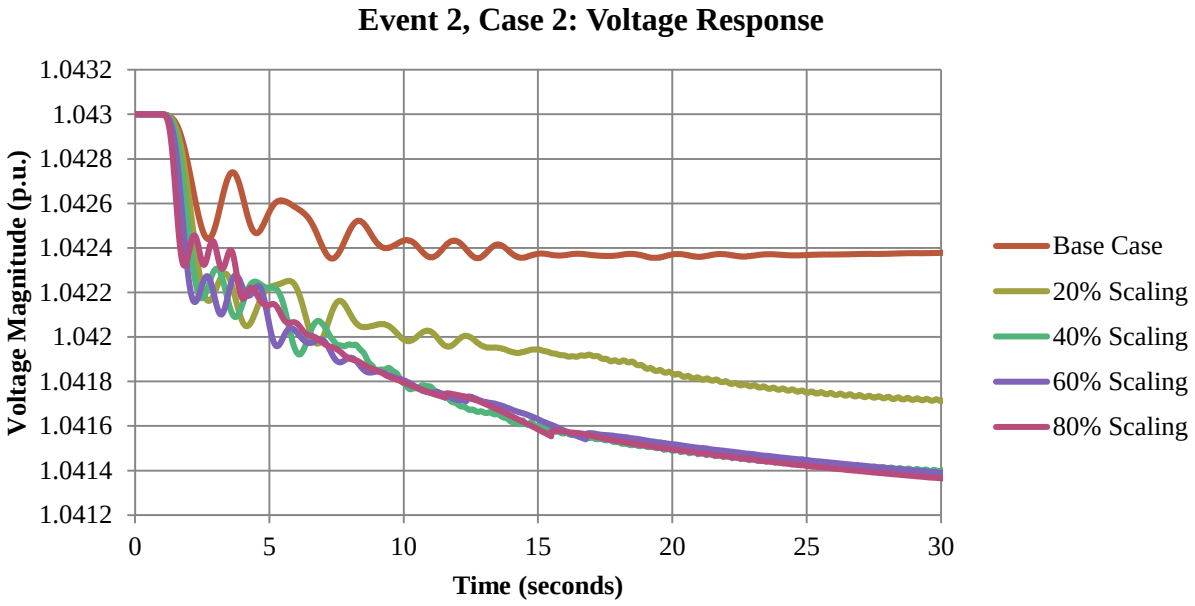

Figure B.8. Event 2, Case 2: Voltage response

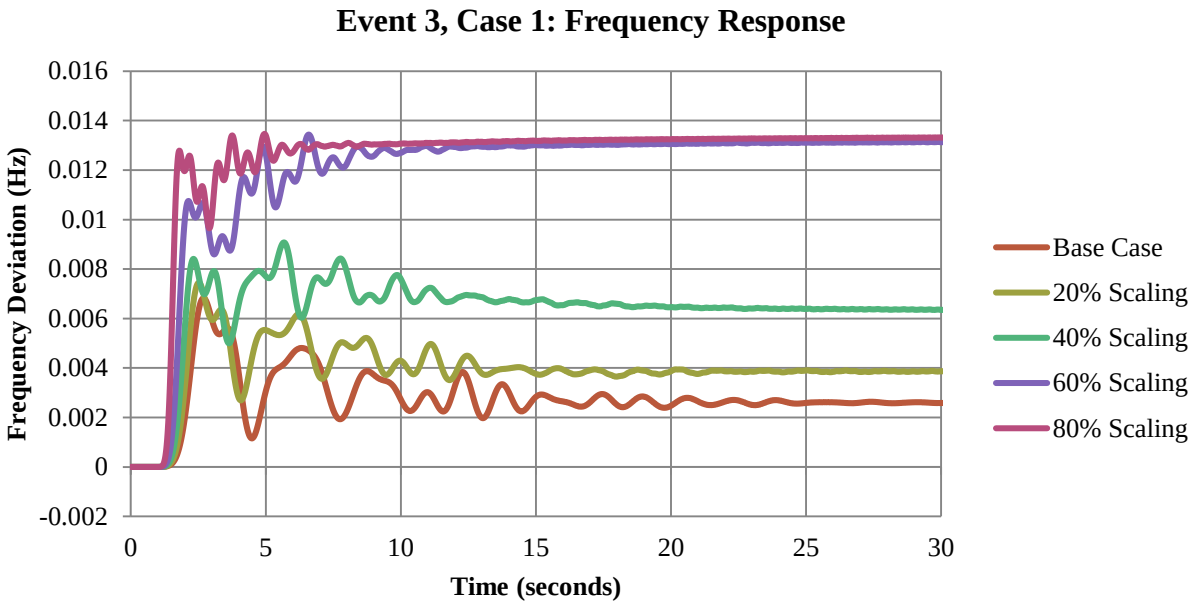

Figure B.9. Event 3, Case 1: Frequency response

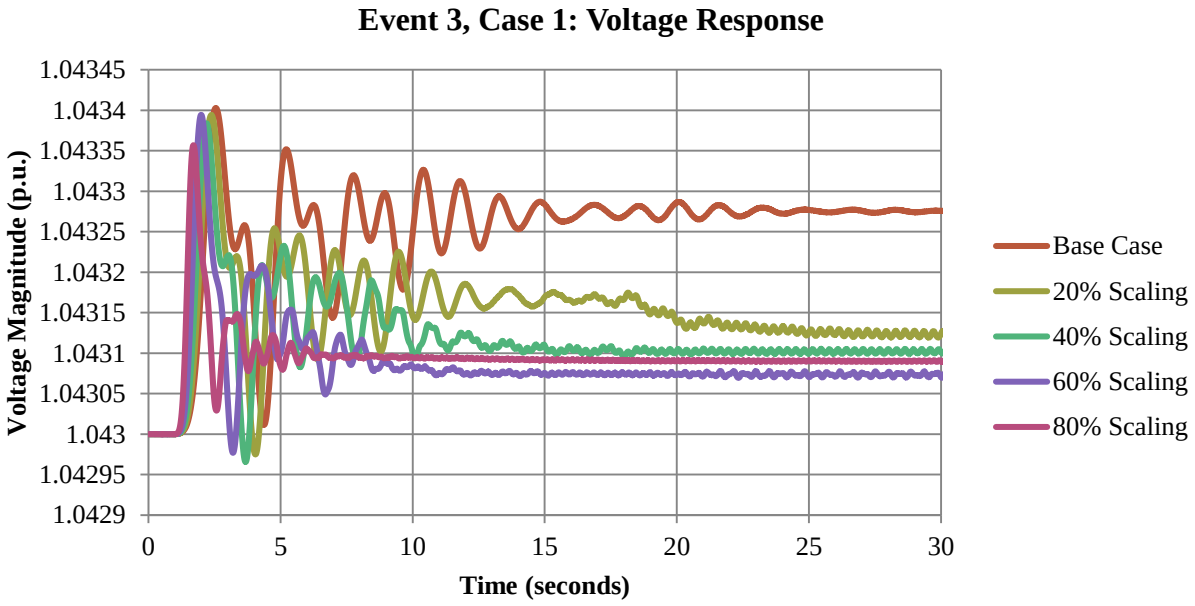

Figure B.10. Event 3, Case 1: Voltage response

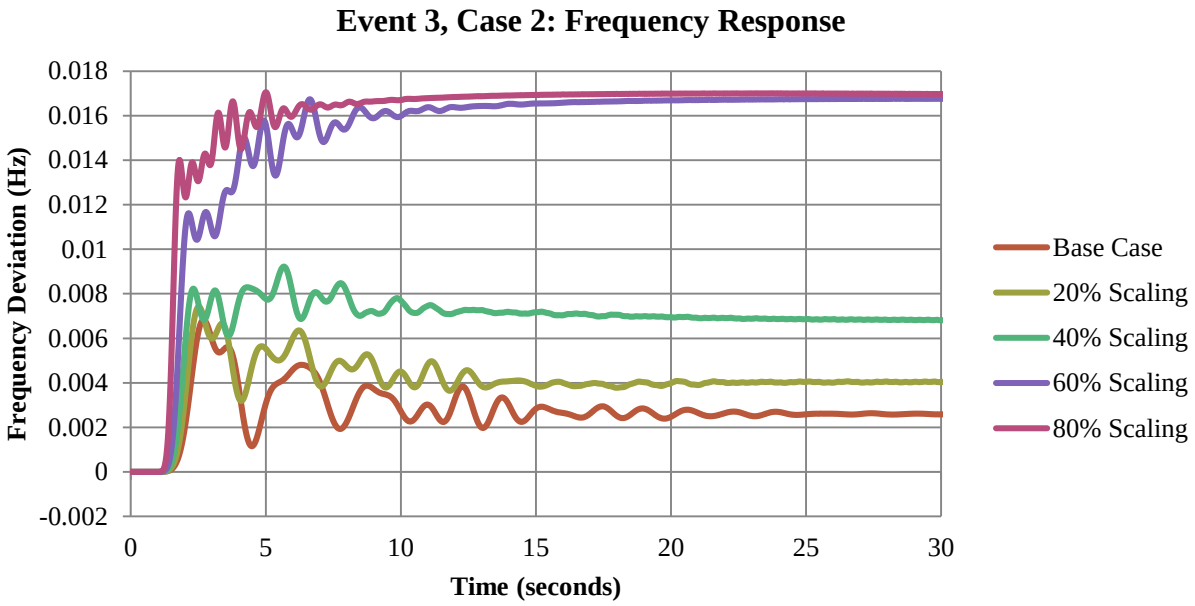

Figure B.11. Event 3, Case 2: Frequency response

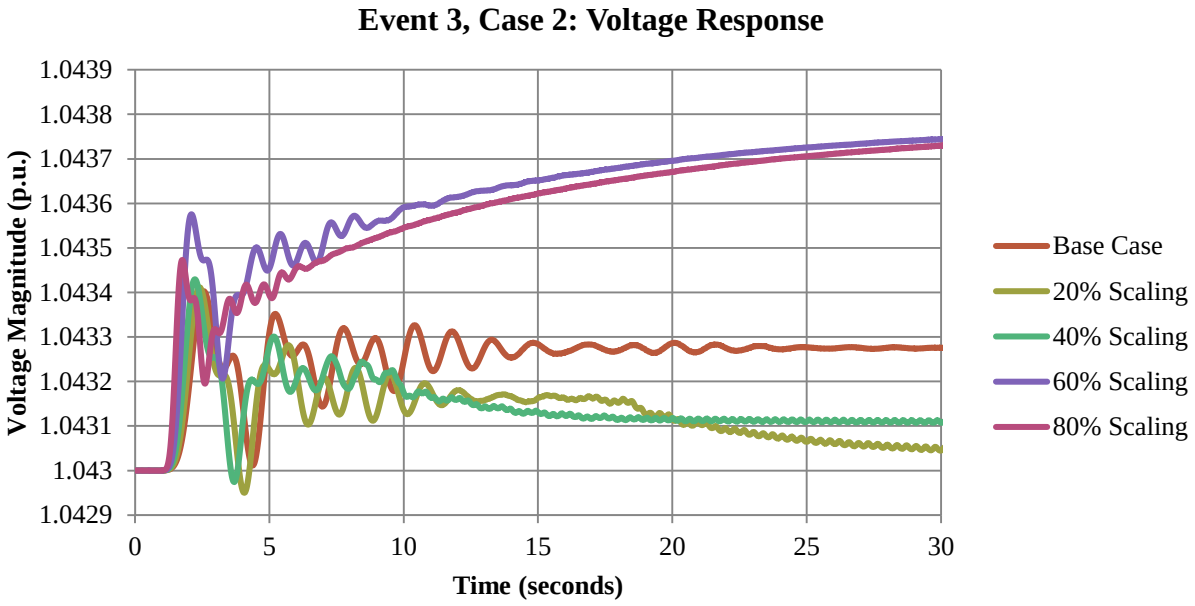

Figure B.12. Event 3, Case 2: Voltage response

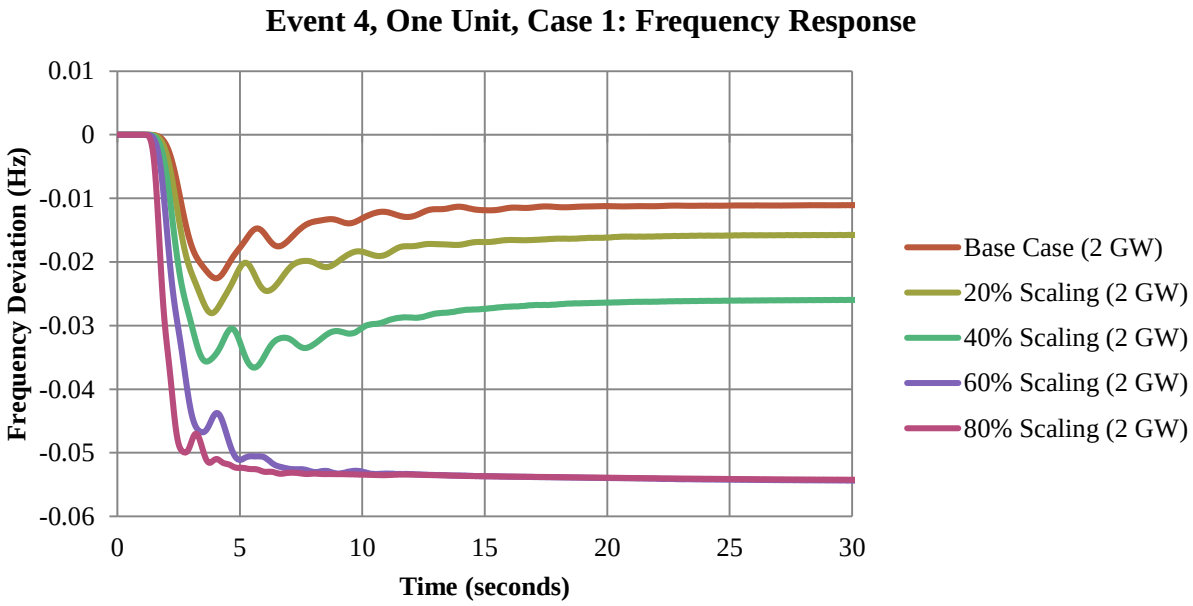

Figure B.13. Event 4, One Unit, Case 1: Frequency response

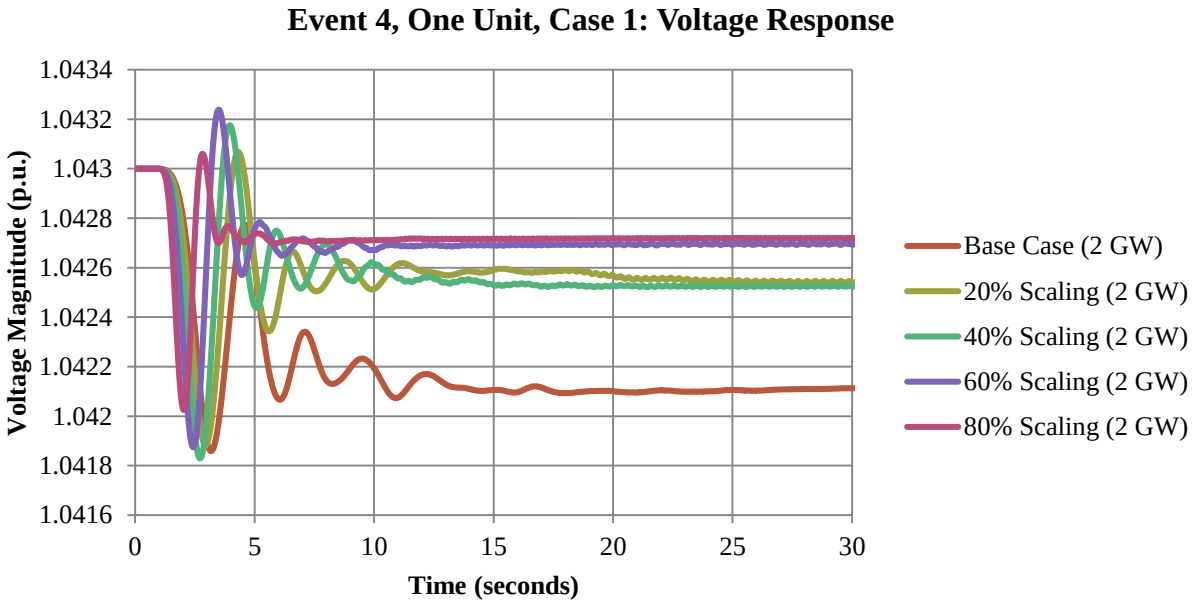

Figure B.14. Event 4, One Unit, Case 1: Voltage response

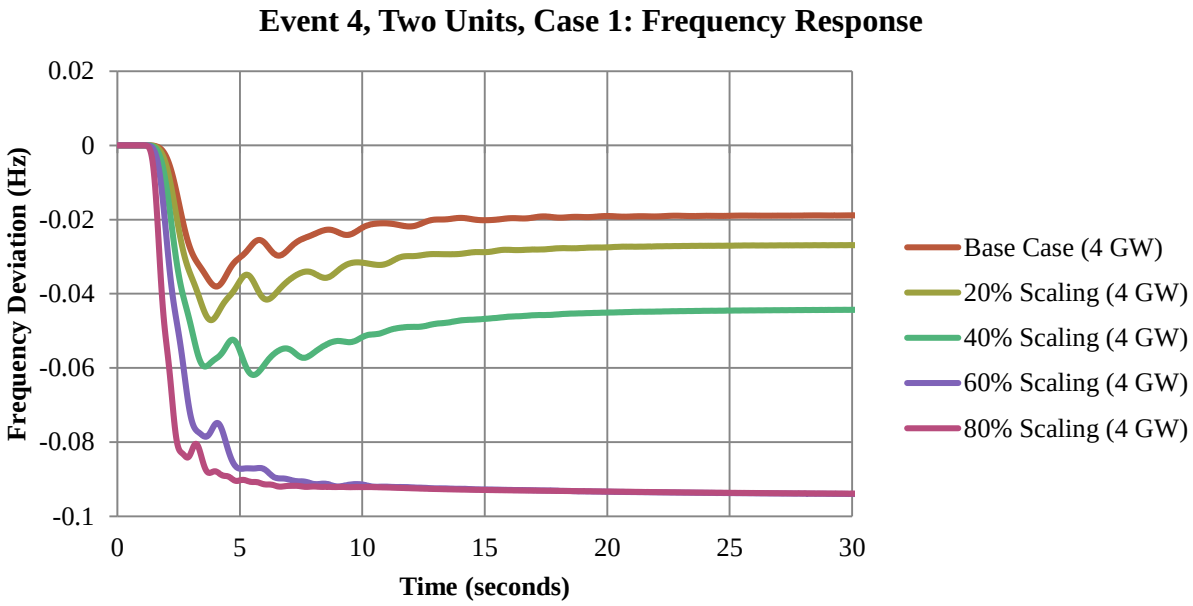

Figure B.15. Event 4, Two Units, Case 1: Frequency response

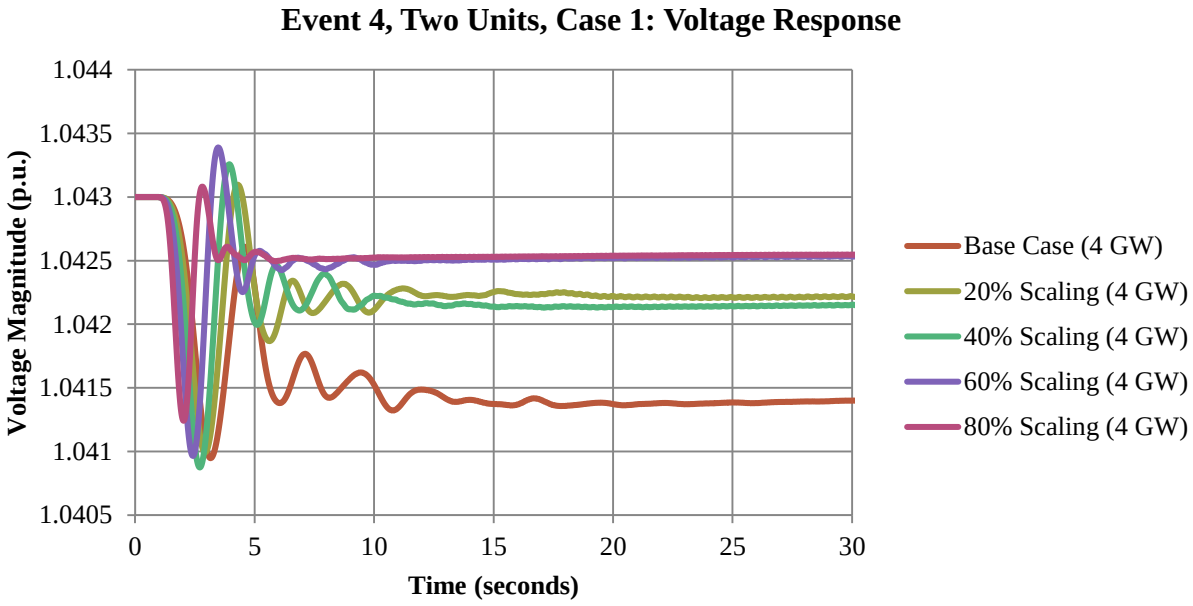

Figure B.16. Event 4, Two Units, Case 1: Voltage response

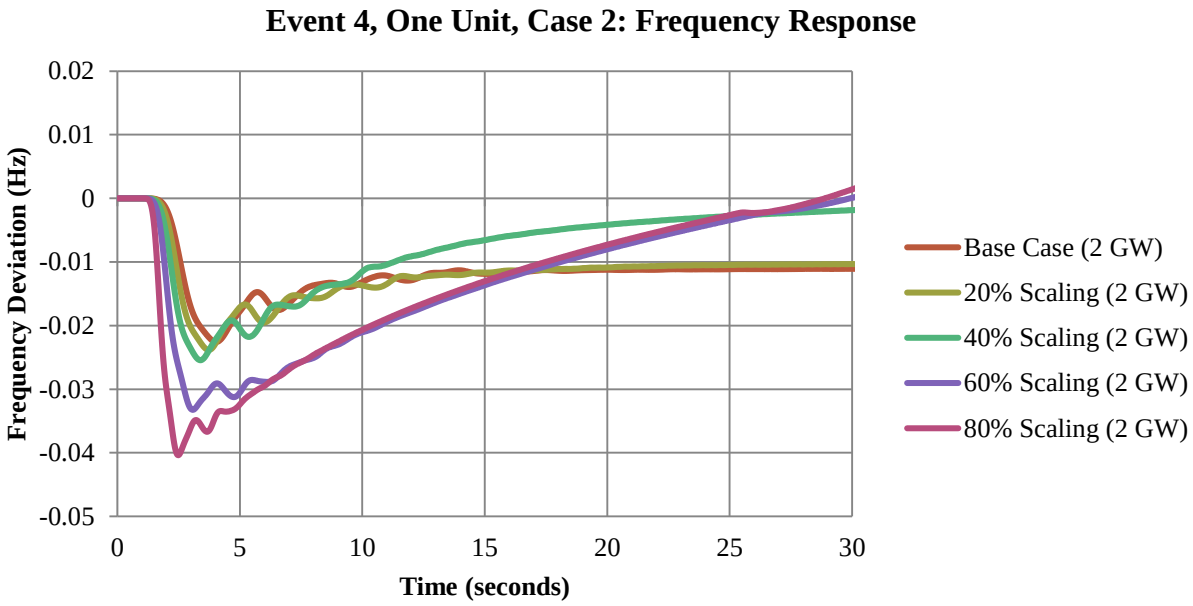

Figure B.17. Event 4, One Unit, Case 2: Frequency response

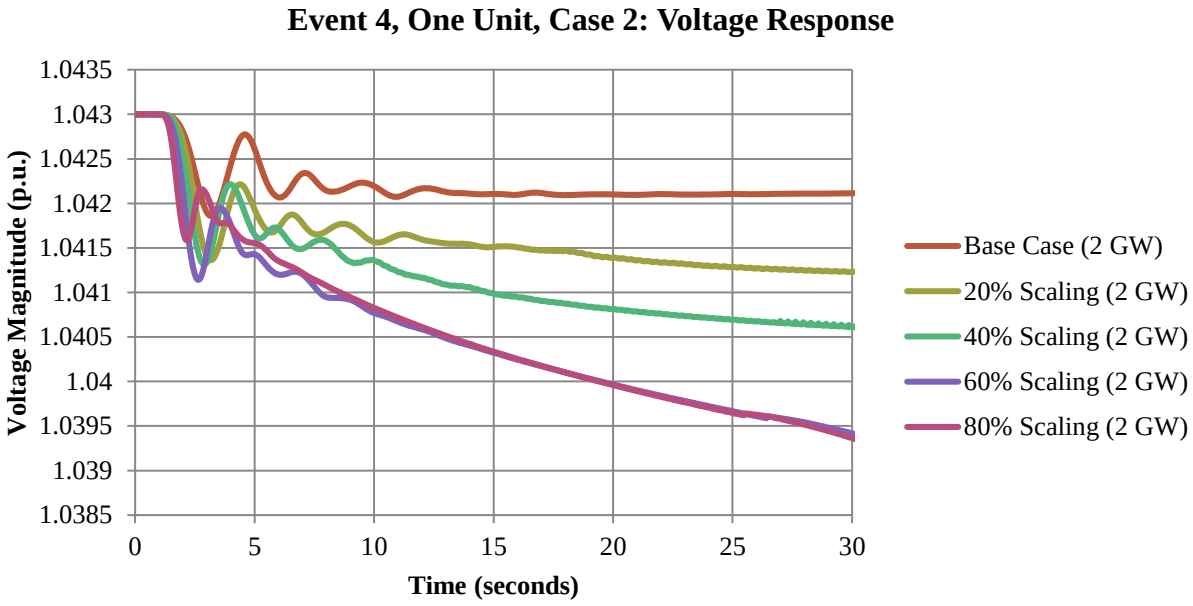

Figure B.18. Event 4, One Unit, Case 2: Voltage response

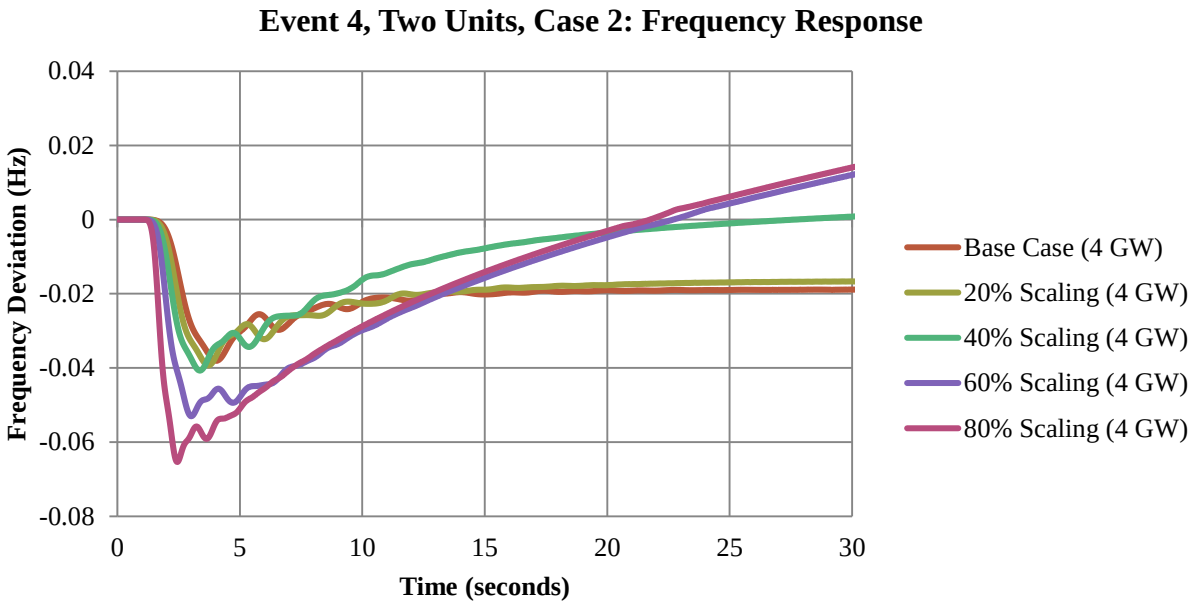

Figure B.19. Event 4, Two Units, Case 2: Frequency response

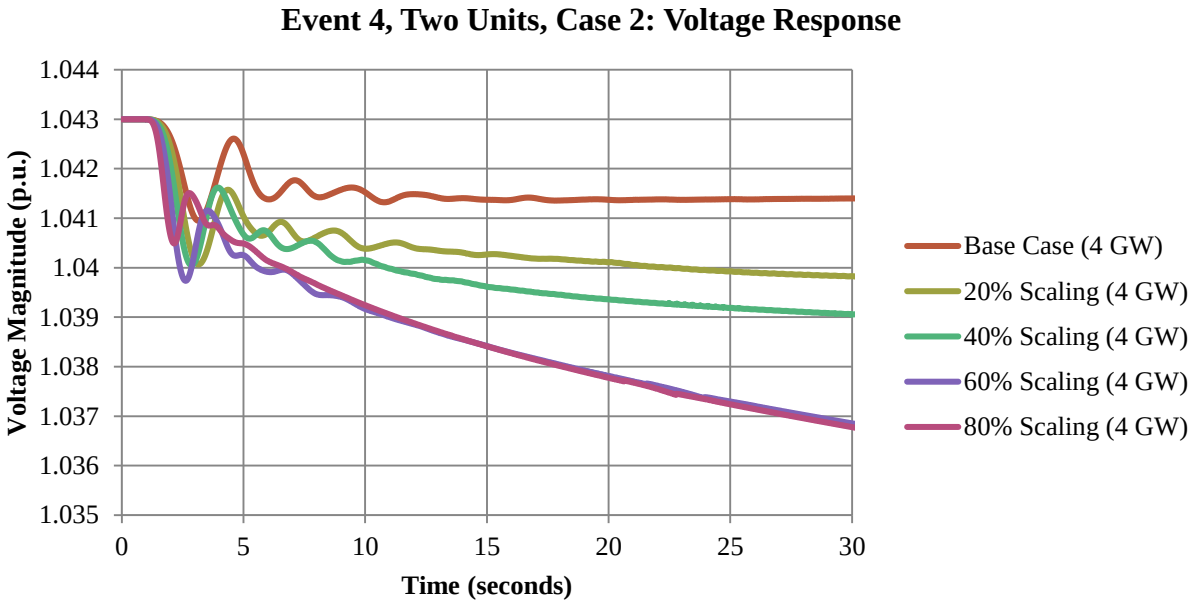

Figure B.20. Event 4, Two Units, Case 2: Voltage response

APPENDIX C: PYTHON HELPER FUNCTIONS CREATED FOR PSS®E

```
#!/usr/bin/env/python
"""Provides functionality for PSS®E simulation.

This functionality is not readily available from the official Python
          API.

Requires Python 2.7 and PSS®E 33
    -or- Python 2.5 and PSS®E 32
"""

import csv, os, re, shutil, sys
from sets import Set
from time import strftime
from random import randint

# Import PSS®E APIs
psse_version = 33
pssbin_path = 'C:\\Program Files
           (x86)\\PTI\\PSSE{0}\\PSSBIN'.format(psse_version)
sys.path.append(pssbin_path)
os.environ['PATH'] = (pssbin_path + ';' + os.environ['PATH'])
import psspy, redirect, dyntools

# Obtain PSS®E defaults
_i = psspy.getdefaultint()
_f = psspy.getdefaultreal()
_s = psspy.getdefaultchar()
redirect.psse2py()

__author__ = 'Micah J. Till'
__copyright__ = 'Copyright 2017'
__version__ = "2.1.1"

def use_best_var_type(str):
    try:
        test_float = float(str)
        test_int = int(test_float)
        if test_float == test_int:
            return test_int
        else:
            return test_float
    except ValueError:
        return str

def load_case(path):
    if path.endswith('.sav'):
        ierr = psspy.case(path)
```

```
    elif path.endswith('.raw'):
        ierr = psspy.read(0, path)
    else:
        ierr = -1
    return ierr

def get_temp_sid(value_if_none = None):
    for sid in range(0, 12):
        if not psspy.bsysisdef(sid):
            psspy.bsysdef(sid, 1)
            return sid
    return value_if_none

def kill_temp_sid(sid):
    psspy.bsysdef(sid, 0)
    return 0

def fdns_solution(opts):
    good_run = False
    ierr = psspy.fdns(opts)
    ival = psspy.solved()
    if (ierr == 0) and (ival == 0):
        good_run = True
    return (good_run, ierr, ival)

def fnsl_solution(opts):
    good_run = False
    ierr = psspy.fnsl(opts)
    ival = psspy.solved()
    if (ierr == 0) and (ival == 0):
        good_run = True
    return (good_run, ierr, ival)

def solve_case():
    SLTN_OPTIONS = [1,0,0,1,1,0,99,0]
    caseStatus = fdns_solution(SLTN_OPTIONS)
    return caseStatus

def solve_with_discrete_locked():
    SLTN_OPTIONS = [1,0,0,1,2,0,99,0]
    caseStatus = fdns_solution(SLTN_OPTIONS)
    return caseStatus

def solve_with_discrete_fully_locked():
    SLTN_OPTIONS = [2,0,0,1,2,0,20,0]
    caseStatus = fdns_solution(SLTN_OPTIONS)
    return caseStatus

def solve_on_lockdown():
    SLTN_OPTIONS = [0,0,0,1,2,0,20,0]
```

```
    caseStatus = fdns_solution(SLTN_OPTIONS)
    return caseStatus

def get_bus_elements_by_bsys(bsys_id):
    ierr, (bs0,) = psspy.abusint(bsys_id,2,'NUMBER')
    ierr, (bs1,) = psspy.abusint(bsys_id,2,'AREA')
    ierr, (bs2,) = psspy.abusreal(bsys_id,2,'PU')
    ierr, (bs3,) = psspy.abusreal(bsys_id,2,'ANGLED')
    ierr, (bs4,) = psspy.abusreal(bsys_id,2,'BASE')
    ierr, (bs5,) = psspy.abusint(bsys_id,2,'TYPE')
    if bs0 is not None:
        bus_elements = zip(bs0,bs1,bs2,bs3,bs4,bs5)
    else:
        bus_elements = ()
    return bus_elements;

def get_branch_elements_by_bsys(bsys_id):
    TIES = 1
    ierr, (br0,) = psspy.abrnint(bsys_id,_i,TIES,2,1,'FROMNUMBER')
    ierr, (br1,) = psspy.abrnint(bsys_id,_i,TIES,2,1,'TONUMBER')
    ierr, (br2,) = psspy.abrnchar(bsys_id,_i,TIES,2,1,'ID')
    ierr, (br3,) = psspy.abrnreal(bsys_id,_i,TIES,2,1,'MVA')
    ierr, (br4,) = psspy.abrnreal(bsys_id,_i,TIES,2,1,'RATEA')
    ierr, (br5,) = psspy.abrnreal(bsys_id,_i,TIES,2,1,'RATEB')
    ierr, (br6,) = psspy.abrnreal(bsys_id,_i,TIES,2,1,'RATEC')
    ierr, (br7,) = psspy.abrnint(bsys_id,_i,TIES,2,1,'STATUS')
    if br0 is not None:
        branch_elements = zip(br0,br1,br2,br3,br4,br5,br6,br7)
    else:
        branch_elements = ()
    return branch_elements;

def get_two_winding_elements_by_bsys(bsys_id):
    TIES = 3
    ierr, (xd0,) = psspy.atrnint(bsys_id,_i,TIES,2,1,'FROMNUMBER')
    ierr, (xd1,) = psspy.atrnint(bsys_id,_i,TIES,2,1,'TONUMBER')
    ierr, (xd2,) = psspy.atrnchar(bsys_id,_i,TIES,2,1,'ID')
    ierr, (xd3,) = psspy.atrnreal(bsys_id,_i,TIES,2,1,'MVA')
    ierr, (xd4,) = psspy.atrnreal(bsys_id,_i,TIES,2,1,'RATEA')
    ierr, (xd5,) = psspy.atrnreal(bsys_id,_i,TIES,2,1,'RATEB')
    ierr, (xd6,) = psspy.atrnreal(bsys_id,_i,TIES,2,1,'RATEC')
    ierr, (xd7,) = psspy.atrnint(bsys_id,_i,TIES,2,1,'STATUS')
    if xd0 is not None:
        two_winding_elements = zip(xd0,xd1,xd2,xd3,xd4,xd5,xd6,xd7)
    else:
        two_winding_elements = ()
    return two_winding_elements;

def get_three_winding_elements_by_bsys(bsys_id):
    TIES = 3
```

```
    ierr, (yd0,) = psspy.atr3int(bsys_id,_i,TIES,2,_i,'WIND1NUMBER')
    ierr, (yd1,) = psspy.atr3int(bsys_id,_i,TIES,2,_i,'WIND2NUMBER')
    ierr, (yd2,) = psspy.atr3int(bsys_id,_i,TIES,2,_i,'WIND3NUMBER')
    ierr, (yd3,) = psspy.atr3char(bsys_id,_i,TIES,2,_i,'ID')
    ierr, (yd4,) = psspy.atr3int(bsys_id,_i,TIES,2,_i,'STATUS')
    if yd0 is not None:
        three_winding_elements = zip(yd0,yd1,yd2,yd3,yd4)
    else:
        three_winding_elements = ()
    return three_winding_elements;

def record_and_remove_islands():
    ierr, (busesBeforeIsland,) = psspy.abusint(-1,1,'NUMBER')
    ierr, genBeforeIsland = psspy.systot('GEN')
    ierr, loadBeforeIsland = psspy.systot('LOAD')
    ierr = psspy.island()
    ierr, (busesAfterIsland,) = psspy.abusint(-1,1,'NUMBER')
    ierr, genAfterIsland = psspy.systot('GEN')
    ierr, loadAfterIsland = psspy.systot('LOAD')
    islandBuses = list(set(busesBeforeIsland)-set(busesAfterIsland))
    islandGen = genBeforeIsland - genAfterIsland
    islandLoad = loadBeforeIsland - loadAfterIsland
    return (islandBuses,islandGen,islandLoad);

def record_and_reset_islands():
    tempdir = os.getcwd()
    temprnd = randint(1000,9999)
    tempfile =
           'temp{0}_{1}.sav'.format(strftime('%Y%m%d%H%M%S'),temprnd)
    tempfullpath = '{0}//{1}'.format(tempdir,tempfile)
    ierr = psspy.save(tempfullpath)
    ierr, (busesBeforeIsland,) = psspy.abusint(-1,1,'NUMBER')
    ierr, genBeforeIsland = psspy.systot('GEN')
    ierr, loadBeforeIsland = psspy.systot('LOAD')
    ierr1 = psspy.island()
    ierr2, (busesAfterIsland,) = psspy.abusint(-1,1,'NUMBER')
    ierr3, genAfterIsland = psspy.systot('GEN')
    ierr4, loadAfterIsland = psspy.systot('LOAD')
    islandBuses = list(set(busesBeforeIsland)-set(busesAfterIsland))
    islandGen = genBeforeIsland - genAfterIsland
    islandLoad = loadBeforeIsland - loadAfterIsland
    ierr = psspy.case(tempfullpath)
    os.remove(tempfullpath)
    return (islandBuses,islandGen,islandLoad);

def last_switched_shunts(progressOutput):
    REGEX_GROUP_SHUNTS = r'''SWITCHED SHUNTS ADJUSTED:[\r|\n|\r\n]X---
           ----- AT BUS ---------X[ |\t]*OLD Q[ |\t]*NEW
           Q[\r|\n|\r\n](?: \d+ \[.*[\r|\n|\r\n])+[\r|\n|\r\n]\d+
           switched shunt[s]? adjusted'''
```

```
    REGEX_INDIVIDUAL_SHUNTS = r'''(?: (\d+) \[.*[\r|\n|\r\n])'''

    iFile = open(progressOutput, 'r')
    logFile = iFile.read()
    iFile.close()

    groupPattern = re.compile(REGEX_GROUP_SHUNTS, re.MULTILINE)
    individualPattern = re.compile(REGEX_INDIVIDUAL_SHUNTS,
           re.MULTILINE)

    shuntGroupSwitched = None
    for shuntGroupSwitched in re.finditer(groupPattern, logFile):
        pass
    lastShuntsSwitched = re.findall(individualPattern,
           shuntGroupSwitched.group(0))
    lastShuntsSwitched = map(int, lastShuntsSwitched)

    return lastShuntsSwitched

def lock_switched_shunt(bus):
    ierr = psspy.switched_shunt_chng_3(bus, [_i, _i, _i, _i, _i, _i,
           _i, _i, _i, _i, _i, 0], [_f, _f, _f, _f, _f, _f, _f, _f,
           _f, _f, _f, _f], _s)
    return ierr

def drop_switched_shunt(bus):
    ierr = psspy.switched_shunt_chng_3(bus, [_i, _i, _i, _i, _i, _i,
           _i, _i, _i, _i, 0, _i], [_f, _f, _f, _f, _f, _f, _f, _f,
           _f, _f, _f, _f], _s)
    return ierr

def create_tltg_report(sub, con, mon, report):
    tempdir = os.getcwd()
    temprnd = randint(1000,9999)
    tempfile = 'temp{0}_{1}.dfx'.format(strftime('%Y%m%d%H%M%S' ),
           temprnd)
    dfx = '{0}//{1}'.format(tempdir,tempfile)
    Sys1 = 'ALLGEN'
    Sys2 = 'ALLLOAD'
    ierr = psspy.dfax([1,1], sub, mon, con, dfx)
    psspy.report_output(2, report, [2, 0])
    ierr = psspy.tltg([_i, _i, _i, _i, _i, _i, _i, _i, _i, _i, _i, _i,
           _i, _i, _i, _i, _i], [_f, _f, _f, _f, _f, _f, _f], [Sys1,
           Sys2, _s, _s, _s, _s, _s, _s], dfx)
    psspy.close_report()
    psspy.report_output(1, _s, [_i, _i])
    os.remove(dfx)
    return 0

def parse_tltg_limiting_element_report(tltgPath):
```

```
    # This still breaks on some report rows; I don't know why
    REGEX_LIMITING_ELEMENTS = (r'''[ ]*(?:(<?[-0-9.]+)[* \t]+'''
                               '''(\d+(?:WNDTR)?)[ \t]+(?:([-_. #&a-
        zA-z0-9]{1,12})[ \t]*([0-9.]+|WND \d+))[ \t]+'''
                               '''(\d+(?:WNDTR)?)[ \t]+(?:([-_. #&a-
        zA-z0-9]{1,12})[ \t]*([0-9.]+|WND \d+)|(PHSHFT [-_. #&a-zA-
        z0-9]{1,12}[0-9.]+))[ \t]+'''
                               '''([&a-zA-Z0-9]{1,2})[ \t]+'''
                               '''([-.\d]+)[ \t]+([-.\d]+)[ \t]+([-
        .\d]+)'''
                               '''[ \t]+(?:-*\n[ \t]+)?(OPEN|BASE
        CASE)[ ]?([^\r\n]*)(?:\r\x0c\.*)?\n)''')

    REGEX_LIM_EL_HEADER = (r'''(?:[ \t]+INCR\.[ \t]+PRE-[
        \t]+RATING\n'''
                           '''[ \t]+TRANS \<-* LIMITING ELEMENT -*\>[
        \t]+DISTR\.[ \t]+SHIFT BAS/CNT\n'''
                           '''[ \t]+CAPAB \<-* F R O M -*\> \<-* T O -
        *\>CKT[ \t]+FACTOR[ \t]+MW[ \t]+A/[AB]{1}[ \t]+\<-*
        CONTINGENCY DESCRIPTION -*\>\n)'''
                           '''('''  + REGEX_LIMITING_ELEMENTS +
        ''')+''')

    iFile = open(tltgPath, 'r')
    logFile = iFile.read()
    iFile.close()

    groupPattern = re.compile(REGEX_LIM_EL_HEADER, re.MULTILINE)
    individualPattern = re.compile(REGEX_LIMITING_ELEMENTS,
           re.MULTILINE)

    allElementsReported = []
    for elementReportPage in re.finditer(groupPattern, logFile):

           allElementsReported.extend(re.findall(individualPattern,ele
           mentReportPage.group(0)))
        pass
    return allElementsReported

def limiting_transfer_capability_contingency(tltgPath):
    INCLUDE_THREE_WINDINGS = True
    KEEP_UNDER_NEGATIVE_99999 = False

    mostLimitingElement = []
    foundWorst = False
    tltgEl = parse_tltg_limiting_element_report(tltgPath)
    for el in tltgEl:
        if not foundWorst:
            if INCLUDE_THREE_WINDINGS or (el[4] != '3WNDTR'):
                if KEEP_UNDER_NEGATIVE_99999 and (el[0] == '<-99999'):
```

```
                    el = [-100000] + list(el[1:])
                if (el[0] != '<-99999'):
                    mostLimitingElement = list(el)
                    for idx, x in enumerate(mostLimitingElement):
                        mostLimitingElement[idx] =
            use_best_var_type(x)
                    foundWorst = True
    return mostLimitingElement

def get_Q_headroom():
    ierr, (QGen,) = psspy.amachreal(-1, 1, 'QGEN')
    ierr, (QMax,) = psspy.amachreal(-1, 1, 'QMAX')
    totalQGen = sum(QGen)
    totalQMax = sum(QMax)
    QHeadroom = totalQMax - totalQGen
    return QHeadroom

if __name__ == '__main__':
    pass
```

APPENDIX D: SUBSTATION BUS LIST SCRIPT

```
#!/usr/bin/env/python
"""Builds substation list for a PSS®E case.

This script contains several functions, many
of which can be used individually, but which
build to substation_lists_to_csv(path). This
functions will parse the pre-loaded PSS®E
case and create a CSV file at the given path
with one row per substation. (Defined as
buses connected by transformers or zero-imp
branch equivalents.)

Requires Python 2.7 and PSS®E 33
    -or- Python 2.5 and PSS®E 32
"""

import sys, os, csv

# Import PSS®E APIs
PSSE_VERSION = 33
PSSBIN_PATH = 'C:\\Program Files
           (x86)\\PTI\\PSSE{0}\\PSSBIN'.format(PSSE_VERSION)
sys.path.append(PSSBIN_PATH)
os.environ['PATH'] = (PSSBIN_PATH + ';' + os.environ['PATH'])
import psspy, redirect, dyntools

# Obtain PSS®E defaults
_i = psspy.getdefaultint()
_f = psspy.getdefaultreal()
_s = psspy.getdefaultchar()
redirect.psse2py()

__author__ = 'Micah J. Till'
__copyright__ = 'Copyright 2017'
__version__ = "1.2.0"

def combine_lists(new, old = []):
    y = old[:]
    for x in new:
        if x not in y:
            y.append(x)
    return y

def get_temp_sid(value_if_none = None):
    for sid in range(0, 12):
        if not psspy.bsysisdef(sid):
            psspy.bsysdef(sid, 1)
```

```
            return sid
    return value_if_none

def kill_temp_sid(sid):
    psspy.bsysdef(sid, 0)
    return 0

def is_dummy_bus(ibus):
    x = False
    if psspy.busint(ibus, 'DUMMY')[1]:
        x = True
    return x

def is_zero_imp(Z):
    ZERO_DEF = [0.0000, 0.0001, 0.0000]
    fake_branch = False
    if abs(Z.real) <= ZERO_DEF[0] and abs(Z.imag) <= ZERO_DEF[1]:
        fake_branch = True
    return fake_branch

def find_zero_branch_ends(ibus):
    sid = get_temp_sid(11)
    jbus = [ibus]
    ierr = psspy.bsys(sid,
                      0, [0, 0],            # kV
                      0 ,[],                # Areas
                      ibus, [ibus],         # Buses
                      0, [],                # Owners
                      0, [])                # Zones

    ierr, (bus1,) = psspy.abrnint(sid, _i, 3, 2, 1, 'FROMNUMBER')
    ierr, (bus2,) = psspy.abrnint(sid, _i, 3, 2, 1, 'TONUMBER')
    ierr, (brID,) = psspy.abrnchar(sid, _i, 3, 2, 1, 'ID')
    kill_temp_sid(sid)

    for i,br in enumerate(brID):
        ierr, brZ = psspy.brndt2(bus1[i], bus2[i], br, 'RX')
        if is_zero_imp(brZ):
            jbus += [bus1[i], bus2[i]]

    jbus = [j for j in jbus if j != ibus]
    jbus = combine_lists(jbus)
    jbus.sort()
    return jbus

def find_tx_ends(ibus):
    sid = get_temp_sid(11)
    jbus = [ibus]
    ierr = psspy.bsys(sid,
                      0, [0, 0],            # kV
```

```
                    0 ,[],                  # Areas
                    ibus, [ibus],           # Buses
                    0, [],                  # Owners
                    0, [])                  # Zones

    ierr, (jbus2,) = psspy.atrnint(sid, _i, 3, 2, 2, 'TONUMBER')
    jbus = combine_lists(jbus2, jbus)

    for idx in (1,2,3):
        ierr, (jbus3,) = psspy.atr3int(sid, _i, 3, 2, _i,
           'WIND{0}NUMBER'.format(idx))
        jbus = combine_lists(jbus3, jbus)
    kill_temp_sid(sid)

    jbus = [j for j in jbus if j != ibus]
    jbus = combine_lists(jbus)
    jbus.sort()
    return jbus

def substation_list_from_bus(ibus, substationBusList = []):
    sbuses = combine_lists([ibus], substationBusList)
    jbus = find_zero_branch_ends(ibus)
    jbus += find_tx_ends(ibus)
    for bus in jbus:
        if bus not in sbuses:
            sbuses.append(bus)
            sbuses = substation_list_from_bus(bus, sbuses)
    return sbuses

def substation_lists_to_csv(csvPath):
    TRACK_PROGRESS = False                  # Displaying progress
           significantly slows this process
    INCLUDE_DUMMY_BUSES = False             # Set to False to exclude
           dummy buses

    sid = get_temp_sid(11)
    ierr = psspy.bsys(sid,
                    1, [0.0, 9999],         # kV
                    0 ,[],                  # Areas
                    0, [],                  # Buses
                    0, [],                  # Owners
                    0, [])                  # Zones

    ierr, (allBuses,) = psspy.abusint(sid, 2, 'NUMBER')
    kill_temp_sid(sid)

    with open(csvPath, 'wb') as f:
        writer = csv.writer(f)
        writer.writerow(['Name', 'Bus List'])
```

```
    checkedBuses = []
    for i,ibus in enumerate(allBuses):
        if ibus not in checkedBuses:
            if INCLUDE_DUMMY_BUSES or not is_dummy_bus(ibus):

                if TRACK_PROGRESS:
                    print 'Bus: {0} ({1:.2f}%)'.format(ibus,
            float(i)/float(len(allBuses))*100.0)

                substationBuses = substation_list_from_bus(ibus)
                substationBuses.sort()
                checkedBuses += substationBuses

                ierr, bName = psspy.notona(ibus)
                substationName = bName[0:11].strip()

                with open(csvPath, 'ab') as f:
                    writer = csv.writer(f)
                    writer.writerow([substationName] +
            substationBuses)

if __name__ == '__main__':
    pass
```

APPENDIX E: TRANSFORMER REPLACEMENT LOCATOR SCRIPT

```
#!/usr/bin/env/python
"""Determines appropriate donor transformers for each unit.

This script contains function definitions leading up to
find_donor_transformers(bsys) that, given subsystem with id of
bsys, will determine which transformers within the subsystem are
suitable donor transformers for each other unit in the
subsystem.

Requires Python 2.7 and PSS®E 33
    -or- Python 2.5 and PSS®E 32
"""

import os, sys, numbers

# Import PSS®E APIs
psse_version = 33
pssbin_path = 'C:\\Program Files
           (x86)\\PTI\\PSSE{0}\\PSSBIN'.format(psse_version)
sys.path.append(pssbin_path)
os.environ['PATH'] = (pssbin_path + ';' + os.environ['PATH'])
import psspy, redirect, dyntools

# Obtain PSS®E defaults
_i = psspy.getdefaultint()
_f = psspy.getdefaultreal()
_s = psspy.getdefaultchar()
redirect.psse2py()

__author__ = 'Micah J. Till'
__copyright__ = 'Copyright 2017'
__version__ = "1.0.1"

def two_winding_transformers(bsys):
    TIES = 3
    ierr, (xd0,) = psspy.atrnint(bsys, _i, TIES, 2, 1, 'FROMNUMBER')
    ierr, (xd1,) = psspy.atrnint(bsys, _i, TIES, 2, 1, 'TONUMBER')
    ierr, (xd2,) = psspy.atrnchar(bsys, _i, TIES, 2, 1, 'ID')
    ierr, (xd3,) = psspy.atrnint(bsys, _i, TIES, 2, 1, 'STATUS')
    if xd0 is not None:
        twoWindingElements = zip(xd0, xd1, xd2, xd3)
    else:
        twoWindingElements = ()
    return twoWindingElements

def three_winding_transformers(bsys):
    TIES = 3
```

```
    ierr, (yd0,) = psspy.atr3int(bsys, _i, TIES, 2, _i, 'WIND1NUMBER')
    ierr, (yd1,) = psspy.atr3int(bsys, _i, TIES, 2, _i, 'WIND2NUMBER')
    ierr, (yd2,) = psspy.atr3int(bsys, _i, TIES, 2, _i, 'WIND3NUMBER')
    ierr, (yd3,) = psspy.atr3char(bsys, _i, TIES, 2, _i, 'ID')
    ierr, (yd4,) = psspy.atr3int(bsys, _i, TIES, 2, _i, 'STATUS')
    if yd0 is not None:
        threeWindingElements = zip(yd0, yd1, yd2, yd3, yd4)
    else:
        threeWindingElements = ()
    return threeWindingElements

def pri_sec_voltage_match(original, donor):
    voltage_match = False

    ierr, bv1a = psspy.busdat(original[0], 'BASE')
    ierr, bv1b = psspy.busdat(original[1], 'BASE')
    ierr, bv2a = psspy.busdat(donor[0], 'BASE')
    ierr, bv2b = psspy.busdat(donor[1], 'BASE')
    if max(bv1a, bv1b) == max(bv2a, bv2b):
        if min(bv1a, bv1b) == min(bv2a, bv2b):
            voltage_match = True

    return voltage_match

def mva_match(original_MVA_flow, donor_MVA_rating):
    mva_match = False
    if donor_MVA_rating >= original_MVA_flow:
        mva_match = True
    return mva_match

def two_winding_mva_match(original, donor):
    ierr, original_flow = psspy.brnmsc(original[0], original[1],
           original[2], 'MVA')

    ierr, mvaA = psspy.brndat(donor[0], donor[1], donor[2], 'RATEA')
    ierr, mvaB = psspy.brndat(donor[0], donor[1], donor[2], 'RATEA')
    ierr, mvaC = psspy.brndat(donor[0], donor[1], donor[2], 'RATEA')
    ratings = [0]
    for m in [mvaA, mvaB, mvaC]:
        if isinstance(m, numbers.Number):
            ratings.append(m)
    donor_rating = max(ratings)

    return mva_match(original_flow, donor_rating)

def three_winding_mva_match(original, donor):
    ierr, original_flow = psspy.wnddat(original[0], original[1],
           original[2], original[3], 'MVA')
```

```
    ierr, mvaA = psspy.wnddat(donor[0], donor[1], donor[2], donor[3],
           'RATEA')
    ierr, mvaB = psspy.wnddat(donor[0], donor[1], donor[2], donor[3],
           'RATEB')
    ierr, mvaC = psspy.wnddat(donor[0], donor[1], donor[2], donor[3],
           'RATEC')
    ratings = [0]
    for m in [mvaA, mvaB, mvaC]:
        if isinstance(m, numbers.Number):
            ratings.append(m)
    donor_rating = max(ratings)

    return mva_match(original_flow, donor_rating)

def imp_match(z_original, z_donor):
    LIMIT_LOW = 1.0
    LIMIT_HIGH = 1.2

    imp_match = False
    ratio = z_donor.imag / z_original.imag
    if ratio >= LIMIT_LOW:
        if ratio <= LIMIT_HIGH:
            imp_match = True
    return imp_match

def two_winding_imp_match(original, donor):
    ierr, z_original = psspy.brndt2(original[0], original[1],
           original[2], 'RX')
    ierr, z_donor = psspy.brndt2(donor[0], donor[1], donor[2], 'RX')

    return imp_match(z_original, z_donor)

def three_winding_imp_match(original, donor):
    ierr, z1_original = psspy.wnddt2(original[0], original[1],
           original[2], original[3], 'RX')
    ierr, z2_original = psspy.wnddt2(original[1], original[0],
           original[2], original[3], 'RX')
    z_original = z1_original + z2_original

    ierr, z1_donor = psspy.wnddt2(donor[0], donor[1], donor[2],
           donor[3], 'RX')
    ierr, z2_donor = psspy.wnddt2(donor[1], donor[0], donor[2],
           donor[3], 'RX')
    z_donor = z1_donor + z2_donor

    return imp_match(z_original, z_donor)

def find_donor_transformers(bsys):
    txResults = [['Bus1', 'Bus2', 'Bus3', 'ckt', 'Replacements:' ]]
```

```
    two_winding_set = two_winding_transformers(bsys)
    for tx2 in two_winding_set:
        dataOrigTx = [tx2[0], tx2[1], 'None', tx2[2]]
        dataReplTx = []

        for txB in two_winding_set:
            if pri_sec_voltage_match(tx2, txB):
                if two_winding_mva_match(tx2, txB):
                    if two_winding_imp_match(tx2, txB):
                        if not tx2 == txB:
                            dataReplTx.append(txB)

        if len(dataReplTx) < 1:
            dataOrigTx.extend(['NONE'])
        else:
            dataOrigTx.extend(dataReplTx)
        txResults.append(dataOrigTx)

    three_winding_set = three_winding_transformers(bsys)
    for tx3 in three_winding_set:
        dataOrigTx = list(tx3[0:4])
        dataReplTx = []

        for txC in three_winding_set:
            if pri_sec_voltage_match(tx3, txC):
                if three_winding_mva_match(tx3, txC):
                    if three_winding_mva_match(tx3, txC):
                        if not tx3 == txC:
                            dataReplTx.append(txC)

        if len(dataReplTx) < 1:
            dataOrigTx.extend(['NONE'])
        else:
            dataOrigTx.extend(dataReplTx)
        txResults.append(dataOrigTx)

    return txResults

if __name__ == '__main__':
    pass
```

VITA

Micah J. Till was born in Knoxville, Tennessee. The son of an engineer and a computer scientist, he was doomed from the start to have “the knack.” He received his B.S. in Electrical Engineering—officially marking him as a third generation power systems engineer—from Tennessee Technological University in 2011 and his M.S. in the same field from the University of Tennessee, Knoxville in 2015. He is a recipient of the Energy Science and Engineering Fellowship and the Dominion Virginia Power Fellowship. Hopefully this document makes enough of his research interests obvious that placing an abbreviated list in this section would be needlessly redundant.